Oxidative Medicine and Cellular Longevity

Diagnostics and Mechanisms of Nanomaterials and Oxidative Stress in Cancer, Inflammatory, and Cardiovascular Disease 2021

Lead Guest Editor: Daoud Ali
Guest Editors: Madhukar Saxena and Khuram Ahmad

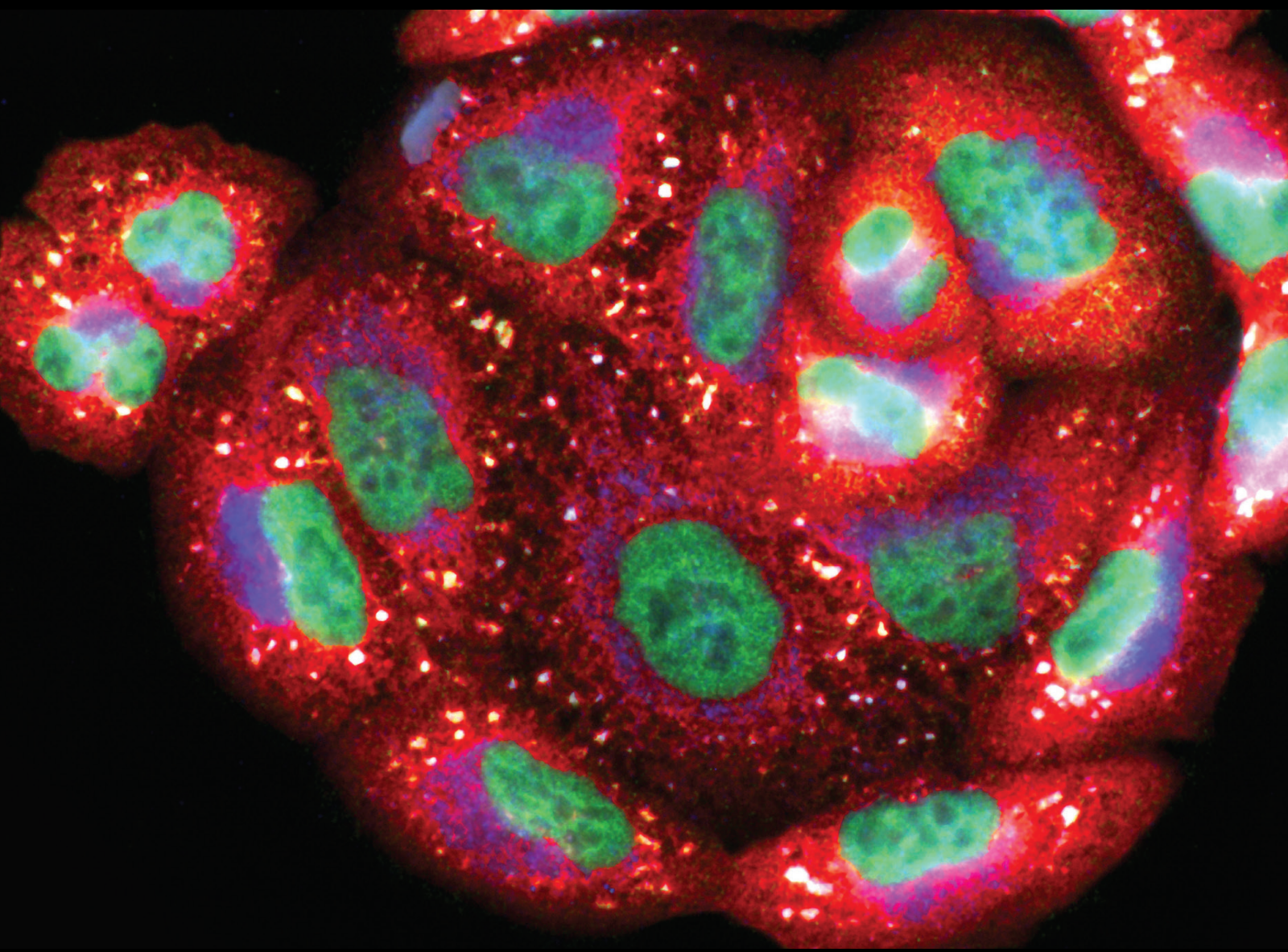

Diagnostics and Mechanisms of Nanomaterials and Oxidative Stress in Cancer, Inflammatory, and Cardiovascular Disease 2021

Oxidative Medicine and Cellular Longevity

Diagnostics and Mechanisms of Nanomaterials and Oxidative Stress in Cancer, Inflammatory, and Cardiovascular Disease 2021

Lead Guest Editor: Daoud Ali
Guest Editors: Madhukar Saxena and Khuram Ahmad

Contents

Hindawi
Oxidative Medicine and Cellular Longevity
Volume 2021, Article ID 4759821, 27 pages
https://doi.org/10.1155/2021/4759821

Research Article

Synthesis, Anticancer Assessment, and Molecular Docking of Novel Chalcone-Thienopyrimidine Derivatives in HepG2 and MCF-7 Cell Lines

Ghada M. Safwat,[1] **Kamel M. A. Hassanin**,[2] **Eman T. Mohammed**,[1] **Essam Kh. Ahmed**,[3] **Mahmoud R. Abdel Rheim**,[1] **Mohamed A. Ameen**,[3] **Mohamed Abdel-Aziz**,[4] **Ahmed M. Gouda**,[5] **Ilaria Peluso**,[6] **Rafa Almeer**,[7] **Mohamed M. Abdel-Daim**,[8] **and Ahmed Abdel-Wahab**[9]

[1]*Department of Biochemistry, Faculty of Veterinary Medicine, Beni Suef University, Beni Suef 62512, Egypt*
[2]*Biochemistry Department, Faculty of Veterinary Medicine, Minia University, Minya 61519, Egypt*
[3]*Chemistry Department, Faculty of Science, Minia University, Minya 61519, Egypt*
[4]*Medicinal Chemistry Department, Faculty of Pharmacy, Minia University, Minya 61519, Egypt*
[5]*Medicinal Chemistry Department, Faculty of Pharmacy, Beni Suef University, Beni Suef 62514, Egypt*
[6]*Research Centre for Food and Nutrition, Council for Agricultural Research and Economics (CREA-AN), Rome, Italy*
[7]*Department of Zoology, College of Science, King Saud University, P.O. Box 2455, Riyadh 11451, Saudi Arabia*
[8]*Pharmacology Department, Faculty of Veterinary Medicine, Suez Canal University, Ismailia 41522, Egypt*
[9]*Physiology Department, Faculty of Veterinary Medicine, Minia University, Minya 61519, Egypt*

Correspondence should be addressed to Eman T. Mohammed; dr_emantaha@yahoo.com

Received 30 July 2021; Revised 6 November 2021; Accepted 29 November 2021; Published 28 December 2021

Academic Editor: Enrico Desideri

Heterocycles containing thienopyrimidine moieties have attracted attention due to their interesting biological and pharmacological activities. In this research article, we reported the synthesis of a series of new hybrid molecules through merging the structural features of chalcones and pyridothienopyrimidinones. Our results indicated that the synthesis of chalcone-thienopyrimidine derivatives from the corresponding thienopyrimidine and chalcones proceeded in a relatively short reaction time with good yields and high purity. Most of these novel compounds exhibited moderate to robust cytotoxicity against HepG2 and MCF-7 cancer cells similar to that of 5-fluorouracil (5-FU). The results indicated that IC_{50} of the two compounds (**3b** and **3g**) showed more potent anticancer activities against HepG2 and MCF-7 than 5-FU. An MTT assay and flow cytometry showed that only **3b** and **3g** had anticancer activity and antiproliferative activities at the G1 phase against MCF-7 cells, while six compounds (**3a-e** and **3g**) had cytotoxicity and cell cycle arrest at different phases against HepG2 cells. Their cytotoxicity was achieved through downregulation of Bcl-2 and upregulation of Bax, caspase-3, and caspase-9. Although all tested compounds increased oxidative stress *via* increment of MDA levels and decrement of glutathione reductase (GR) activities compared to control, the **3a**, **3b**, and **3g** in HepG2 and **3b** and **3g** in MCF-7 achieved the target results. Moreover, there was a positive correlation between cytotoxic efficacy of the compound and apoptosis in both HepG2 ($R^2 = 0.531$; $P = 0.001$) and MCF-7 ($R^2 = 0.219$; $P = 0.349$) cell lines. The results of molecular docking analysis of **3a-g** into the binding groove of Bcl-2 revealed relatively moderate binding free energies compared to the selective Bcl-2 inhibitor, DRO. Like venetoclax, compounds **3a-g** showed 2 violations from Lipinski's rule. However, the results of the ADME study also revealed higher drug-likeness scores for compounds **3a-g** than for venetoclax. In conclusion, the tested newly synthesized chalcone-pyridothienopyrimidinone derivatives showed promising antiproliferative and apoptotic effects. Mechanistically, the compounds increased ROS production with concomitant cell cycle arrest and apoptosis. Therefore, regulation of the cell cycle and apoptosis are possible targets for anticancer therapy. The tested compounds could be potent anticancer agents to be tested in future clinical trials after extensive pharmacodynamic, pharmacokinetic, and toxicity profile investigations.

1. Introduction

Cancer is a multifactorial disease that results from the mutation of certain genes that regulate cell function upon exposure to specific environmental factors. It is characterized by out-of-control cell growth leading to expansive masses of abnormal cells that infiltrate and damage nearby normal tissues. According to the World Health Organization [1], cancer is the second leading cause of death globally and accounted for 7.4 million deaths in 2004 and will continue to increase with an expected 11.5 million deaths in 2030. Although significant progress has been made in cancer treatment, adverse side effects and drug resistance remain serious problems. Therefore, the search is still on for safe and effective chemotherapeutic agents for cancer treatment.

Apoptosis is a physiological process that involves programmed cell death to help the body eliminate aging and nonfunctioning cells *via* the autodigestion process [2]. Apoptosis has a critical role in cancer therapy. Any disturbance in the apoptotic pathway results in many diseases, including cancer. Therefore, the design of a novel anticancer agent that can recover the normal apoptotic pathways is a promising strategy for cancer treatment [3]. Apoptosis in tumor cells can be triggered by various natural and synthetic agents [4]. Synthetic products are frequently more potent than their original compounds [4]. Combinations of chalcones with other pharmacologically interesting scaffolds increase their advantage as anticancer therapy. Previous studies highlighted the ability of chalcones to enhance apoptosis [5].

The heterocycles of thienopyrimidine moiety are structural analogs of the natural pyrimidines "cytosine, thymine, and uracil" [6]. They consist of a thiophene ring bonded with the pyrimidine ring. Their thiophene moiety is identical to the imidazole ring in the purine ring [7]. 2-Thiouracil (a natural equivalent of thiopyrimidines) is a minor component of t-RNA. Their sulfur- or/and nitrogen-disubstituted components showed anticancer effects due to their incorporation into DNA and consequently act as effective inhibitors of nucleic acid syntheses [8]. Thienopyrimidine moiety is a constitutional part of several biologically active compounds [9]. The anticancer effects of thienopyrimidines were recently studied *via* suppression of the protein kinase family [10] and STAT protein family [11]. Due to their interesting biological activities, we have focused our interests on the synthesis of a large number of thienopyrimidine derivatives to find compounds endowed with anticancer activity.

Chalcones or 1,3-diaryl-2-propen-1-ones are an essential class of natural flavonoids and isoflavonoids that are found in many nutritional materials such as vegetables, tea, spices, and fruits. Chalcones have antibacterial [12], antifungal [13], anti-inflammatory [14], and antioxidant [15] activities. The anticancer and antiproliferative activities of chalcones have also been intensively studied against different cancer cell lines [16]. Their biological activities are due to their chemical structure and α,β-unsaturated carbonyl derivatives [17]. The most striking is that chalcones do not induce undesirable genotoxic effects as done with many useful anticancer drugs that may interact with the amino groups of purine and pyrimidine nucleotides of nucleic acids [18].

Several chemotherapeutic drugs have been demonstrated to cause the production of ROS, which aids in cancer cell death [19]. Oxidative stress is induced in HCT116, OV2008, and A2780 cells by thieno[2,3d]pyrimidine derivatives [20]. Furthermore, chalcone derivatives may contribute to the apoptosis of HepG2 cells through increased generation of ROS that ultimately alters the mitochondrial membrane potential of HepG2 cells [21]. In addition, chalcone analogs with a thieno[2,3-d]pyrimidin-2-yl group were found to cause mitochondrial membrane potential depolarization, accelerate ROS generation in HCT-116 cells, and increase the percentage of early and late apoptotic cells [22].

High levels of ROS, such as hydrogen peroxide, superoxide, and hydroxyl radicals, have been shown to cause cell cycle arrest, apoptosis, and irreversible cell damage in cancer cells [23]. Besides, excessive quantities of ROS oxidize and nitrate macromolecules such as lipids, proteins, and DNA, resulting in significant cellular damage [24].

As a result, it is critical to design and manufacture a number of chalcone-thienopyrimidine derivatives, as well as to investigate their mechanisms of promoting apoptosis in the tumor cell.

Over the last three decades, many hybrid molecules have been of great importance in the development of new drugs and have undergone clinical trials for the treatment of various diseases [25]. A hybridization strategy has been used to develop new anticancer drugs by fusing more than two or more active pharmacophores in a single hybrid molecule with synergistic anticancer activity [26]. Hybrid molecules are designed to enhance the biological spectrum and efficacy, overcome drug cross resistance, and reduce potential toxicity compared to the parent drugs. For example, hybridization of the 1,2,4-triazole ring with chalcone moiety in compound I (Figure 1) exhibited significant growth inhibition and induced caspase-3-dependent apoptosis in A549 human lung adenocarcinoma cells with IC_{50} value of 4.4 μM relative to cisplatin with IC_{50} value of 15.3 μM [27].

Following the previous study on the importance of hybrid molecules in the treatment of different types of cancer and pathways, herein, we report the design and synthesis of certain novel thienopyrimidine/chalcone derivatives (**3a-g**, Scheme 1) that incorporate thienopyrimidine and chalcone moieties into a single compact structure for synergistic anticancer activity, manage drug resistance development, and reduce possible side effects. The synthesized compounds have different substitutions for the electron-donating and the electron-withdrawing groups for the SAR study of these compounds. The synthesized derivatives were evaluated for the cytotoxic assay and in vitro antiproliferative activity against HepG2 and MCF-7 cancer cell lines. Furthermore, the synthesized compounds were subjected to the MTT assay, cell cycle analysis, and cellular DNA content measurement. Apoptosis was measured using the Annexin V-FITC/PI apoptotic assay. Additionally, the evaluation of the relative expression levels of Bax, Bcl-2, caspase-3, and caspase-9 was measured. Finally, compounds **3a-g** were also docked into the active site of Bcl-2 to investigate the binding interaction of these compounds with different amino acids.

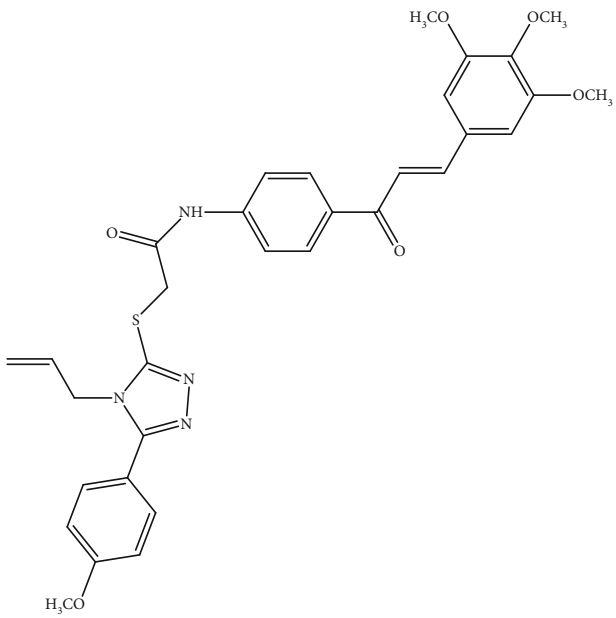

Figure 1: Compound I.

2. Materials and Methods

2.1. Chemicals. All used chemicals were obtained from Alfa Aesar and Fluka corporations and were used without further refinement. 5-Flurouracil was used as a standard reference anticancer agent (fluorouracil 500 mg/10 ml intravenous solution, manufactured by APP Pharmaceuticals Inc., 3 Corporate Dr, Lake Zurich, IL 60047, USA). The other used chemicals were of high purity grade and were obtained from the Aldrich Chemical Company, USA.

2.2. Cell Cultures. The human liver cancer cell line (HepG2 cells) and human breast cancer cell line (MCF-7 cells) were obtained from cell culture lab., Vacsera company, Egypt.

2.3. Synthesis of Chalcone-Thienopyrimidine Derivatives **3a-g**. The melting points of the compounds (**3a-g**) were estimated with a Gallenkamp device. Chalcone **2** (3 mmol) was mixed with a suspension of thienopyrimidine **1** (3 mmol) and K_2CO_3 (0.82 g, 6 mmol) in acetone (15 ml). The reaction mixture was stirred at reflux temperature for 4-6 hours. Then, the solvent was vaporized to dryness in a vacuum. The residue was diluted with water and then extracted with CH_2Cl_2 (3×30 ml). The combined organic extracts were dried over anhydrous Na_2SO_4, filtered, and evaporated under reduced pressure to obtain the corresponding colorless crystal product.

The synthesis of chalcone-thienopyrimidine derivatives (**3a-g**) was done according to the general pathway charted in Scheme 1. Primarily, the chalcones were created by Claisen–Schmidt condensation reaction of aromatic aldehydes with 4-methoxy acetophenone (1 : 1), using 40% potassium hydroxide as a base in ethanol. Then, compound **2** reacted with different pyridothienopyrimidine derivatives in the presence of K_2CO_3 under reflux in acetone to give the corresponding chalcone conjugates in 79-89% yield.

2.4. Identification of Compounds **3a-g**. The reactions and compounds purity were monitored by TLC, on aluminum plates coated with silica gel with a fluorescent indicator (Merck, 60 F254). The NMR spectra were performed on a JHA-LAA 400 WB-FT spectrometer (300 MHz for ^{1}H NMR, 75 MHz for ^{13}C NMR) and a Bruker Avance (400 MHz for ^{1}H and 100 MHz for ^{13}C) with either deuterated DMSO-d6 or $CDCl_3$ as a solvent. Chemical shifts are expressed in δ using TMS as a reference. The mass spectra were recorded on Agilent 6240 Triple Quad LC-MS with methanol as a solvent.

2.5. Determination of the Cytotoxicity. All synthesized chalcone-thienopyrimidine derivatives **3a-g** were screened against two different cancer cell lines: HepG-2 cells and MCF-7. The MTT assay, cell cycle analysis, and apoptotic assays were used to identify the cytotoxic effect of these novel derivatives.

2.5.1. Cell Lines and Culture Maintenance. Cancer cell lines were manipulated according to the method described by Sigounas et al. [28]. In this method, the cell lines were grown as adherent monolayers in T75 flasks with Dulbecco's modified Eagle's medium (DMEM) supplemented with 10% Fetal Bovine Serum (FBS), 2 mM L-glutamine, and 1% streptomycin/penicillin. The cells were left to grow in a CO_2 incubator at 37°C, 5% CO_2, and 95% humidity until their confluence.

2.5.2. MTT Assay for Determination of Cell Proliferation. The 3-[4,5-dimethylthiazol-2-yl]-2,5-diphenyltetrazolium bromide (MTT) colorimetric assay was used to examine the sensitivity of cells to tested compounds (as anticancer drugs), as previously described [29]. This assay depends on the production of a purple formazan derivative from the yellow tetrazolium bromide (MTT) by mitochondrial succinate dehydrogenase in viable cells. The percentage of cell survival was calculated as follows:

$$\text{Percentage of survival} = \frac{\text{O.D.treated cells}}{\text{O.D.control cells}} \times 100. \quad (1)$$

For preliminary screening of the cytotoxicity of synthesized compounds **3a-g**, cells exposed to DMSO were used as a control. Plotting the relationship between the survival score and the compound concentration and calculating the IC_{50} (the concentration required to inhibit cell viability by 50%) were performed for each test compound according to Li et al. [30] in comparison with the reference standard anticancer agent, 5-FU.

2.5.3. Cell Cycle Analysis and Cellular DNA Content Measurement. Cell cycle analysis was performed to decide if the newly synthesized thienopyrimidine derivatives arrested the cell cycle and at what phase of the cell cycle, the HepG2 and MCF-7 cell lines were arrested. The experiments were performed as previously described by Tolba et al. [31]. HepG2 and MCF-7 cell lines were seeded and incubated with the tested compounds in 6-well plates. After incubation overnight, the cells were washed twice with ice-

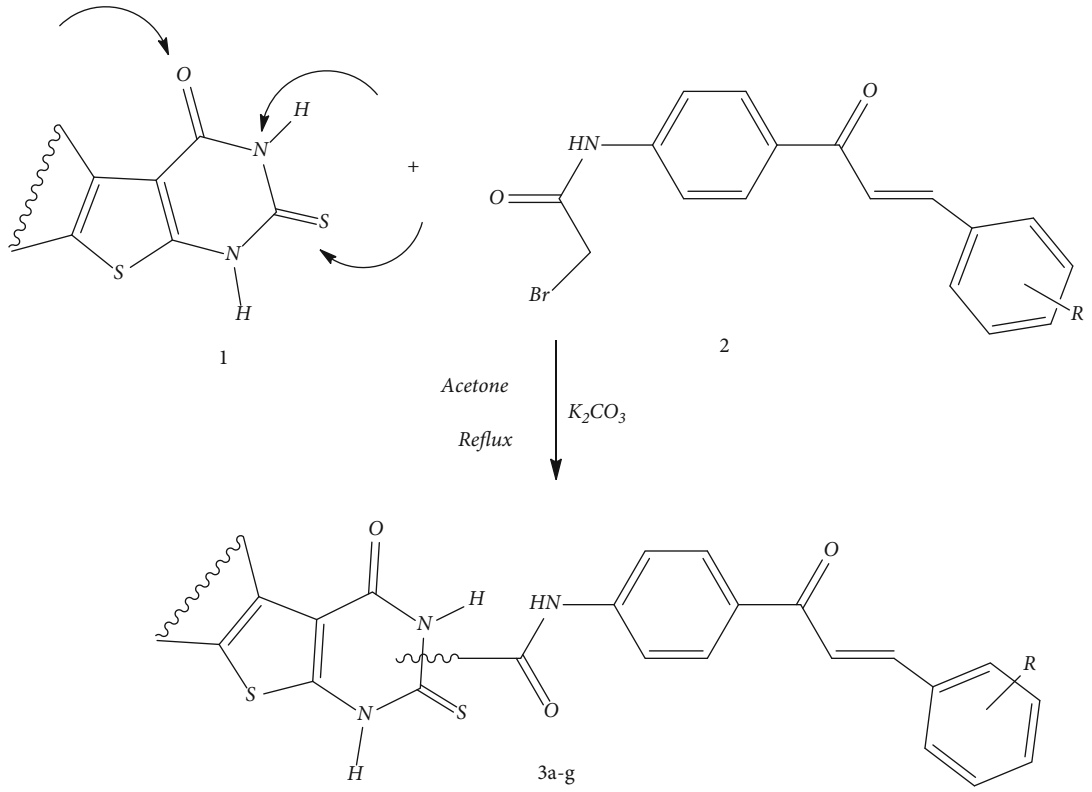

Scheme 1: Synthesis of chalcone-thienopyrimidines **3a-g**.

cold phosphate-buffered saline (PBS), detached by EDTA-trypsinization from the plates, harvested by centrifugation, fixed in ice-cold 70% (*v*/*v*) ethanol, and washed with phosphate-buffered saline (PBS, pH 7.2 ± 0.2). The cells were resuspended with 0.1 mg/ml RNase, stained with 40 mg/ml propidium iodide (PI), and analyzed by flow cytometry using a FACSCalibur flow cytometer (BD Biosciences, San Jose, CA). CellQuest software (Becton Dickinson) was used to determine the cell cycle distributions after incubation with 5-FU or tested compounds. Exposure of HepG2 and MCF-7 cell lines to these compounds could interfere with the normal cell cycle distribution.

2.5.4. Measurement of Apoptosis Using the Annexin V-FITC/PI Apoptotic Assay. Annexin V-fluorescein isothiocyanate (FITC) and counterstaining with propidium iodide (PI) using the Annexin V-FITC/PI apoptosis detection kit (BD Biosciences, San Diego, CA) were employed to distinguish early and late apoptotic cells according to the manufacturer's directions. Annexin V conjugated with fluorescein isothiocyanate was used to quantify the loss of phosphatidylserine asymmetry in cell membranes involved in apoptosis, and propidium iodide can distinguish between early apoptosis, late apoptotic, and necrotic cells [32]. Analyses were achieved by using a FACSCalibur flow cytometer (BD Biosciences, San Jose, CA).

2.6. Evaluation of the Relative Expression Levels of Bax, Bcl-2, Caspase-3, and Caspase-9. We determined the effect of IC_{50} concentration of newly synthesized thienopyrimidine derivatives (**3a**-**e** and **3g** and **3b** and **3g**) on the relative expression levels of some markers of apoptosis in HepG2 and MCF-7 cell lines, respectively. These included the antiapoptotic marker Bcl-2 as well as the apoptotic markers Bax, caspase-3, and caspase-9 [33]. BIORAD iScript™ One-Step RT-PCR kit with SYBR® Green was used to assess the relative levels of expression of apoptosis markers. The measurement was carried out according to the technique of reverse transcription polymerase chain reaction (RT-PCR) using the Rotor-Gene RT-PCR system, and the method of the used kit was done based on the manufacturer's instructions. The procedure of this assay included the following:

2.6.1. RNA Purification Using RNeasy Technology. Based on the manufacturer's instructions, the Qiagen RNeasy Extraction Kit (Qiagen Ltd., UK) was used to isolate mRNA from approximately 1×10^7 cells according to the cell line.

2.6.2. Master Mix Preparation. Mix all the following reagents to get the total volume (50 μl): 2X SYBR® Green RTPCR reaction mixture (25 μl), forward primer (10 mM) (1.5 μl), reverse primer (10 mM) (1.5 μl), nuclease-free water (11 μl), RNA template (1 pg-100 ng total RNA) (10 μl), and iScript reverse transcriptase (1 μl) for One-Step RT-PCR. The real-time PCR sequences of the forward and reverse primers of the following genes were shown in Table 1.

The thermal cycler (Rotor-Gene) program used was as follows: one cycle for reverse transcription at 50°C for 10 minutes and one cycle for RT inactivation/Hot-start activation at 95°C for 5 minutes and then 45 cycles for qPCR

Table 1: Primer sequences used for RT-PCR.

Parameter	Primer sequence
Bax	Forward primer: 5′-GTTTCA TCC AGG ATC GAG CAG-3′ Reverse primer: 5′-CATCTT CTT CCA GAT GGT GA-3′
Cas3	Forward primer: 5′-CTCGGTCTGGTACAGATGTCGA-3′ Reverse primer: 5′-CATGGCTCAGAAGCACACAAAC-3′
Cas9	Forward primer: 5′-CTCCAACATCGACTGTGAGAAGTT-3′ Reverse primer: 5′-GCGCCAGCTCCAGCAA-3′
Bcl-2	Forward primer: 5′-CCTGTG GAT GAC TGA GTA CC-3′ Reverse primer: 5′-GAGACA GCC AGG AGA AAT CA-3′
β-Actin	Forward primer: 5′-GTGACATCCACACCCAGAGG-3′ Reverse primer: 5′-ACAGGATGTCAAAACTGCCC-3′

(10 s at 95°C, 30 seconds for annealing at 55°C, and 30 seconds for extension at 72°C), and this is followed by the final extension (one cycle) at 72°C for 10 minutes.

2.7. Molecular Docking. The docking analysis was carried out using AutoDock 4.2 [34] to perform the docking study of compounds **3a-g** into the active site of Bcl-2 (pdb code: 2W3L) [35]. The crystal structure of Bcl-2 was retrieved from the Protein Data Bank (https://www.rcsb.org/structure). Preparation of ligands and protein files was carried out in accordance with the previous report [36]. In addition, the docking study was completed in accordance with the previous report [37]. Discovery Studio Visualizer was used to visualize the binding modes/interaction of the test compound [38].

2.8. ADME Study. The SwissADME web server (http://www.swissadme.ch/) [39] was used to calculate the physicochemical properties of compounds **3a-g**. The Molsoft web server (http://molsoft.com/mprop/) was also used to calculate the drug-likeness scores of the seven compounds.

2.9. Determination of Lipid Peroxidation (MDA). MDA is described as a lipid peroxidation product. It reacts with thiobarbituric acid to produce a red substance that is absorbed at 535 nm [40].

2.10. Determination of Glutathione Reductase (GR) Activity. The activity of GR was determined by the decrease in absorbance caused by the oxidation of NADPH during the reduction of oxidized GSH [41].

2.11. Statistical Analysis. The obtained data were subjected to statistical analysis by the one-way analysis of variance (ANOVA) test followed by Duncan's multiple tests for comparison using the SPSS 10.0 (SPSS, Chicago, IL, USA) software program. The values were summarized as means and standard error of mean (SEM) for three replicates. The values were considered statistically significant if the P value was $^{*}P < 0.05$ from control and $^{\#}P < 0.05$ from 5FU. In addition, the correlation between cytotoxicity and apoptosis was determined by the Pearson correlations.

3. Results

3.1. Chemistry

3.1.1. Synthesis of Chalcone-Thienopyrimidine Derivatives. Our data indicated that in general, the synthesis of chalcone-thienopyrimidine compounds from the correspondent thienopyrimidine proceeds in a relatively short reaction time with good yield and high purity. The reaction produces only one diastereomer, which is considered Z-isomer, as shown in Scheme 1. The ^{1}H NMR proves that there is an olefinic-H proton that is affected by the carbonyl group, since this proton appeared deshielded in the ^{1}H NMR spectra of **3a-g** at $\delta > 7.60$ and low coupling constant referring to the Z-isomer. In this study, we synthesized a series of novel chalcone-pyridothienopyrimidinone derivatives **3a-g** by reacting chalcones with different pyridothienopyrimidinone **2** according to the methods of Sauter et al. [42] and Ameen et al. [43] under reflux temperature as indicated in Figure 2.

Melting points were determined on a Boetius melting point apparatus and are uncorrected. Elemental analyses were performed on Carlo Erba CHN-S Elemental analyses 1108. The NMR spectra were obtained using a Bruker Avance (400 MHz for ^{1}H and 100 MHz for ^{13}C), Institute of Organic Chemistry, Karlsruhe University, Karlsruhe, Germany, with deuterated DMSO-d_6 as a solvent. Chemical shift is quoted in δ and is referenced to TMS. Mass spectrometry was performed by electron impact at 70 eV (FAB-MS): Finnigan MAT 95, Institute of Organic Chemistry, Karlsruhe Institute of Technology, Karlsruhe, Germany. The reactions and purity were monitored by TLC, on aluminum plates coated with silica gel with a fluorescent indicator (Merck, 60 F254).

The IUPAC nomenclature, chemical formula, molecular weight, melting point (m.p.), and NMR (^{1}H NMR and ^{13}C NMR) analysis (Supplementary 3) of the synthesized chalcone-thienopyrimidine derivatives are presented as follows.

3.2. Compound 3a

3.2.1. Ethyl (Z)-2-((2-((4-(3-(2-Chlorophenyl)acryloyl)phenyl)amino)-2-oxoethyl)thio)-3-(2-ethoxy-2-oxoethyl)-4-oxo-3,5,6,8-tetrahydropyrido[4′,3′:4,5]thieno[2,3-d]pyrimidine-7(4H)-carboxylate. Colorless crystals from DMF-H_2O; Yield (79%); m.p. 181-182°C. ^{1}H NMR (400 MHz, *DMSO*, ppm): δ 1.26 (t, 6H, J = 7.1 Hz, $2COOCH_2CH_3$), 2.71 (t, 2H, J = 5.6 Hz, H-5), 2.87 (t, 2H, J = 5.1 Hz, H-6), 4.09 (q, 2H, J = 7.0 Hz, $COOCH_2CH_3$), 4.21 (q, 2H, J = 7.0 Hz, $COOCH_2CH_3$), 4.29 (s, 2H, SCH_2), 4.59 (s, 2H, H-8). 4.92 (s, 2H, NCH_2),

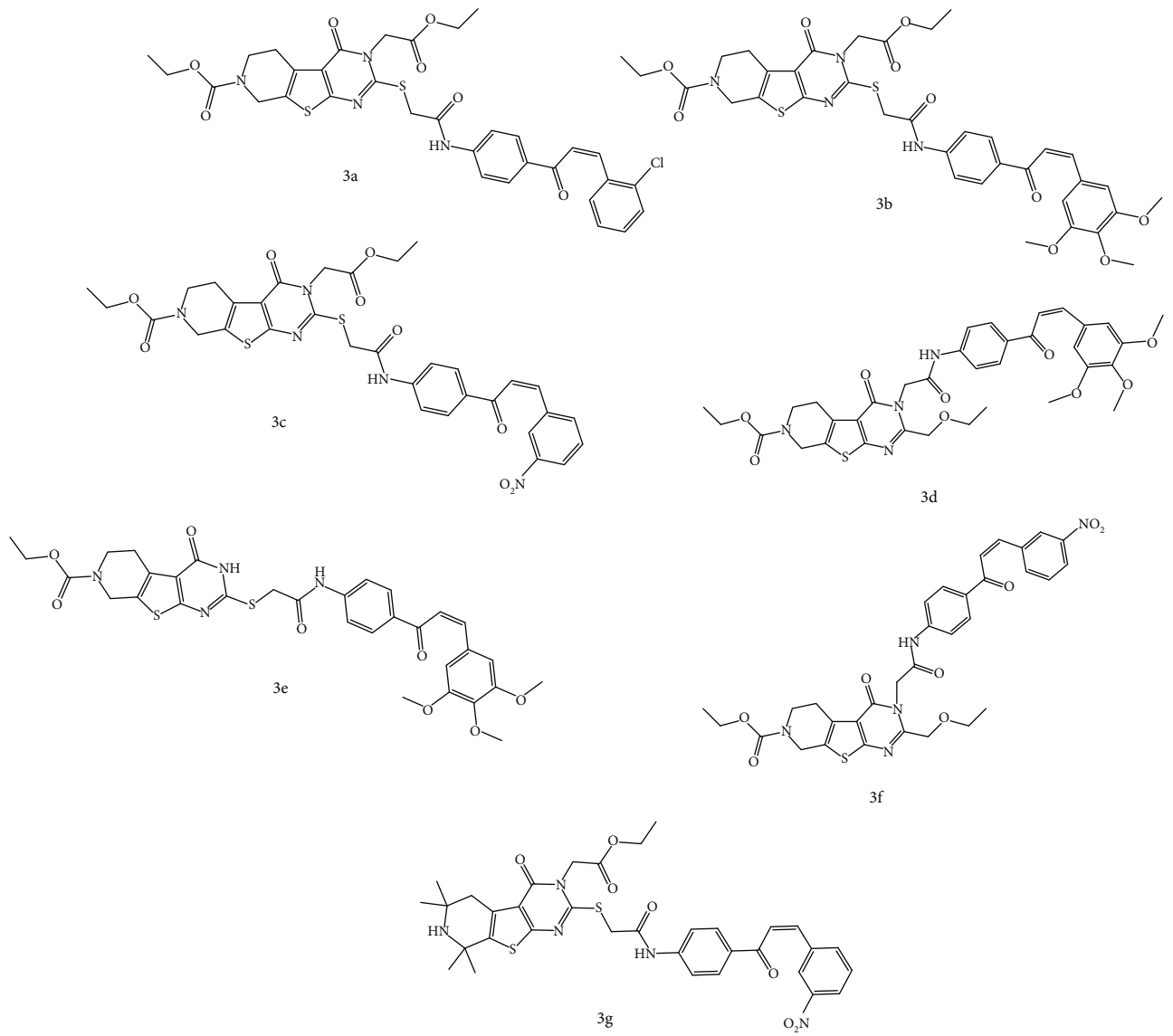

Figure 2: Chemical structures of synthesized chalcone-thienopyrimidines **3a-g**.

7.45-7.60 (m, 4H, Ar-H), 7.79 (d, 2H, J=9.0 Hz, Ar-H), 8.01 (d, 2H, J=4.0 Hz, 2CH), 8.20 (d, 2H, J=9.0 Hz, Ar-H), 10.78 (s, 1H, NH). ^{13}C NMR (100 MHz, *DMSO*, ppm): δ 14.4 (CH_3), 14.7 (CH_3), 30.1 (C-5), 35.7 (SCH_2), 40.7 (C-6), 42.8 (C-8), 44.7 (NCH_2), 61.1 (CH_2, carbamate), 61.6 (CH_2, carbamate), 117.1 (C-4a), 124.6 (C-4b), 127.6 (C-8a), 128.4, 129.2, 129.9, 130.1, 131.8, 132.2, 132.4, 134.3, 137.9, 141.3 (12 C-Ar, 2 CH-olefine), 154.6 (C-9a), 154.9, 156.8, 161.7, 162.3, 185.3 (5 C=O), (EI-MS): *m/z* calcd. $C_{33}H_{31}ClN_4O_7S_2$ $[M]^+$: 694.13, found: 694.11. Anal. Calcd for $C_{33}H_{31}ClN_4O_7S_2$ (695.20): C, 57.01; H, 4.49; Cl, 5.10; N, 8.06; Found: C, 56.96; H, 4.38; Cl, 5.02; N, 7.98.

3.3. Compound **3b**

3.3.1. Ethyl (Z)-3-(2-Ethoxy-2-oxoethyl)-4-oxo-2-((2-oxo-2-((4-(3-(3,4,5 trimethoxyphenyl) acryloyl)phenyl)amino)ethyl) thio)-3,5,6,8 tetra-hydropyrido[4′,3′:4,5]thieno[2,3-d]pyrimidine-7(4H)-carboxylate. Colorless crystals from DMF-H_2O; Yield (81%); m.p. 172-173°C. ^{1}H NMR (400 MHz, *DMSO*, ppm): δ 1.11, 1.22 (t, 6H, J=7.1 Hz, $2COOCH_2CH_3$), 2.86 (t, 2H, J=5.6 Hz, H-5), 3.61 (t, 2H, J=5.1 Hz, H-6), 3.86 (s, 3H, OCH_3), 3.97 (s, 6H, $2OCH_3$), 4.08 (q, 2H, J=7.0 Hz, $COOCH_2CH_3$), 4.20 (q, 2H, J=7.0 Hz, $COOCH_2CH_3$), 4.26 (s, 2H, SCH_2), 4.55 (s, 2H, H-8). 4.87 (s, 2H, NCH_2), 7.65-7.95 (m, 2H, Ar-H, d, 2H, J=9.0 Hz, Ar-H, d, 2H, J=4.0 Hz, 2CH), 8.20 (d, 2H, J=9.0 Hz, Ar-H), 10.77 (s, 1H, NH). ^{13}C NMR (100 MHz, *DMSO*, ppm): δ 13.9 (CH_3), 14.5 (CH_3), 30.1 (C-5), 35.5 (SCH_2), 39.7 (C-6), 42.5 (C-8), 44.5 (NCH_2), 56.1 ($2OCH_3$), 59.2 (OCH_3), 61.1 (CH_2, carbamate), 61.6 (CH_2, carbamate), 105.6 (2CH-Ar), 117.1 (C-4a), 120.1 (CH-Ar), 122.2, (CH-olefine), 124.6 (C-4b), 127.6, 128.8 (C-8a), 129.9, 130.1, 131.8, 132.2, 132.6, 137.9, 139.5 (6 C-Ar, CH-Ar), 143.2 (CH-olefine), 152.6 (C-9a), 155.6, 156.7, 162.6, 165.3, 186.6 (5 C=O), (EI-MS): *m/z* calcd. $C_{36}H_{38}N_4O_{10}S_2$ $[M]^+$: 750.20, found: 750.23. Anal. Calcd for $C_{36}H_{38}N_4O_{10}S_2$ (750.84): C, 57.59; H, 5.10; N, 7.46; Found: C, 57.47; H, 5.01; N, 7.36.

3.4. Compound **3c**

3.4.1. Ethyl (Z)-3-(2-Ethoxy-2-oxoethyl)-2-((2-((4-(3-(3-nitrophenyl)acryloyl)phenyl)amino)-2-oxoethyl)thio)-4-oxo-3,5,6,8-tetrahydropyrido[4′,3′:4,5]thieno[2,3-d]pyrimidine-7(4H)-carboxylate. Pale yellow crystals from DMF-H_2O; Yield (86%); m.p. 189-190°C. ^{1}H NMR (400 MHz, *DMSO*, ppm): δ 1.14 (t, 3H, J=7.1 Hz, $COOCH_2CH_3$), 1.21 (t, 3H, J=7.1 Hz, $COOCH_2CH_3$), 2.78 (t, 2H, J=5.6 Hz, H-5), 3.64 (t, 2H, J=5.1 Hz, H-6), 4.11 (q, 2H, J=7.0 Hz, $COOCH_2CH_3$), 4.21 (q, 2H, J=7.0 Hz, $COOCH_2CH_3$), 4.31 (s, 2H, SCH_2), 4.58 (s, 2H, H-8). 4.95 (s, 2H, NCH_2), 7.51-7.68 (m, 4H, Ar-H), 7.79 (d, 2H, J=9.0 Hz, Ar-H), 8.12 (d, 2H, J=4.0 Hz, 2CH), 8.20 (d, 2H, J=9.0 Hz, Ar-H), 10.82 (s, 1H, NH). ^{13}C NMR (100 MHz, *DMSO*, ppm): δ 14.0 (CH_3), 14.7 (CH_3), 31.1 (C-5), 35.6 (SCH_2), 40.8 (C-6), 42.9 (C-8), 44.7 (NCH_2), 61.2 (CH_2, carbamate), 61.6 (CH_2, carbamate), 118.1 (C-4a), 125.6 (C-4b), 127.6 (C-8a), 128.4, 129.3, 129.9, 130.2, 131.9, 132.4, 132.6, 134.5, 137.9, 141.4 (12 C-Ar, 2 CH-olefine), 154.6 (C-9a), 155.6, 156.8, 162.6, 165.6, 185.4 (5 C=O), (EI-MS): *m*/*z* calcd. $C_{33}H_{31}N_5O_9S_2$ $[M]^+$: 705.16, found: 705.21. Anal. Calcd for $C_{33}H_{31}N_5O_9S_2$ (705.76): C, 56.16; H, 4.43; N, 9.92; Found: C, 56.04; H, 4.32; N, 9.81.

3.5. Compound **3d**

3.5.1. Ethyl (Z)-2-(Ethoxymethyl)-4-oxo-3-(2-oxo-2-((4-(3-(2,3,4-trimethoxyphenyl)acryloyl)-phenyl)amino)ethyl)-3,5,6,8-tetrahydropyrido[4′,3′:4,5]thieno[2,3-d]pyrimidine-7(4H)-carboxylate. Pale yellow crystals from DMF-H_2O; Yield (80%); m.p. 157-158°C. ^{1}H NMR (400 MHz, *DMSO*, ppm): δ 1.07 (t, 3H, J=7.1 Hz, OCH_2CH_3), 1.22 (t, 3H, J=7.1 Hz, $COOCH_2CH_3$), 2.89 (t, 2H, J=5.6 Hz, H-5), 3.48 (q, 2H, J=7.0 Hz, OCH_2CH_3), 3.65 (t, 2H, J=5.1 Hz, H-6), 3.76 (s, 3H, OCH_3), 3.87 (s, 6H, $2OCH_3$), 4.10 (q, 2H, J=7.0 Hz, OCH_2CH_3), 4.20 (q, 2H, J=7.0 Hz, $COOCH_2CH_3$), 4.51 (s, 2H, OCH_2), 4.59 (s, 2H, H-8). 4.98 (s, 2H, NCH_2), 7.14 (d, 2H, J=9.0 Hz, Ar-H), 7.71-7.96 (m, 2H, Ar-H, d, 2H, J=4.0 Hz, 2CH), 8.20 (d, 2H, J=9.0 Hz, Ar-H), 10.79 (s, 1H, NH). ^{13}C NMR (100 MHz, *DMSO*, ppm): δ 14.5 (CH_3), 14.7 (CH_3), 39.5 (C-5), 35.7 (OCH_2), 39.9 (C-6), 42.5 (C-8), 55.5 (NCH_2), 56.1 ($2OCH_3$), 60.1 (OCH_3), 61.1 (CH_2, OCH_2CH_3), 65.6 (CH_2, carbamate), 110.6 (2CH-Ar), 111.2 (C-4a), 121.1, 122.3 (4 CH-Ar), 124.6 (C-4b), 127.6, (C-8a), 132.2, 133.6, 137.9, 138.5 (C-Ar), 143.2 (2 CH-olefine), 150.1 (C-9a), 157.6, 159.1 (3 *C*-OCH_3), 162.6, 162.3, 171.2, 191.4 (4 C=O), (EI-MS): *m*/*z* calcd. $C_{35}H_{38}N_4O_9S$ $[M]^+$: 690.24, found: 690.16. Anal. Calcd for $C_{35}H_{38}N_4O_9S$ (690.77): C, 60.86; H, 5.55; N, 8.11; Found: C, 60.77; H, 5.43; N, 8.04.

3.6. Compound **3e**

3.6.1. Ethyl (Z)-4-Oxo-2-((2-oxo-2-((4-(3-(3,4,5-trimethoxyphenyl) acryloyl)phenyl)amino)ethyl)-thio)-3,5,6,8-tetrahydropyrido[4′,3′:4,5]thieno[2,3-d]pyrimidine-7(4H)-carboxylate. Pale yellow crystals from DMF-H_2O; Yield (89%); m.p. 167-168°C. ^{1}H NMR (400 MHz, *DMSO*, ppm): δ 1.18 (t, 3H, J=7.1 Hz, $COOCH_2CH_3$), 2.86 (t, 2H, J=5.6 Hz, H-5), 3.64 (t, 2H, J=5.1 Hz, H-6), 3.86 (s, 3H, OCH_3), 3.88 (s, 6H, $2OCH_3$), 4.22 (q, 2H, J=7.0 Hz, $COOCH_2CH_3$), 4.27 (s, 2H, SCH_2), 4.58 (s, 2H, H-8), 7.55-7.95 (m, 2H, Ar-H, d, 2H, J=9.0 Hz, Ar-H, d, 2H, J=4.0 Hz, 2CH), 8.20 (d, 2H, J=9.0 Hz, Ar-H), 10.77 (s, 1H, NH), 11.17 (s, 1H, NH). ^{13}C NMR (100 MHz, *DMSO*, ppm): δ 14.5 (CH_3), 30.1 (C-5), 35.5 (SCH_2), 39.7 (C-6), 42.5 (C-8), 56.1 ($2OCH_3$), 59.2 (OCH_3), 61.6 (CH_2, carbamate), 107.6 (2CH-Ar), 117.4 (C-4a), 120.5 (CH-Ar), 121.2, (CH-olefine), 123.6 (C-4b), 128.6, 128.8 (C-8a), 129.7, 130.1, 130.8, 132.1, 132.7, 137.9, 139.5 (6 C-Ar, CH-Ar), 143.3 (CH-olefine), 152.9 (C-9a), 153.6, 156.5, 164.3, 186.7 (4 C=O), (EI-MS): *m*/*z* calcd. $C_{32}H_{32}N_4O_8S_2$ $[M]^+$: 664.17, found: 664.25. Anal. Calcd for $C_{32}H_{32}N_4O_8S_2$ (664.75): C, 57.82; H, 4.85; N, 8.43; Found:): C, 57.71; H, 4.75; N, 8.32.

3.7. Compound **3f**

3.7.1. Ethyl (Z)-2-(Ethoxymethyl)-3-(2-((4-(3-(3-nitrophenyl) acryloyl)phenyl)amino)-2-oxoethyl)-4-oxo-3,5,6,8-tetrahydropyrido[4′,3′:4,5]thieno[2,3-d]pyrimidine-7(4H)-carboxylate. Pale yellow crystals from DMF-H_2O; Yield (82%); m.p. 178-179°C. ^{1}H NMR (400 MHz, *DMSO*, ppm): δ 1.14 (t, 3H, J=7.1 Hz, OCH_2CH_3), 1.21 (t, 3H, J=7.1 Hz, $COOCH_2CH_3$), 2.78 (t, 2H, J=5.6 Hz, H-5), 3.64 (t, 2H, J=5.1 Hz, H-6), 4.11 (q, 2H, J=7.0 Hz, OCH_2CH_3), 4.21 (q, 2H, J=7.0 Hz, $COOCH_2CH_3$), 4.31 (s, 2H, CH_2O), 4.58 (s, 2H, H-8). 4.95 (s, 2H, NCH_2), 7.51-7.68 (m, 4H, Ar-H), 7.79 (d, 2H, J=9.0 Hz, Ar-H), 8.12 (d, 2H, J=4.0 Hz, 2CH), 8.20 (d, 2H, J=9.0 Hz, Ar-H), 10.82 (s, 1H, NH). ^{13}C NMR (100 MHz, *DMSO*, ppm): δ 14.1 (CH_3), 14.6 (CH_3), 31.4 (C-5), 35.8 (OCH_2), 41.5 (C-6), 42.7 (C-8), 44.8 (NCH_2), 61.2 (CH_2, OCH_2CH_3), 61.6 (CH_2, carbamate), 117.9 (C-4a), 124.6 (C-4b), 127.6 (C-8a), 128.3, 129.5, 129.9, 130.6, 131.2, 131.8, 132.4, 132.6, 134.5, 137.9, 141.4 (12 C-Ar, 2 CH-olefine), 154.6 (C-9a), 155.7, 156.7, 166.5, 184.4 (4 C=O), (EI-MS): *m*/*z* calcd. $C_{32}H_{31}N_5O_8S$ $[M]^+$: 645.19, found: 645.21. Anal. Calcd for $C_{32}H_{31}N_5O_8S$ (645.69); C, 59.53; H, 4.84; N, 10.85; Found: C, 59.42; H, 4.73; N, 10.75.

3.8. Compound **3g**

3.8.1. Ethyl (Z)-2-(6,6,8,8-Tetramethyl-2-((2-((4-(3-(3-nitrophenyl)acryloyl)-phenyl)amino)-2-oxoethyl)thio)-4-oxo-5,6,7,8-tetrahydropyrido[4′,3′:4,5]thieno[2,3-d]pyrimidin-3(4H)-yl)acetate. Pale yellow crystals from DMF-H_2O; Yield (80%); m.p. 194-195°C. ^{1}H NMR (400 MHz, *DMSO*, ppm): δ 1.13 (t, 3H, J=7.1 Hz, $COOCH_2CH_3$), 1.23 (s, 6H, $2CH_3$), 1.23 (s, 6H, $2CH_3$), 2.03 (s, H, NH), 2.76 (t, 2H, J=5.6 Hz, H-5), 4.12 (q, 2H, J=7.0 Hz, $COOCH_2CH_3$), 4.33 (s, 2H, SCH_2), 4.88 (s, 2H, NCH_2), 7.67-7.65 (m, 4H, Ar-H), 7.76 (d, 2H, J=9.0 Hz, Ar-H), 8.09 (d, 2H, J=4.0 Hz, 2CH), 8.21 (d, 2H, J=9.0 Hz, Ar-H), 10.67 (s, 1H, NH). ^{13}C NMR (100 MHz, *DMSO*, ppm): δ 14.1 (CH_3), 28.1 ($2CH_3$), 33.2 (C-5), 34.1 ($2CH_3$), 35.7 (SCH_2), 44.6 (NCH_2), 58.9 (C-6), 61.1 (C-8), 61.3 (CH_2, carbamate), 117.2 (C-4a), 124.6 (C-4b), 127.7 (C-8a), 128.3, 129.3, 130.1, 131.2, 131.8, 132.6, 132.5, 134.8, 136.9, 141.6 (12 C-Ar, 2 CH-olefine), 153.6 (C-9a), 155.7, 156.4, 161.8, 184.3 (4 C=O), (EI-MS): *m*/*z* calcd. $C_{34}H_{35}N_5O_7S_2$ $[M]^+$: 689.20, found: 689.27. Anal.

Calcd for $C_{34}H_{35}N_5O_7S_2$ (689.80); C, 59.20; H, 5.11; N, 10.15; Found: C, 59.04; H, 5.07; N, 10.08.

3.9. Cytotoxic Activity (MTT Assay). The results presented in Tables 2 and 3 indicate the percentage of survival of the two cell lines (HepG2 and MCF-7) after exposure to serial dilution of the synthesized chalcone-thienopyrimidine derivatives **3a-g** as well as DMSO.

DMSO (at dilution rate 1.5625) showed no cytotoxicity on MCF-7 and HepG2 cell lines producing survival percentages of 102.6 ± 0.632 and 103.6 ± 0.051, respectively. Therefore, we suggested that the tested compounds showing cell survival percentage less than 100% at the corresponding dilution had cytotoxic efficacy and then they were used in further experiments.

The MTT assay results revealed that the six compounds **3a**, **3b**, **3c**, **3d**, **3e**, and **3g** exhibited potent cytotoxicity with IC_{50} values ranging from 0.0332 ± 0.0028 to $0.1321 \pm 0.0152\,\mu$M against the HepG2 cell line. Moreover, the two compounds **3b** and **3g** showed the maximum anticancer effects with the lowest IC_{50} values of 0.0073 ± 0.0016 and $0.0332 \pm 0.0028\,\mu$M, respectively. The two compounds **3b** and **3g** showed anticancer effects which represented 4046.90- and 420.94-fold more potent activity than 5-FU ($13.9753 \pm 0.149\,\mu$M) (Figure 3(a)).

The MTT assay results of the tested compounds **3a**, **3b**, and **3c** on the HepG2 cell line indicate that compound **3b** containing 3-methoxy-donating function groups on chalcone moiety exhibited remarkable anticancer activity (~18 times more activity) compared to compounds **3a** and **3c** containing an electron-withdrawing function group on chalcone moiety.

Compounds **3d** and **3e** containing 3-methoxy-donating function groups on chalcone moiety either on the sulfur atom or on the nitrogen atom of thienopyrimidine exhibited nearly equal anticancer activity with IC_{50} of $0.0837\,\mu$M and $0.0871\,\mu$M, respectively.

Compound **3g** containing an electron-withdrawing function group (NO_2) with the absence of ethoxycarbonyl moiety on the nitrogen of piperidine moiety exhibited good anticancer activity with IC_{50} of $0.0033\,\mu$M.

On the other hand, only **3b** and **3g** compounds were the most potent cytotoxic compounds with IC_{50} values of 0.0349 ± 0.0047 and $0.0843 \pm 0.0066\,\mu$M, respectively, representing 846.5- and 350.4-fold more effective anticancer activity than 5-FU ($29.5424 \pm 0.264\,\mu$M) against the MCF-7 cell line (Figure 3(b)).

The MTT assay results of the tested compounds **3b** and **3g** on the MCF-7 cell line indicate that compound **3b** containing 3-methoxy-donating function groups on chalcone moiety exhibited remarkable anticancer activity (~2.5 times more activity) compared to compound **3g** containing an electron-withdrawing function group (NO_2) on chalcone moiety.

The most active newly synthesized compounds were selected for further evaluation.

3.10. Cell Cycle Analysis. The molecular mechanism of antiproliferation induction of the HepG2 cell line by the six tested compounds **3a**, **3b**, **3c**, **3d**, **3e**, and **3g** as well as the MCF-7 cell line by two compounds **3b** and **3g** was evaluated by measuring their impacts on cell cycle progression using propidium iodide. The data presented in Figures 4 and 5 illustrated the flow cytometry analyses of cell cycle distribution in the untreated cell (control), 5-fluorouracil (5-FU), and tested newly synthesized chalcone-thienopyrimidine derivatives.

Flow cytometry analysis displayed that the treatment of the HepG2 cell line with compounds **3a**, **3e**, and **3g** showed substantial increase in the cell population in G2/M while compounds **3a**, **3b**, **3d**, **3e**, and **3g** induced a significant increase in pre-G1 phases compared with control cells (Figure 4). Interestingly, the application of compound **3c** exhibited a significant increase in the G1 phase cell population ($P < 0.05$). Worthwhile, compound **3c** induced a significant ($P < 0.05$) increase in the cell population in the G1 phase up to 55.32%. Additionally, compound **3d** induced a significant ($P < 0.05$) increase in the S phase cell population (Figure 4).

Regarding the MCF-7 cell line, our results revealed that compounds **3b** and **3g** significantly ($P < 0.05$) induced G1 and pre-G1 arrest. Results indicated the increased cell population in G1 and pre-G1 phases compared with control cells (Figure 5).

3.11. Induction of Apoptosis. To further demonstrate that the antiproliferative activities of the six tested compounds relied mainly on apoptosis, Annexin V-FITC/PI staining by flow cytometry (Figure 6) was used to determine the quantitative assessment of apoptosis. For HepG2 cells treated with the six compounds, the total apoptosis was evaluated; also, the cells undergoing early apoptosis (Annexin+/PI−), late apoptosis (Annexin+/PI+), and necrosis (Annexin−/PI+) were evaluated (Figure 6).

Interestingly, our results revealed that the HepG2 cell line treated with all tested compounds except **3c** showed significant induction of total apoptosis in relation to control ($P < 0.05$). On exposure to compounds **3a**, **3b**, and **3g**, the HepG2 cell line significantly exhibited early and late apoptosis ($P < 0.05$). All of these compounds elicited apoptotic effects comparable to that of 5-FU ($P > 0.05$). Moreover, no one of the tested derivatives displayed a necrotic effect in comparison with the control ($P > 0.05$) (Figure 6).

Concerning the MCF-7 cells, their treatment with the compounds **3a** and **3b** showed a significant increase in the total, early, and late apoptosis as well as necrosis relative to the control cells ($P < 0.05$) together with enhancing the translocation of phosphatidylserine (Annexin V-positive cells) (Figure 7).

3.12. Gene Expression of Bcl-2, Bax, Caspase-3, and Caspase-9. For further understanding of the mechanism by which the tested compounds induced apoptosis, the gene expression levels of proapoptotic factors Bax, caspase-9, and caspase-3 and antiapoptotic one Bcl-2 were measured by RT-PCR and compared to that of 5-FU (Figure 8).

For the HepG2 cell line, it is worth mentioning that all tested compounds significantly increased the expression

Table 2: Preliminary screening of the cytotoxic efficacy of the synthesized chalcone-thienopyrimidine derivatives **3a-g** against human breast cancer cell line (MCF-7) compared to DMSO. The cytotoxic efficacy of the compounds is expressed as the mean of survival percentage ± SEM.

Compound concentration (μg/ml)	**3a**	**3b**	**3c**	**3d**	**3e**	**3f**	**3g**	*DMSO*
10000	6.0 ± 0.063	17.3 ± 0.001	5.9 ± 0.002	5.8 ± 0.001	15.9 ± 0.002	4.6 ± 0.002	15.3 ± 0.000	4.2 ± 0.071
5000	6.0 ± 0.001	19.7 ± 0.002	6.4 ± 0.007	6.12 ± 0.003	16.0 ± 0.000	5.1 ± 0.003	18.9 ± 0.001	4.2 ± 0.121
2500	6.28 ± 0.003	20.1 ± 0.001	6.4 ± 0.003	6.2 ± 0.005	17.9 ± 0.002	6.2 ± 0.004	19.0 ± 0.001	6.8 ± 0.257
1250	9.8 ± 0.003	20.3 ± 0.001	7.4 ± 0.003	8.5 ± 0.006	27.8 ± 0.021	47.5 ± 0.181	19.9 ± 0.002	11.5 ± 0.112
625	64.9 ± 0.008	20.3 ± 0.002	11.3 ± 0.026	26.5 ± 0.120	38.0 ± 0.030	67.1 ± 0.086	19.9 ± 0.001	15.1 ± 0.313
312.5	101.6 ± 0.022	21.0 ± 0.001	71.1 ± 0.156	35.3 ± 0.044	61.5 ± 0.112	92.0 ± 0.141	19.4 ± 0.004	26.8 ± 0.245
156.25	101.8 ± 0.284	21.3 ± 0.013	110.9 ± 0.063	103.1 ± 0.202	104.2 ± 0.026	119.7 ± 0.182	20.1 ± 0.003	102.6 ± 0.632
78.125	108.4 ± 0.084	27.7 ± 0.026	121.5 ± 0.183	113.1 ± 0.171	109.2 ± 0.084	120.2 ± 0.150	28.0 ± 0.015	113.0 ± 0.334
39.0625	129.1 ± 0.038	31.8 ± 0.009	132.0 ± 0.136	132.7 ± 0.231	129.1 ± 0.033	122.6 ± 0.121	81.0 ± 0.009	116.8 ± 0.277
19.53125	124.4 ± 0.079	83.2 ± 0.022	140.3 ± 0.197	133.2 ± 0.116	123.4 ± 0.070	127.7 ± 0.180	96.4 ± 0.003	129.7 ± 0.299
9.765625	132.9 ± 0.132	102.6 ± 0.015	135.4 ± 0.066	146.0 ± 0.065	131.6 ± 0.132	132.2 ± 0.214	98.2 ± 0.023	130.2 ± 0.226
4.8828125	150.0 ± 0.171	104.9 ± 0.016	149.3 ± 0.082	133.8 ± 0.227	147.1 ± 0.051	149.7 ± 0.082	105.3 ± 0.032	145.8 ± 0.072

Table 3: Preliminary screening of the cytotoxic efficacy of the synthesized chalcone-thienopyrimidine derivatives 3a-g against human liver cancer cell line (HepG2) compared to DMSO. The cytotoxic efficacy of the compounds is expressed as the mean of survival percentage ± SEM.

Compound concentration (μg/ml)	**3a**	**3b**	**3c**	**3d**	**3e**	**3f**	**3g**	*DMSO*
10000	18.5 ± 0.001	12.1 ± 0.002	18.0 ± 0.001	18.4 ± 0.002	14.1 ± 0.002	10.7 ± 0.004	12.3 ± 0.002	10.6 ± 0.018
5000	19.1 ± 0.001	12.1 ± 0.001	18.8 ± 0.001	18.5 ± 0.003	16.8 ± 0.003	11.6 ± 0.002	12.5 ± 0.001	11.2 ± 0.001
2500	19.5 ± 0.001	12.2 ± 0.001	19.0 ± 0.002	19.4 ± 0.004	17.4 ± 0.002	11.7 ± 0.009	12.7 ± 0.002	11.6 ± 0.028
1250	20.5 ± 0.004	12.7 ± 0.002	20.1 ± 0.004	19.5 ± 0.001	18.4 ± 0.003	12.6 ± 0.019	12.5 ± 0.001	14.4 ± 0.028
625	21.7 ± 0.012	12.9 ± 0.006	20.6 ± 0.003	20.0 ± 0.001	18.9 ± 0.001	15.3 ± 0.005	13.0 ± 0.003	14.4 ± 0.061
312.5	28.4 ± 0.009	13.3 ± 0.004	21.1 ± 0.004	20.5 ± 0.002	19.8 ± 0.005	77.8 ± 0.071	14.1 ± 0.002	44.4 ± 0.012
156.25	40.1 ± 0.021	16.2 ± 0.004	22.1 ± 0.011	20.5 ± 0.002	21.1± 0.012	112.0 ± 0.460	14.5 ± 0.003	103.6 ± 0.051
78.125	66.9 ± 0.018	17.3 ± 0.007	62.4 ± 0.051	31.0 ± 0.017	21.4 ± 0.073	115.9 ± 0.157	17.5 ± 0.002	109.4 ± 0.040
39.0625	73.8 ± 0.019	18.4 ± 0.006	63.0 ± 0.030	91.2 ± 0.138	45.1 ± 0.072	119.1 ± 0.122	64.1 ± 0.038	113.6 ± 0.052
19.53125	74.2 ± 0.012	23.2 ± 0.012	69.8 ± 0.027	99.2 ± 0.026	91.9 ± 0.060	144.7 ± 0.140	97.8 ± 0.053	118 ± 0.045
9.765625	87.8 ± 0.087	67.9 ± 0.048	81.6 ± 0.027	111.0 ± 0.041	114.3 ± 0.141	149.1 ± 0.106	115.9 ± 0.098	174.4 ± 0.129
4.8828125	103.5 ± 0.033	110.1 ± 0.046	91.5 ± 0.013	123.0 ± 0.026	127.5 ± 0.033	149.7 ± 0.200	131.3 ± 0.033	183.0 ± 0.078

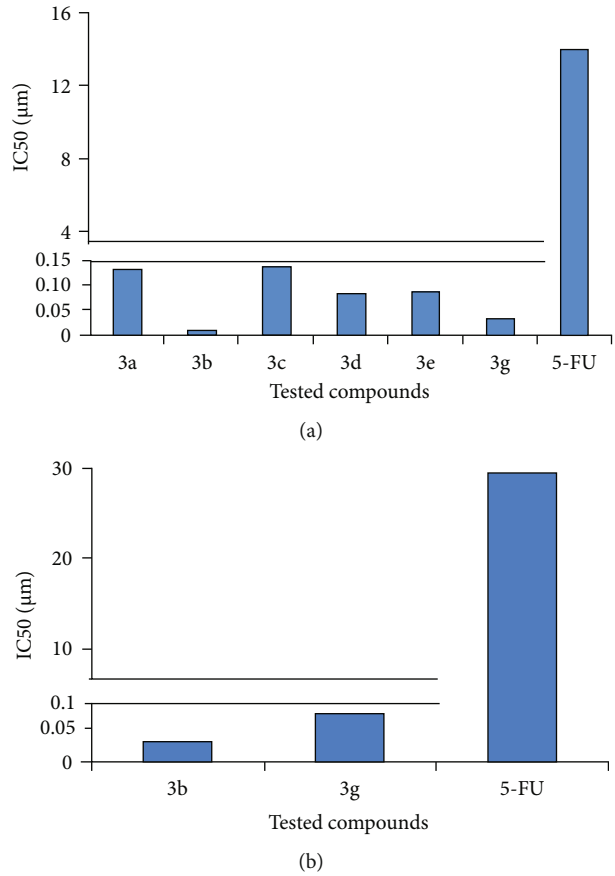

Figure 3: Cytotoxicity for some newly synthesized thienopyrimidine derivatives **3a-g** against (a) HepG2 and (b) MCF-7 cancer cell lines in comparison to the traditional anticancer drug 5-FU. IC_{50} of triplicates was expressed as μM.

levels of caspase-3 in comparison to control ($P < 0.05$). However, all tested compounds except **3c** revealed a marked increase in the expression levels of Bax. Furthermore, the expression levels of caspase-9 were significantly elevated with all tested compounds except **3e**. On the other side, the expression levels of Bcl-2 were noticeably decreased with **3a**, **3d**, and **3g** in comparison with untreated control cells ($P < 0.05$), while expression levels of Bcl-2 were insignificantly decreased with the other compounds ($P > 0.05$). Therefore, all tested compounds except **3c** had been shown to produce significant altitude in the Bax/Bcl-2 ratio ($P < 0.05$) in comparison to control, which supported their ability to promote the apoptotic response in HepG2 cells (Figure 8(a)).

Remarkably, in the MCF-7 cell line, the two compound chalcone-thienopyrimidine derivatives **3b** and **3g** showed significant elevation of the expression levels of the key genes of apoptosis (Bax, caspase-3, and caspase-9) and a remarkable decrease in the expression levels of Bcl-2 in relation to the control ($P < 0.05$). Therefore, Bax/Bcl-2 ratios were strikingly elevated with both **3b** and **3g** (Figure 8(b)).

3.13. Correlation between Cytotoxic Efficacy of the Compounds and Apoptosis. As shown in Figure 9, there was a positive correlation between cytotoxic efficacy of the compounds and apoptosis in both HepG2 ($R^2 = 0.531$; $P = 0.001$; Figure 9(a)) and MCF-7 ($R^2 = 0.219$; $P = 0.349$; Figure 9(b)) cell lines.

3.14. Molecular Docking. Recently, several small molecules (1 and 2) were reported as Bcl-2 inhibitors [35, 44] (Figure 10). The ability of these molecules to inhibit the antiapoptotic Bcl-2 protein was associated with the sensitization of cancer cells to apoptosis [35]. The mechanism of action of these inhibitors was dependent on their binding to the binding groove in Bcl-2 which resulted in the inhibition of the anti-apoptotic effect of Bcl-2.

In the current study, compounds **3a-g** induced apoptosis and repressed Bcl-2 gene expression in HepG2 and/or MCF-7. To investigate the ability of these compounds to bind to and inhibit Bcl-2, a comparative molecular docking study was performed. The aim of this study was to assess the potential binding affinities, modes, and interactions of the new compounds against those of a selective Bcl-2 inhibitor [35]. The crystal structure of Bcl-2/Bcl-xL bound to the DRO inhibitor (pdb: 2W3L) [26] was used in this study (Figure 11(a)). The binding mode of DRO into Bcl-2 was also illustrated (Figure 11(b)). Investigation of the inhibitory activity of DRO against Bcl-2 revealed IC_{50} values of 0.03 and 0.10 μM against Bcl-2 16me and Bcl-2 26me, respectively [35]. Accordingly, DRO was used as a reference drug in this study.

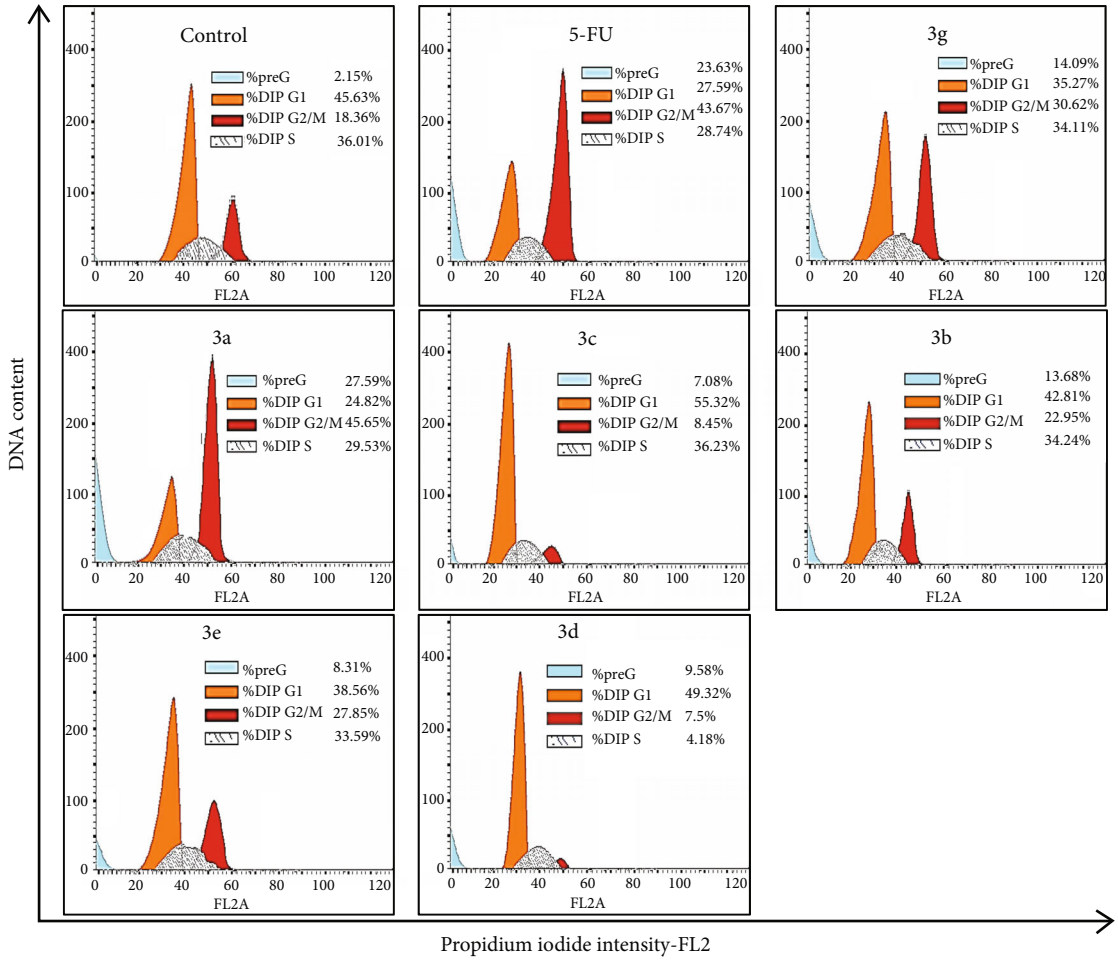

FIGURE 4: Effect of six tested compounds (**3g**, **3a**, **3c**, **3b**, **3d**, and **3e**) on cell proliferation and cell cycle phases of HepG2. (a) Change in the cell cycle of untreated (cont.), 5-fluorouracil (5-FU), and treated HepG2 was analyzed using a flow cytometer. (b) The percentage of the cell population in the phases of the HepG2 cell cycle. Data were expressed for each bar as mean ± standard error of mean. $^{*}P < 0.05$ from control, $^{\#}P < 0.05$ from 5FU.

Validation of the docking study was initially performed, where DRO was redocked into Bcl-2 using AutoDock 4.2 [34]. The results of this validation revealed a binding free energy (ΔG_b) of -9.67 kcal/mol for the best fitting conformation of DRO. Investigation of the binding mode of DRO revealed superposition with the cocrystallized ligand with RMSD of 0.79 Å (Figure 11(c)). Analysis of the binding interactions of DRO revealed one carbon-hydrogen bond and one electrostatic (pi-anion) interaction with Asp70. In addition, multiple hydrophobic (pi-sigma/alkyl, pi-pi T-

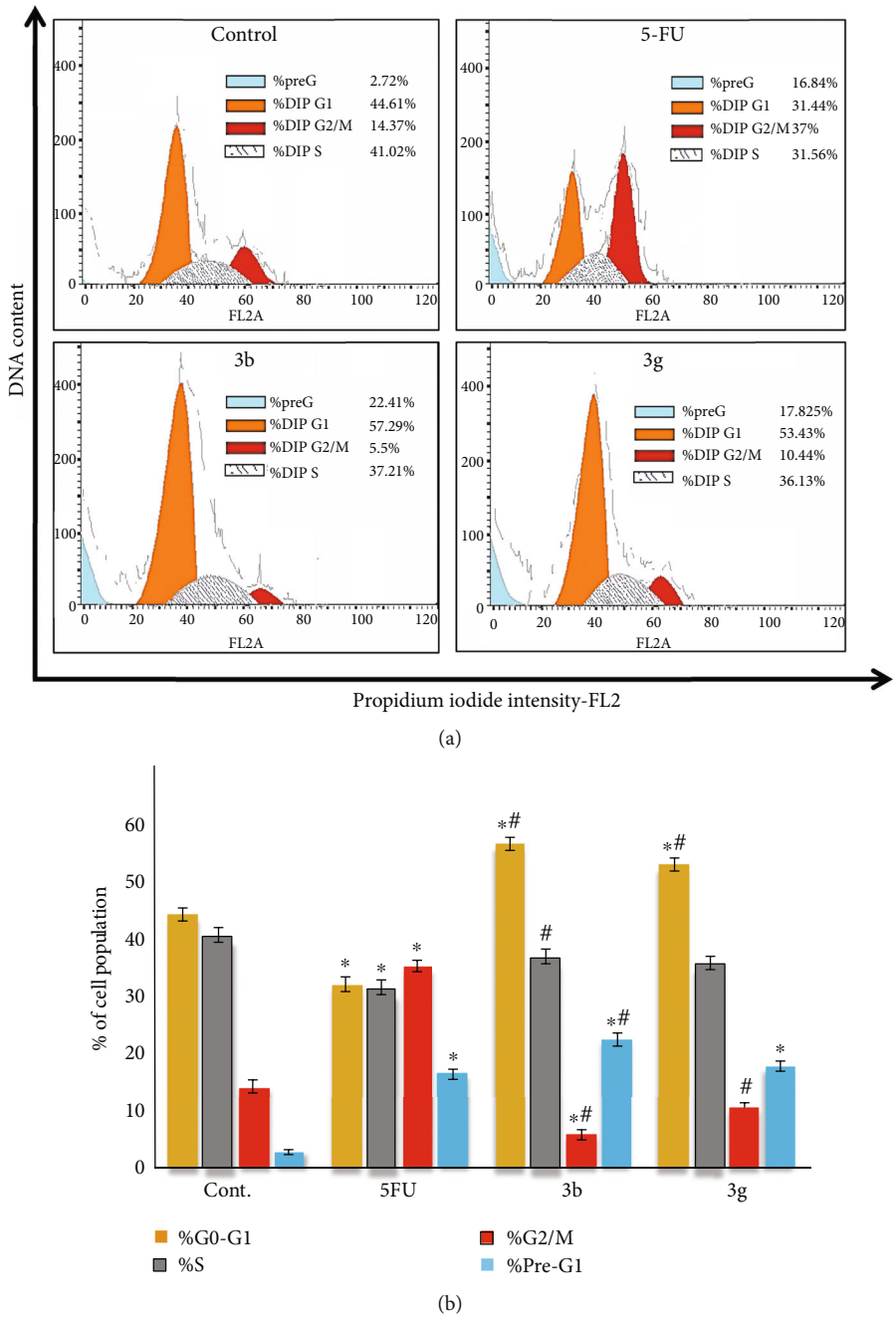

Figure 5: Effect of two tested compounds (**3b** and **3g**) on cell proliferation and cell cycle phases of MCF-7. (a) Change in the cell cycle of untreated (cont.), 5-fluorouracil (5-FU), and treated MCF-7 was analyzed using a flow cytometer. (b) The percentage of the cell population in the phases of the MCF-7 cell cycle. Data were expressed for each bar as mean ± standard error of mean. $^{*}P < 0.05$ from control, $^{\#}P < 0.05$ from 5FU.

shaped, and alkyl) interactions were also observed between DRO and amino acids into Bcl-2.

Compounds **3a-g** were also docked into the active site of Bcl-2. The results revealed binding free energies in the range of -5.73 to -7.57 kcal/mol, where **3g** exhibited the highest affinity toward Bcl-2. In addition to the multiple hydrophobic interactions, the new compounds **3a-g** also showed 1-5 hydrogen bonds of the conventional/carbon types with amino acids in Bcl-2 (Table 4).

Among the new compounds, **3a** displayed a binding free energy of (ΔG_b) of -5.94 kcal/mol toward Bcl-2 compared to -9.67 kcal/mol for DRO. Analysis of the best fitting conformation of **3a** revealed partial superposition of the thieno[2,3-*d*]pyrimidine moiety with the tetrahydroisoquinoline moiety in DRO. Investigation of the binding interaction of **3a** revealed one conventional hydrogen bond with Ala108, one carbon hydrogen bonds with Leu96, and one pi-donor bond with Arg105. Like DRO, compound **3a**

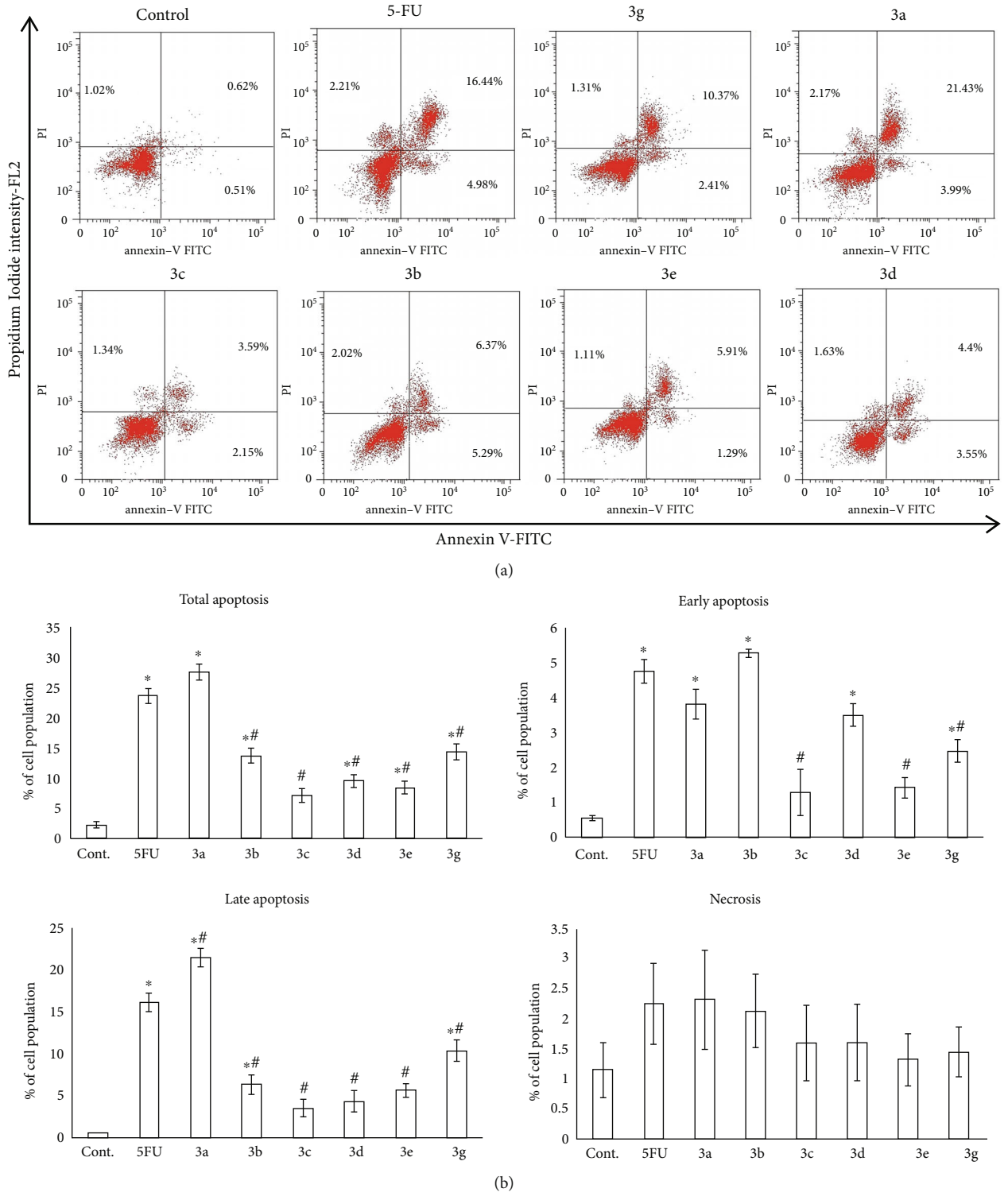

FIGURE 6: Evaluation of apoptosis in HepG2 cells treated with the six tested compounds (**3g**, **3a**, **3c**, **3b**, **3e**, and **3d**). (a) Apoptosis was analyzed using Annexin V-FITC/PI staining and flow cytometry. The right lower quadrant demonstrates early apoptotic cells, and the right upper quadrant demonstrates late apoptotic cells. (b) The bar graph showed quantification of the percentage of early and late apoptotic HepG2 cells. Data were expressed for each bar as mean ± standard error of mean. $^{*}P < 0.05$ from control, $^{\#}P < 0.05$ from 5FU.

exhibited similar hydrophobic interaction with Tyr67, Met74, and Val92 (Figure 12).

Compound **3b** also displayed a binding free energy of -5.73 kcal/mol toward Bcl-2. Analysis of the best fitting conformation of **3b** revealed superposition of the pyrimidine ring with the pyrazole ring in DRO, where the ethyl ester moiety in **3b** occupied the position of one of the two phenyl rings of the diphenylamine moiety in DRO. The trimethoxyphenyl moiety

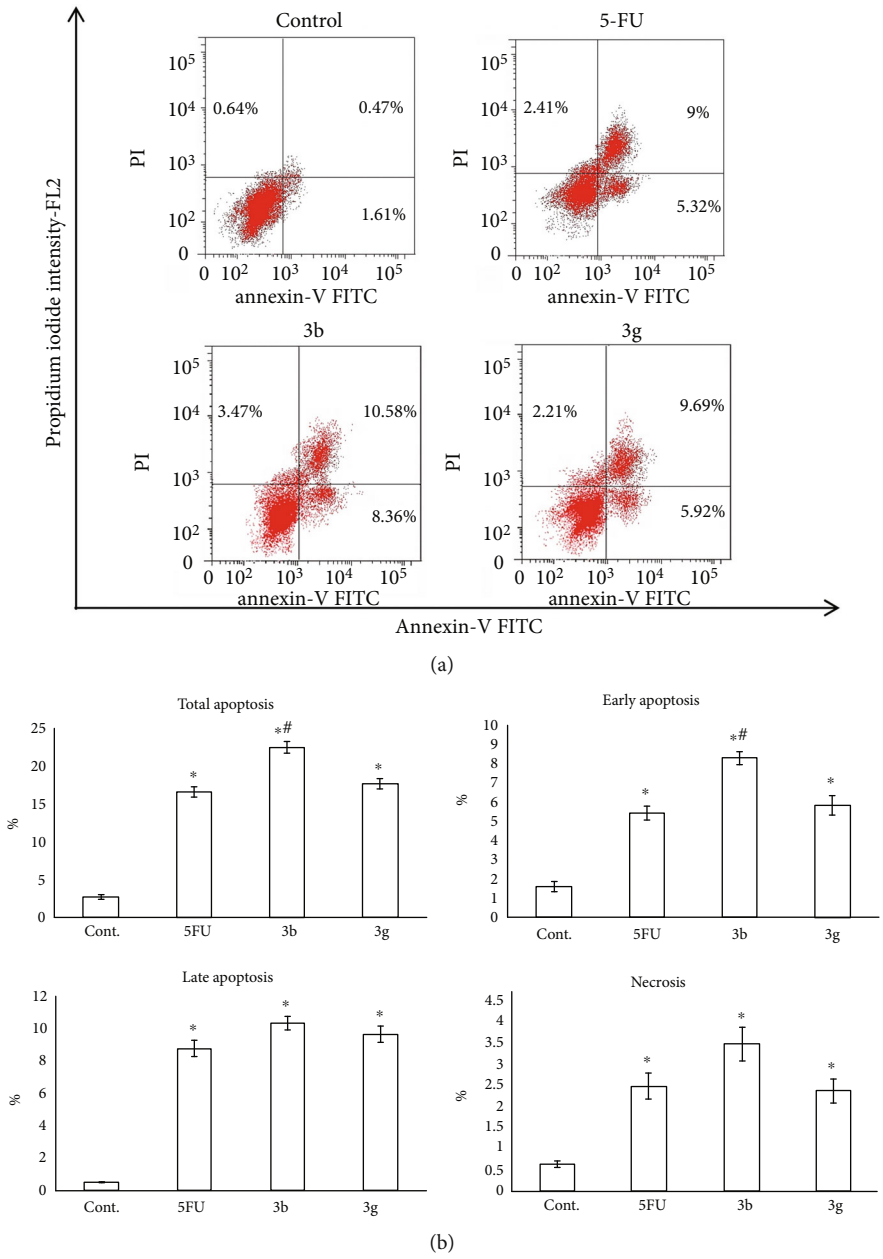

Figure 7: Evaluation of apoptosis in the MCF-7 cell line treated with the six tested compounds (**3b** and **3g**). (a) Apoptosis was analyzed using Annexin V-FITC/PI staining and flow cytometry. The right lower quadrant demonstrates early apoptotic cells, and the right upper quadrant demonstrates late apoptotic cells. (b) The bar graph showed quantification of the percentage of the early and late apoptotic MCF-7 cell line. Data were expressed for each bar as mean ± standard error of mean. $^{*}P < 0.05$ from control, $^{\#}P < 0.05$ from 5FU.

in **3b** is also superposed with the tetrahydroisoquinoline in DRO (Figure 13).

Like DRO, compound **3b** exhibited one electrostatic interaction with Asp70. The two compounds also exhibited similar hydrophobic interactions with the same amino acids (Phe63, Phe71, Leu96, and Ala108). In addition, **3b** showed two additional conventional hydrogen Asn102 and Arg105 (Figure 13). Moreover, compound **3g** showed different types of interactions with amino acids in Bcl-2 (Figure 14).

The 2/3D binding modes and interactions of the remaining compounds (**3c-f**) are provided in the supplementary data (Figures S1–S4).

In conclusion, the results of the docking analysis revealed a relatively moderate binding affinity of the seven compounds toward the antiapoptotic protein, Bcl-2. Among these derivatives, **3g** showed the highest binding free energy. The new compounds also exhibit different types of binding interaction including hydrogen bonds and electrostatic and hydrophobic interactions.

3.15. ADME Study. The physicochemical properties related to drug-likeness of compounds **3a-g** were calculated using SwissADME (http://www.swissadme.ch/) [45] and Molsoft L.L.C (http://molsoft.com/mprop/). This study was aimed

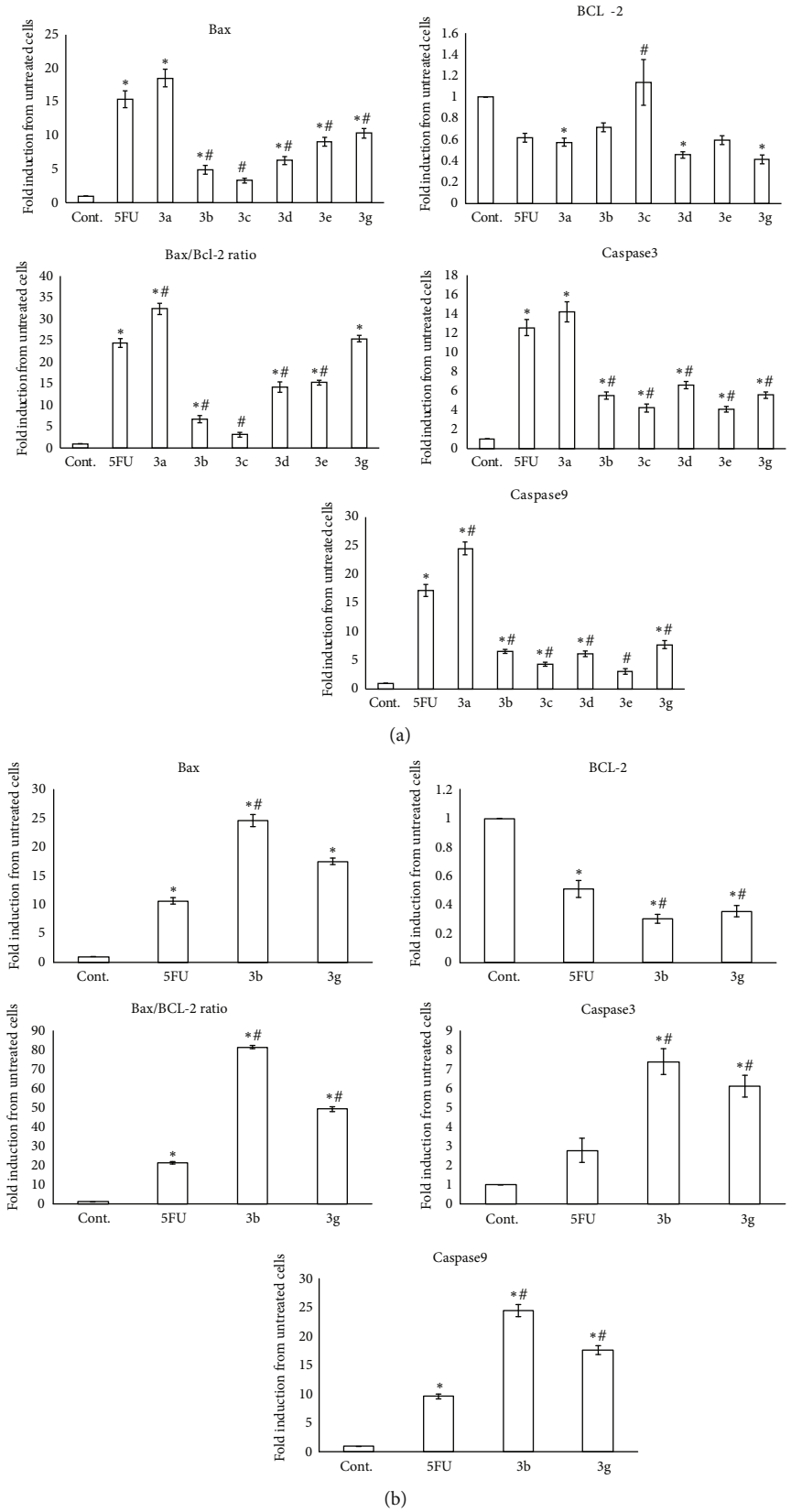

FIGURE 8: Effect of newly synthesized chalcone-thienopyrimidine derivatives **3a-e** and **3g** (IC_{50}) (a) and the newly synthesized chalcone-thienopyrimidine derivatives **3b** and **3g** (IC_{50}) (b) on the gene expression of Bcl-2, Bax, Bax/Bcl-2 ratio, caspase-3, and caspase-9 in HepG2 (a) and MCF-7 (b) cell lines after 8-hour incubation. Data were expressed for each bar as mean ± standard error of mean. $^{*}P < 0.05$ from control, $^{\#}P < 0.05$ from 5FU.

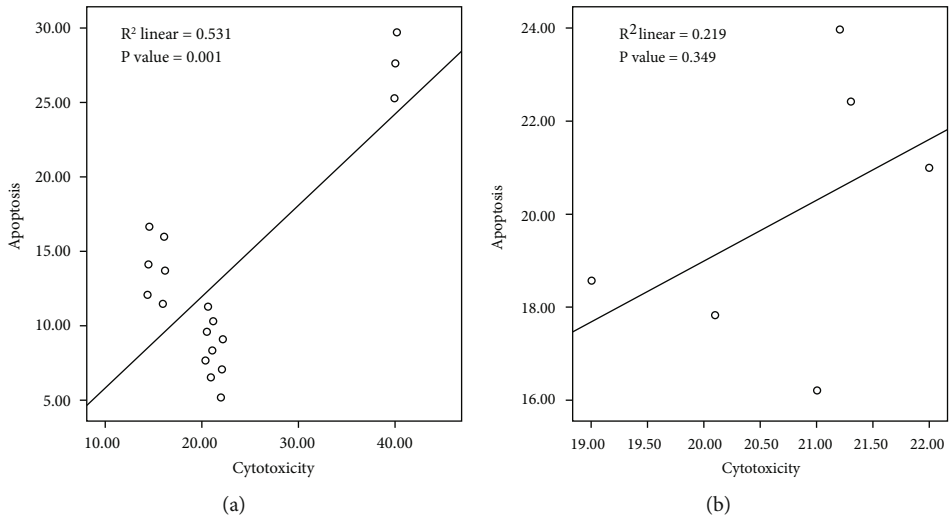

Figure 9: Correlation of cytotoxic efficacy of the compounds vs. apoptosis in HepG2 (a) and MCF-7 (b) cell lines.

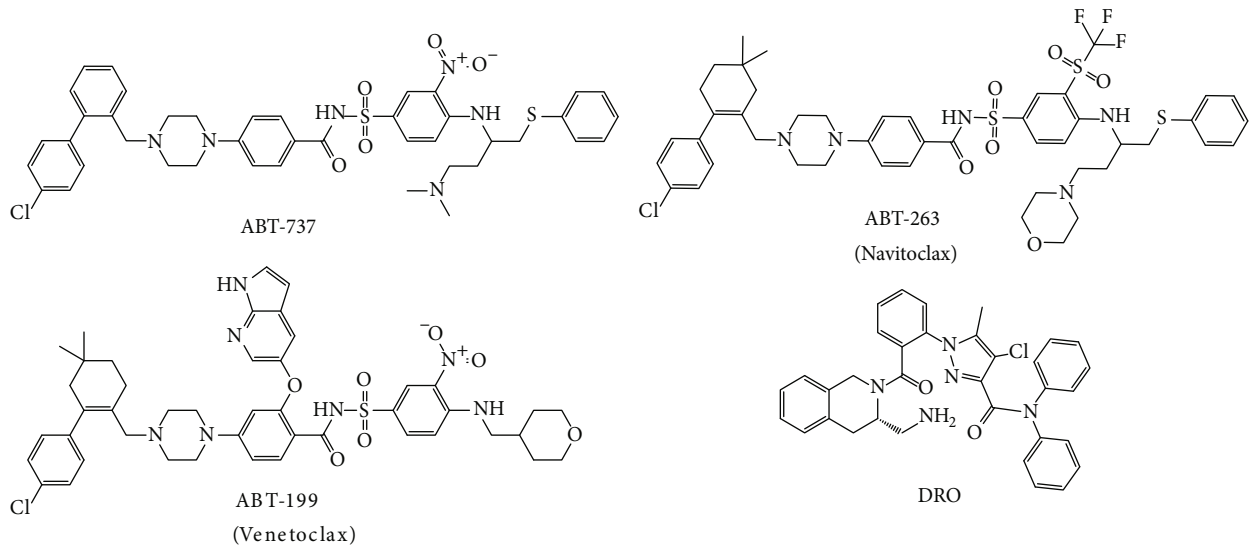

Figure 10: Chemical structure of Bcl-2 inhibitors.

at evaluating the physicochemical properties of the new compounds against those of the selective Bcl-2 inhibitor DRO and the FDA-approved Bcl-2 inhibitor venetoclax. The results are presented in Table 5. The detailed results of the ADME study are provided in Supplementary 4 (Tables S1–S18).

The results of the ADME study revealed that hits **3a-g** have molecular weights (MWs) in the range of 645.68-750.84 Daltons, compared to DRO (MW = 576.09 Da) or venetoclax (MW = 868.44 Da). In addition, many of the small-molecule Bcl-2 inhibitors showed also molecular weights > 500 [46].

The designed compounds also showed lower MVs in the range of 650.41-764.06 $Å^3$, which lay in between those of DRO (559.71 $Å^3$) and venetoclax (854.36 $Å^3$).

Compounds **3a-g** displayed calculated logP (mlogP) values in the range of 1.15-2.95, which was either equal to or lower than the mlogP value of venetoclax (2.95). These results also indicate that all the new compounds (**3a-g**) have lower lipophilicity than DRO (4.76).

The new compounds have a total number of 13-18 rotatable bonds compared to 14 for venetoclax. The new compounds also have 8-11 hydrogen bond acceptor (H_A) compared to 9 for venetoclax, while the hydrogen bond donors (H_D) in the new compounds were less than venetoclax.

Considering the rule of five of Lipinski which stated that the orally active drug should have no more than one violation from this rule [47]. The results in Table 5 showed that all the new compounds have two violations like DRO and venetoclax.

The physicochemical properties related to bioavailability and drug-likeness scores (DLSs) were also calculated for compounds **3a-g**. The results are presented in Table 6.

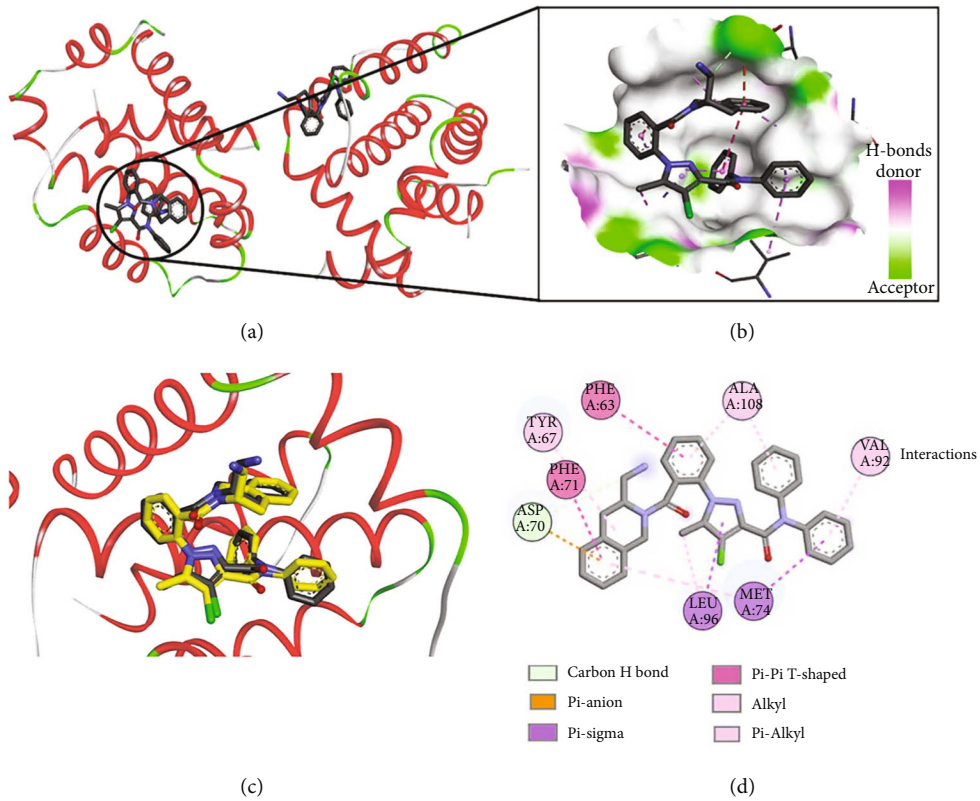

FIGURE 11: Binding mode/interactions of DRO (shown as sticks colored by element) into Bcl-2/Bcl-xL (pdb: 2W3L): (a) Bcl-2/Bcl-xL showing the binding site of DRO; (b) 3D binding mode of DRO into Bcl-2, a receptor shown as the H-bond surface; (c) 3D binding mode of the redocked DRO overlaid with the cocrystallized ligand (yellow sticks) into the active site of Bcl2; (d) 2D binding mode of the cocrystallized DRO showing different types of interactions with amino acids in Bcl2.

TABLE 4: Docking results of **3a-g** into Bcl-2 in comparison to its cocrystallized ligand (DRO).

Ligand	ΔG_b [a]	K_i [b]	HBs[c]	Amino acids involved in the hydrogen bonds
3a	-5.94	44.57 μM	3	Leu96*, Arg105*, Ala108
3b	-5.73	62.76 μM	2	Asn102 and Arg105
3c	-6.27	25.48 μM	2	Asn102, Arg105
3d	-6.47	18.18 μM	4	Asp70*, Glu73*, Arg88, Glu95
3e	-7.39	3.86 μM	5	Met74*, Gly77*, Leu87*, Arg88*, Val92*
3f	-7.41	3.71 μM	1	Arg105
3g	-7.57	2.85 μM	2	Asp99, Asn102
DRO	-9.67	81.01 nM	1	Asp70*

[a]Binding free energy (kcal/mol). [b]Inhibition constant. [c]Number of hydrogen bonds. *Amino acids indicated by the asterisk are involved in carbon hydrogen bonds with the ligands.

The new compounds **3a-g** showed that log *S* values are in the range of -5.64 to -6.99 compared to DRO (-7.14) and venetoclax (-9.78). They also showed TPSAs in the range of 175.76-236.26 Å^2 compared to 183.09 for venetoclax (Table 6).

All the new compounds exhibited a similar bioavailability score of 0.17, which was equal to that of venetoclax. The fraction of the new compounds that could be absorbed from the GIT was calculated according to the previous method [47]. The calculated fractions of the new compounds **3a-g** that could be absorbed from GIT were in the range of 27.49%-48.36% compared to 45.83% for venetoclax (Table 6).

The results of the ADME study revealed that the drug-likeness scores (DLSs) are in the range of 0.17-1.68 for compounds **3a-g** compared to DRO (0.38) and venetoclax (0.57). These results also indicate that compounds **3a-g** have DLSs higher than those of DRO and venetoclax (Table 6).

3.16. Oxidant/Antioxidant Status in HepG2 Cells and MCF-7 Cells. All tested compounds induced a significant increase ($P < 0.05$) in the MDA levels together with a marked

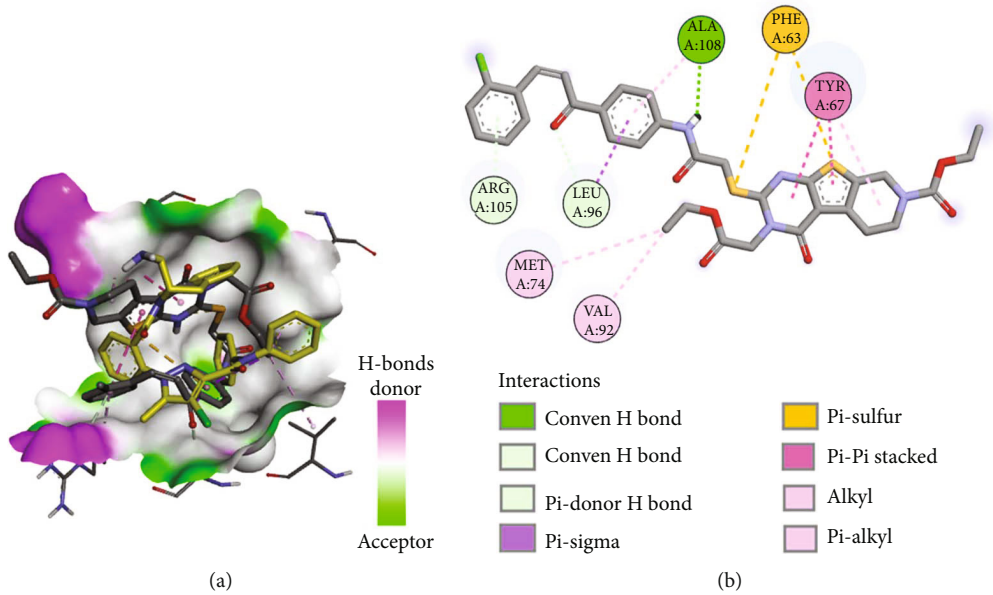

FIGURE 12: Binding mode/interactions of **3a** (shown as sticks colored by element) in Bcl-2: (a) 3D binding mode of **3a** overlaid with the cocrystallized DRO (yellow sticks) into the active site of Bcl-2; (b) 2D binding mode of **3a** showing the hydrogen bonds and electrostatic and hydrophobic interactions with amino acids in Bcl-2.

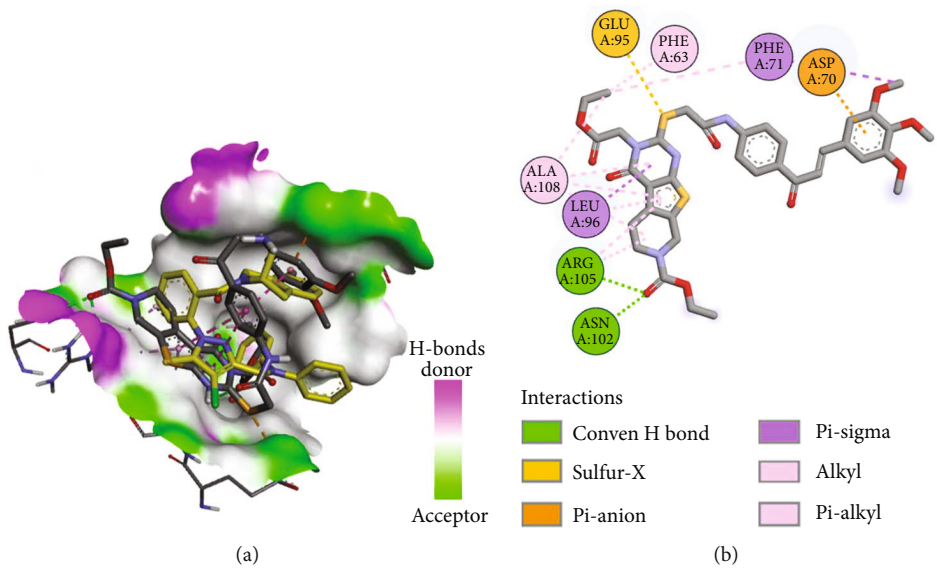

FIGURE 13: Binding mode/interactions of **3b** (shown as sticks colored by element) in Bcl-2: (a) 3D binding mode of **3b** overlaid with the cocrystallized DRO (yellow sticks) into the active site of Bcl-2; (b) 2D binding mode of **3b** showing the hydrogen bonds and electrostatic and hydrophobic interactions with amino acids in Bcl-2.

reduction of GR activity in the HepG2 cell line compared to control cells (Figure 15(a)).

Similarly, significant elevation of MDA along with a significant decline of GR activity was noticed in MCF-7 cells exposed to **3b** and **3g** compounds in comparison to untreated cells ($P < 0.05$) (Figure 15(b)).

4. Discussion

As a step to progress in the field of medicine, several trials were made to join many biological activities with different moieties to develop novel compounds that have powerful anticancer effects [48]. Therefore, we synthesized novel chalcone-thienopyrimidine conjugates to develop efficient anticancer candidates. In our manuscript, we used 5-flurouracil as a standard anticancer chemotherapeutic reference which has been used in several studies dealing with the assay of the anticancer activities of thienopyrimidine [49] and other substituted pyrimidine derivatives [50]. Selection of 5-flurouracil is based on its mechanism of action that has been attributed to apoptosis induction in cancer cells [51].

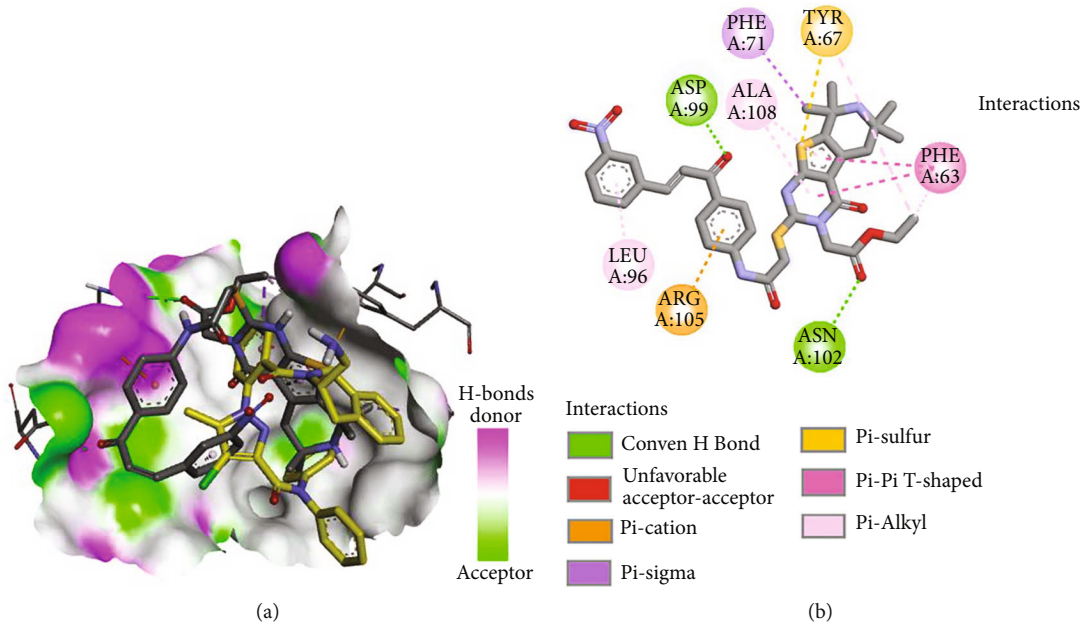

Figure 14: Binding mode/interactions of **3g** (shown as sticks colored by element) in Bcl-2: (a) 3D binding mode of **3g** overlaid with the cocrystallized Pro (yellow sticks) into the active site of Bcl-2; (b) 2D binding mode of **3g** showing different types of interactions with amino acids in Bcl-2.

Table 5: Physicochemical properties and DLSs of compounds **3a-g**, DRO, and venetoclax.

Comp.	Physicochemical properties						Lipinski's rule	
	MW	MV	mlogP	NorO	H_A	H_D	Obey	Comments
3a	695.20	683.62	2.95	15	8	1	No	2 violations: MW > 500, NorO > 10
3b	750.84	764.06	1.59	18	11	1	No	2 violations: MW > 500, NorO > 10
3c	705.76	694.58	1.74	16	10	1	No	2 violations: MW > 500, NorO > 10
3d	690.76	720.46	1.15	16	10	1	No	2 violations: MW > 500, NorO > 10
3e	664.75	672.18	1.61	14	9	2	No	2 violations: MW > 500, NorO > 10
3f	645.68	650.41	1.55	14	9	1	No	2 violations: MW > 500, NorO > 10
3g	689.80	692.96	1.85	13	9	2	No	2 violations: MW > 500, NorO > 10
DRO	576.09	559.71	4.76	8	4	1	No	2 violations: MW > 500, mlogP > 4.15
LBM	868.44	854.36	2.95	14	9	3	No	2 violations: MW > 500, NorO > 10

MW: molecular weight (Da); MV: molecular volume ($Å^3$); mlogP: logP calculated using the topological method implemented from Moriguchi et al. [86]; NorO: number of rotatable bonds; LBM: venetoclax.

The disturbance in the balance between cell death and cell division is the main eliciting factor of cancer. Apoptosis, autophagy, and necrosis are variant processes that develop cell death. Apoptosis is the physiological pathway through it, and programmed cell death occurs. Any disturbance in the process of apoptosis usually develops cancer. Thus, most of anticancer therapies were found to act mechanistically *via* induction of apoptosis [52].

During apoptosis, different biochemical markers were produced in a sequential manner. These markers include phosphatidylserine externalization, the release of proapoptotic proteins, and caspase activation. To elucidate the mechanism by which these compounds exert their anticancer activities *in vitro*, different assays were performed including MTT, cell cycle analysis, apoptosis, and molecular expressions of antiapoptotic protein Bcl-2 as well as the proapoptotic Bax, caspase-3, caspase-9, and oxidant/antioxidant markers.

The MTT assay was performed to assess the viability of cells when subjected *in vitro* to the novel chalcone-thienopyrimidine derivatives. The current results showed that only **3b** and **3g** compounds at their IC_{50} values (Figure 3(b)) exhibited promising antiproliferative potential against MCF-7 cells. On the other side, the IC_{50} of the six compounds (**3a**, **3b**, **3c**, **3d**, **3e**, and **3g**) provoked marked cytotoxic effects against the HepG2 cell line compared to 5-FU, which is one of the well-known anticancer agents (Figure 3(a)). The compound **3f** had the lowest cytotoxic

Table 6: Physicochemical properties and DLSs of compounds **3a-g**, DRO, and venetoclax.

Comp.	Log *S*	Solubility	TPSA	%Abs	BS	DLS
3a	-6.99	7.05*e* – 05 mg/ml	190.44	43.30	0.17	1.01
3b	-6.66	1.66*e* – 04 mg/ml	218.13	33.75	0.17	1.35
3c	-6.48	2.36*e* – 04 mg/ml	236.26	27.49	0.17	0.81
3d	-5.82	1.06*e* – 03 mg/ml	175.76	48.36	0.17	1.42
3e	-6.13	4.95*e* – 04 mg/ml	202.69	39.07	0.17	1.68
3f	-5.64	1.48*e* – 03 mg/ml	193.89	42.11	0.17	0.82
3g	-6.90	8.63*e* – 05 mg/ml	218.75	33.53	0.17	0.17
DRO	-7.14	4.20*e* – 05 mg/ml	84.46	79.86	0.17	0.38
LBM	-9.78	1.44*e* – 07 mg/ml	183.09	45.83	0.17	0.57

Log *S*: 10-based logarithm of the solubility; TPSA: topological polar surface area (Å^2); %Abs: % absorbed orally, %Abs = 109$^-$ (0.345 × TPSA); BS: bioavailability score; LBM: venetoclax. DLSs were calculated using Molsoft (http://molsoft.com/mprop).

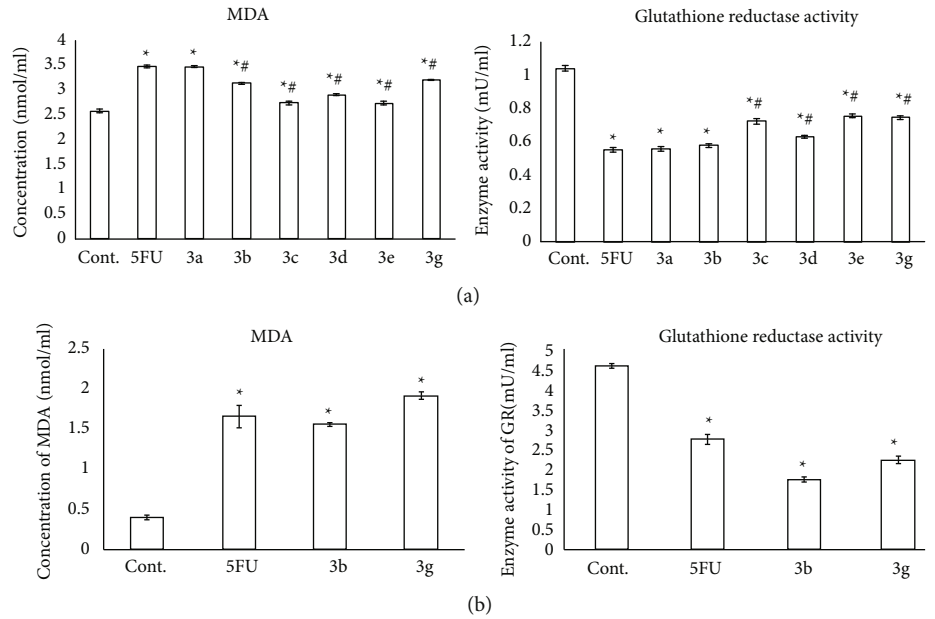

Figure 15: Determination of MDA and GR activity after treatment of the HepG2 cell line (a) with IC50 of some newly synthesized chalcone-thienopyrimidines (3**a**, 3**b**, 3**c**, 3**d**, 3**e**, and 3**g**) and the MCF-7 cell line (b) with IC50 of some newly synthesized chalcone-thienopyrimidine (3**a** and 3**g**) derivatives in comparison to the traditional anticancer drug 5-FU. Data were expressed for each bar as mean ± standard error of mean. $^*P \leq 0.05$ from control, $^\#P \leq 0.05$ from 5FU.

activity against HepG2 and MCF-7 cell lines. The potent compounds were considered for further mechanistic studies of apoptosis and oxidative stress.

The discrepancies in the IC_{50} values might be ascribable to several issues such as the structure and functionality of the ring system and the genetic and biochemical background of the cell lines. The obvious potency of **3b** and **3g** compounds as promising anticancer agents against HepG2 and MCF-7 cell lines was attributed to the presence of 3-methoxy-donating function groups on chalcone moiety that exhibited remarkable anticancer activity (~2.5 times more activity) compared to compound **3g** containing an electron-withdrawing function group (NO_2) on chalcone moiety.

Several reports addressed the *in vitro* potency of numerous synthesized chalcones against cancers of different organs including the lung, colon, and breast [53]. Bagul et al. [54] found that chalcone-linked pyrazoloij1,5-a] pyrimidine hybrids induced antiproliferative actions when incubated *in vitro* with MDA-MB-231 (breast cancer), -549 (lung cancer), and DU-145 (prostate cancer) cells and that the results were comparable with the used reference treatment (erlotinib). Moreover, thiopyrimidines were studied against leukemia and colon and breast cell lines, and the results indicated promising antitumor activities [55]. In addition, some novel morpholinylchalcone (the building blocks for the formation of a series of pyridopyrimidinethiones and pyrido[2,3-d][1,2,4]triazolo[4,3-a]pyrimidin-5(1H)-ones) synthesized

compounds were observed to induce significant anticancer actions equivalent to the standard treatment cisplatin when applied *in vitro* against A-549 and HepG-2 cells [56]. Further, many synthesized 2-thiopyrimidine/chalcone derivatives have been noticed to have remarkable antitumor effects against various cancer cell lines including MCF-7 [11].

Cell cycle analysis of the tested novel compounds was evaluated to elucidate the molecular mechanism of antiproliferation induction in HepG2 and MCF-7 cell lines. Analysis of the cell cycle that was accomplished by propidium iodide (PI) staining in Figure 4 showed arresting of the cell cycle of the HepG2 cell line at different phases by application of the newly synthesized six tested compounds **3a**-**e** and **3g**. In this regard, the arrest in G2/M was observed with compounds **3a**, **3e**, and **3g**, while the arrest in pre-G1 phases was accompanied by compounds **3a**, **3b**, **3d**, **3e**, and **3g**. Worthwhile, compound **3c** induced a significant increase in the G1 phase cell population up to 55.32%. However, compound **3d** induced a significant increase in the S phase cell population. On the other side, in the MCF-7 cell line, compounds **3b** and **3g** significantly induced G1 and pre-G1 arrest (Figure 5). A similar data was achieved when some benzimidazole-chalcone derivatives were applied in MCF-7 cell lines [57] and thyroid carcinoma (BHT-101) cells treated with 50 μM curcumin [58]. The antimitotic action of chalcones *via* arresting the cell proliferation at G2/M was first documented almost 20 years ago [59].

The results of quantitative estimation of apoptosis given by Annexin V-FITC/PI staining with flow cytometry (Figures 6 and 7) revealed that the HepG2 cell line treated with all tested compounds except **3c** showed a significant induction of total apoptosis when compared to control ($P < 0.05$). The compounds **3a**, **3b**, and **3g** significantly exhibited early and late apoptosis. Moreover, none of the tested compounds displayed a necrotic effect compared to the control ($P > 0.05$) (Figure 6). The treatment of MCF-7 cells with compounds **3a** and **3b** showed a significant increase in the total, early, and late apoptosis as well as necrosis in comparison to untreated cells ($P < 0.05$) together with enhancing the phosphatidylserine (Annexin V-positive cells) translocation. In line with these observations, some chalcone analogs showed a significantly higher percentage of apoptotic cells in HepG2 [60] and MCF-7 cells [61] than in the control cells. Takac et al. [62] reported that chalcones halted the proliferation of cancer cells *via* arresting the cell cycle. These anticancer activities of chalcone analogs might be attributed to the identity in the structure of these compounds with 5-FU as the thiopyrimidine ring in these compounds is an analogue to the pyrimidine ring in 5-FU. In this concern, 5-FU was found to inhibit thymidylate synthase, preventing DNA synthesis and inducing apoptosis [63]. Thus, the apoptotic changes that were observed in the cells of the present study might be attributed to the inhibition of DNA synthesis and the subsequent cell cycle arrest.

Apoptosis refers to the physiological mechanism that involves many signaling pathways, provoked by different stimuli primarily oxidative stress [64]. Apoptosis is induced intrinsically when the subclasses of the Bcl-2 protein family interact with the outer mitochondrial membrane. BH3 (Bcl-2 homology 3) proteins are the provoking key of apoptotic signals [65]. BH3 proteins are activated by cytotoxic stress which causes alterations in the permeability of mitochondrial membrane *via* stimulation of Bax and BAK that results in the liberation of cytochrome c (apoptogenic compound) [66]. Cytochrome c is the main activator of caspase-9 which in turn leads to the activation of both caspase-3 and caspase-7 [67], causing a cascade of proteolytic activities that lead to apoptosis [68].

The aforementioned apoptotic mechanism is inhibited by Bcl-2 proteins that interact with BH3-only proteins and accordingly inhibit Bax and BAK [65]. However, cancer cells resist apoptosis by downregulation of Bax and upregulation of Bcl-2. To observe the molecular mechanism *via* which chalcone-thienopyrimidine derivatives exert their antiproliferative activity, we investigated the effect of the most active synthesized chalcone-thienopyrimidine derivatives on the abundance of the specific genes responsible for the cell cycle and apoptosis (Bcl-2, Bax, caspase-3, and caspase-9) in both HepG2 and MCF-7 cells.

Many chalcones have been observed to target the mitochondrial pathway as a means to induce apoptosis [69]. In the HepG2 cell line, all tested compounds except **3c** have been shown to produce significant altitude in the Bax/Bcl-2 ratio ($P < 0.05$) in comparison to control. Caspase-3 levels were remarkably elevated with all tested compounds, while those of caspase-9 were raised with all tested compounds except **3e**. In the MCF-7 cell line, compounds **3b** and **3g** were associated with significant increments in proapoptotic genes (Bax, caspase-3, and caspase-9) and remarkable decrements in the antiapoptotic Bcl-2 in comparison to control ($P < 0.05$). In addition, there was a positive correlation between cytotoxic efficacy of the compounds and apoptosis in both HepG2 and MCF-7 cell lines.

These results support the notion that the mechanism of antitumor activity by these novel chalcone-thienopyrimidine derivatives includes the intrinsic (mitochondrial) apoptotic pathway. In accordance with our results, chalcones have been demonstrated to activate Bak and Bax and inhibit Bcl-2 [70], as well as activate caspase-9. Deeb et al. [71] clarified that a chalcone (xanthohumol) enhanced both intrinsic and extrinsic apoptotic pathways. Similarly, other studies demonstrated that chalcones induced apoptosis in the MCF-7 cell line by both pathways [72]. Moreover, recent studies had shown that chalcones also function as an apoptotic regulator in human lung and hepatic cancer cells and restrain cancer cell metastasis [73]. Further, the indole-chalcone-based benzopyran chalcones when used *in vitro* against cancer cells resulted in antiproliferation of the cells by eliciting DNA nick-sealing activity *via* inhibition of DNA ligases [74]. In addition, the proliferation of K562 was inhibited by chalcone derivatives through induction of apoptosis [75]. The chemical structures of chalcones seem to play a pivotal role in detecting their molecular targets. The apoptotic effect of the tested compounds was elucidated by upregulation of Bax, caspase-3, and caspase-9 and downregulation of Bcl-2. The aforementioned results were supported by the findings of the molecular docking

analysis into Bcl-2 that exhibited moderate binding affinity of the seven tested compounds for Bcl-2 comparable to one of the well-known Bcl-2 inhibitors, DRO [35, 44]. Among them, **3g** showed the highest binding free energy. The remaining tested compounds showed different types of binding interactions including hydrogen bonds and electrostatic and hydrophobic interactions.

Generation of free radicals during oxidation results in a chain of reactions that results in cell damage and develops an oxidative stress state that causes several chronic diseases such as cancer [76]. During oxidative stress, the redox system is altered together with the disturbance in cell proliferation and apoptosis [77]. However, chalcones possess antioxidant properties, but under certain circumstances, chalcones may act as oxidants [78], and this effect can be associated with their antitumor activity [79]. Cancer cells are highly sensitive to the prooxidants [80] due to higher concentrations of some ions and higher metabolic activity [81] in comparison with noncancer cells. The mechanisms through which the chalcones revealed prooxidant actions are either elevation of the superoxide levels [81], elimination of cellular glutathione [82], or formation of phenoxyl radicals [82].

Recently, it has been established that chalcones (either natural or synthetic) exert their antiproliferative activities *via* induction of oxidative stress [83]. Therefore, we investigated the impact of newly synthesized chalcone-thienopyrimidine derivatives on MDA as an indicator of lipid peroxidation and GR activity 5as one of the intracellular antioxidant defense mechanisms. All tested compounds induced a significant increase in the MDA levels together with a marked reduction of GR activity in HepG2 cells in comparison to untreated cells ($P < 0.05$). Similarly, significant elevation of MDA along with a significant decline of GR activity was noticed in MCF-7 cells exposed to **3b** and **3g** compounds in comparison to untreated cells ($P < 0.05$) (Figure 15). These findings supported the efficacy of the tested compounds for causing the oxidative stress-induced apoptosis by suppression of GR activity and increasing lipid peroxidation in cancer cells. In line with our findings, Takac et al. [62] detected significant increases in superoxide, nitric oxide, and lipid peroxide concentrations and a significant drop in GSH levels when the colorectal cancer HCT116 cell line was treated with chalcone. These results were echoed in similar studies [84, 85]. Furthermore, as venetoclax, compounds **3a-g** exhibited 2 violations from Lipinski's rule. However, the findings of the ADME study also indicated higher drug-likeness scores for compounds **3a-g** than for venetoclax.

The present study suggested that the newly synthesized chalcone-thienopyrimidine derivatives had the ability to generate oxidative stress, subsequently inducing apoptosis in MCF-7 and HepG2 cells through the intrinsic pathway as a possible mechanism of their anticancer activity.

5. Conclusion

Novel chalcone-pyridothienopyrimidinone derivatives were synthesized when chalcones reacted with different pyridothienopyrimidine under reflux temperature. It is interesting to observe that the IC_{50} of the two compounds **3b** and **3g** showed a higher cytotoxicity than 5-FU against HepG2 and MCF-7 cell lines. The six tested compounds (**3a**-**e** and **3g**) arrested the proliferation of HepG2 and MCF-7 cell lines at different cell cycle phases. Interestingly, our results revealed that treatment of HepG2 and MCF-7 cells with the newly synthesized tested compound elicited apoptotic effects comparable to that with 5-FU. The mechanism by which the tested compounds induced apoptosis included upregulation of the proapoptotic genes (Bax, caspase-9, and caspase-3) and downregulation of the antiapoptotic Bcl-2. The data of the molecular docking analysis of **3a-g** compounds into the binding groove of the antiapoptotic protein Bcl-2 revealed relatively moderate binding free energies compared to the selective Bcl-2 inhibitor DRO. Among the new compounds, **3g** showed the highest binding free energy toward Bcl-2. Analysis of the binding interactions of **3a-g** revealed multiple hydrophobic interactions besides the hydrogen bonds and electrostatic interactions with amino acids in the active site of Bcl-2. Compounds **3a-g**, like venetoclax, revealed two violations of Lipinski's rule. However, compounds **3a-g** have greater drug-likeness scores in the ADME study than venetoclax.

Intriguingly, all tested compounds were associated with significant increases in MDA levels together with a marked reduction in GR activity in HepG2 and MCF-7 cell lines compared to control cells. This suggested that the newly synthesized chalcone-thienopyrimidine derivatives had the ability to induce anticancer activity *via* inducing oxidative stress which in turn triggered apoptosis in MCF-7 and HepG2 cells through the intrinsic pathway. Anticancer compounds act mechanistically by interfering with the cell cycle and by triggering oxidative stress-dependent apoptosis. Therefore, regulation of the cell cycle and apoptosis are suggested to be active therapeutic strategies for the development of novel therapies in oncology. The tested compounds have the potential to be taken up for further modern clinical trials after extensive pharmacodynamic, pharmacokinetic, and toxicity profile investigations, particularly against liver and breast cancer.

Data Availability

All generated data in this study are included in the article and the supplementary files.

Conflicts of Interest

The authors declare no conflict of interest.

Authors' Contributions

G.M.S., K.M.A.H., E.T.M, E.Kh.A., M.R.A., M.A.A., M.A, A.M.G., I.P., R.A., M.M.A., and A.A. contributed equally to this work. Methodology, analysis of data, and writing of the manuscript were done mostly by all authors. K.M.A.H., E.T.M, and A.A. finished the final version of the manuscript and approved the final form.

Acknowledgments

The authors would like to extend their sincere appreciation to the Researchers Supporting Project number (RSP-2021/96), King Saud University, Riyadh, Saudi Arabia.

Supplementary Materials

Supplementary 1. Figures S1–S4.

Supplementary 2. Experiment.

Supplementary 3. ^{1}H NMR, ^{13}C NMR, and DEPT.

Supplementary 4. ADME study and Tables S1–S18.

References

[1] World Health Organization, *WHO technical specifications: cryosurgical equipment for the treatment of precancerous cervical lesions and prevention of cervical cancer*, World Health Organization, 2012, https://apps.who.int/iris/handle/10665/75853.

[2] S. W. Lowe and A. W. Lin, "Apoptosis in cancer," *Carcinogenesis*, vol. 21, no. 3, pp. 485–495, 2000.

[3] L. Cordeu, E. Cubedo, E. Bandrés et al., "Biological profile of new apoptotic agents based on 2,4-pyrido[2,3- _d_]pyrimidine derivatives," *Bioorganic & Medicinal Chemistry*, vol. 15, no. 4, pp. 1659–1669, 2007.

[4] U. Sirion, S. Kasemsook, K. Suksen, P. Piyachaturawat, A. Suksamrarn, and R. Saeeng, "New substituted C-19-andrographolide analogues with potent cytotoxic activities," *Bioorganic & Medicinal Chemistry Letters*, vol. 22, no. 1, pp. 49–52, 2012.

[5] T. Sakai, R. N. Eskander, Y. Guo et al., "Flavokawain B, a kava chalcone, induces apoptosis in synovial sarcoma cell lines," *Journal of Orthopaedic Research*, vol. 30, no. 7, pp. 1045–1050, 2012.

[6] M. Sayed and N. Ahmed, "Synthesis and biological value of thiouracils and fused thiouracils (a review)," *Journal of Advanced Pharmacy Research*, vol. 1, no. 2, pp. 75–88, 2017.

[7] V. S. Dinakaran, B. Bomma, and K. K. Srinivasan, "Fused pyrimidines: the heterocycle of diverse biological and pharmacological significance," *Der Pharma Chemica*, vol. 4, pp. 255–265, 2012.

[8] W. A. El-Sayed, A. E. Rashad, S. M. Awad, and M. M. Ali, "Synthesis and in vitro antitumor activity of new substituted thiopyrimidine acyclic nucleosides and their thioglycoside analogs," *Nucleosides, Nucleotides and Nucleic Acids*, vol. 28, no. 4, pp. 261–274, 2009.

[9] L. Y. El-Sharkawy, R. A. El-Sakhawy, M. Abdel-Halim et al., "Design and synthesis of novel annulated thienopyrimidines as phosphodiesterase 5 (PDE5) inhibitors," *Archiv der Pharmazie*, vol. 351, no. 5, 2018.

[10] E. Z. Elrazaz, R. A. T. Serya, N. S. M. Ismail, D. A. Abou El Ella, and K. A. M. Abouzid, "Thieno [2, 3-d] pyrimidine based derivatives as kinase inhibitors and anticancer agents," *Future Journal of Pharmaceutical Sciences*, vol. 1, pp. 33–41, 2015.

[11] P. F. Lamie and J. N. Philoppes, "2-Thiopyrimidine/chalcone hybrids: design, synthesis, ADMET prediction, and anticancer evaluation as STAT3/STAT5a inhibitors," *Journal of Enzyme Inhibition and Medicinal Chemistry*, vol. 35, no. 1, pp. 864–879, 2020.

[12] K. Parikh and D. Joshi, "Antibacterial and antifungal screening of newly synthesized benzimidazole-clubbed chalcone derivatives," *Medicinal Chemistry Research*, vol. 22, no. 8, pp. 3688–3697, 2013.

[13] C. Tratrat, M. Haroun, I. Xenikakis et al., "Design, synthesis, evaluation of antimicrobial activity and docking studies of new thiazole-based chalcones," *Current Topics in Medicinal Chemistry*, vol. 19, no. 5, pp. 356–375, 2019.

[14] D. K. Mahapatra, S. K. Bharti, and V. Asati, "Chalcone derivatives: anti-inflammatory potential and molecular targets perspectives," *Current Topics in Medicinal Chemistry*, vol. 17, no. 28, pp. 3146–3169, 2017.

[15] M. Sökmen and M. Akram Khan, "The antioxidant activity of some curcuminoids and chalcones," *Inflammopharmacology*, vol. 24, no. 2-3, pp. 81–86, 2016.

[16] W. Yan, C. Xiangyu, L. Ya, W. Yu, and X. Feng, "An orally antitumor chalcone hybrid inhibited HepG2 cells growth and migration as the tubulin binding agent," *Investigational New Drugs*, vol. 37, no. 4, pp. 784–790, 2019.

[17] H. A. Al-Hazam, Z. A. Al-Shamkani, N. A. Al-Masoudi, B. A. Saeed, and C. Pannecouque, "New chalcones and thiopyrimidine analogues derived from mefenamic acid: microwave-assisted synthesis, anti-HIV activity and cytotoxicity as anti-leukemic agents," *Zeitschrift Für Naturforschung B*, vol. 72, no. 4, pp. 249–256, 2017.

[18] H.-J. Zhang, Y. Qian, D.-D. Zhu, X.-G. Yang, and H.-L. Zhu, "Synthesis, molecular modeling and biological evaluation of chalcone thiosemicarbazide derivatives as novel anticancer agents," *European Journal of Medicinal Chemistry*, vol. 46, no. 9, pp. 4702–4708, 2011.

[19] G. Huang and S.-T. Pan, "ROS-mediated therapeutic strategy in chemo-/radiotherapy of head and neck cancer," *Oxidative Medicine and Cellular Longevity*, vol. 2020, Article ID 5047987, 30 pages, 2020.

[20] H. Amawi, C. Karthikeyan, R. Pathak et al., "Thienopyrimidine derivatives exert their anticancer efficacy via apoptosis induction, oxidative stress and mitotic catastrophe," *European Journal of Medicinal Chemistry*, vol. 138, pp. 1053–1065, 2017.

[21] H. Zhu, L. Tang, C. Zhang et al., "Synthesis of chalcone derivatives: inducing apoptosis of HepG2 cells via regulating reactive oxygen species and mitochondrial pathway," *Frontiers in Pharmacology*, vol. 10, 2019.

[22] F.-C. Wang, B. Peng, S.-L. Cao et al., "Synthesis and cytotoxic activity of chalcone analogues containing a thieno [2, 3-d] pyrimidin-2-yl group as the A-ring or B-ring," *Bioorganic Chemistry*, vol. 94, 2020.

[23] A. Mannan, Z. P. Germon, J. Chamberlain, J. R. Sillar, B. Nixon, and M. D. Dun, "Reactive oxygen species in acute lymphoblastic leukaemia: reducing radicals to refine responses," *Antioxidants*, vol. 10, no. 10, 2021.

[24] K. Li, B. Wang, L. Zheng et al., "Target ROS to induce apoptosis and cell cycle arrest by 5,7-dimethoxy-1,4-naphthoquinone derivative," *Bioorganic & Medicinal Chemistry Letters*, vol. 28, no. 3, pp. 273–277, 2018.

[25] Y.-Q. Hu, C. Gao, S. Zhang et al., "Quinoline hybrids and their antiplasmodial and antimalarial activities," *European Journal of Medicinal Chemistry*, vol. 139, pp. 22–47, 2017.

[26] W.-B. Kuang, R.-Z. Huang, J.-L. Qin et al., "Design, synthesis and pharmacological evaluation of new 3-(1H-benzimidazol-2-yl)quinolin-2(1H)-one derivatives as potential antitumor

agents," *European Journal of Medicinal Chemistry*, vol. 157, pp. 139–150, 2018.

[27] F. F. Ahmed, A. A. Abd El-Hafeez, S. H. Abbas, D. Abdelhamid, and M. Abdel-Aziz, "New 1,2,4-triazole-Chalcone hybrids induce Caspase-3 dependent apoptosis in A549 human lung adenocarcinoma cells," *European Journal of Medicinal Chemistry*, vol. 151, pp. 705–722, 2018.

[28] G. Sigounas, J. Hooker, A. Anagnostou, and M. Steiner, "*S*-Allylmercaptocysteine inhibits cell proliferation and reduces the viability of erythroleukemia, breast, and prostate cancer cell lines," vol. 27, 1997.

[29] N. Hussein, H. Amawi, C. Karthikeyan et al., "The dopamine D_3 receptor antagonists PG01037, NGB2904, SB277011A, and U99194 reverse ABCG2 transporter-mediated drug resistance in cancer cell lines," *Cancer Letters*, vol. 396, pp. 167–180, 2017.

[30] K. Li, Q. Zheng, X. Chen, Y. Wang, D. Wang, and J. Wang, "Isobavachalcone induces ROS-mediated apoptosis via targeting thioredoxin reductase 1 in human prostate cancer PC-3 cells," *Oxidative Medicine and Cellular Longevity*, vol. 2018, Article ID 1915828, 13 pages, 2018.

[31] M. F. Tolba, A. Esmat, A. M. Al-Abd et al., "Caffeic acid phenethyl ester synergistically enhances docetaxel and paclitaxel cytotoxicity in prostate cancer cells," *IUBMB Life*, vol. 65, no. 8, pp. 716–729, 2013.

[32] C.-W. Phang, S. A. Karsani, G. Sethi, and S. N. Abd Malek, "Flavokawain C inhibits cell cycle and promotes apoptosis, associated with endoplasmic reticulum stress and regulation of MAPKs and Akt signaling pathways in HCT 116 human colon carcinoma cells," *PLoS One*, vol. 11, no. 2, 2016.

[33] T. Miyashita, S. Krajewski, M. Krajewska et al., "Tumor suppressor p53 is a regulator of bcl-2 and bax gene expression in vitro and in vivo," *Oncogene*, vol. 9, pp. 1799–1805, 1994.

[34] G. M. Morris, R. Huey, W. Lindstrom et al., "AutoDock4 and AutoDockTools4: Automated docking with selective receptor flexibility," *Journal of Computational Chemistry*, vol. 30, no. 16, pp. 2785–2791, 2009.

[35] J. Porter, A. Payne, B. de Candole et al., "Tetrahydroisoquinoline amide substituted phenyl pyrazoles as selective Bcl-2 inhibitors," *Bioorganic & Medicinal Chemistry Letters*, vol. 19, no. 1, pp. 230–233, 2009.

[36] F. A. Almalki, A. N. Abdalla, A. M. Shawky, M. A. El Hassab, and A. M. Gouda, "In silico approach using free software to optimize the antiproliferative activity and predict the potential mechanism of action of pyrrolizine-based Schiff bases," *Molecules*, vol. 26, no. 13, 2021.

[37] A. M. Shawky, N. A. Ibrahim, A. N. Abdalla, M. A. S. Abourehab, and A. M. Gouda, "Novel pyrrolizines bearing 3, 4, 5-trimethoxyphenyl moiety: design, synthesis, molecular docking, and biological evaluation as potential multi-target cytotoxic agents," *Journal of Enzyme Inhibition and Medicinal Chemistry*, vol. 36, no. 1, pp. 1313–1333, 2021.

[38] D.S. BIOVIA, "Discovery studio modeling environment, release 2017, San Diego: DassaultSystèmes, 2016," https://Accelrys.Com/Products/Collaborativescience/Biovia-Discoverystudio/Visualization.Download.Php.

[39] A. Daina, O. Michielin, and V. Zoete, "SwissADME: a free web tool to evaluate pharmacokinetics, drug-likeness and medicinal chemistry friendliness of small molecules," *Scientific Reports*, vol. 7, 2017.

[40] S. Kei, "Serum lipid peroxide in cerebrovascular disorders determined by a new colorimetric method," *Clinica Chimica Acta*, vol. 90, no. 1, pp. 37–43, 1978.

[41] S. A. Malik, S. Khole, S. P. K. Mittal, T. Urmode, R. Kusurkar, and S. S. Ghaskadbi, "Differential response of antioxidant defense in HepG2 cells on exposure of Livotrit®, in a concentration dependent manner," *Journal of Traditional and Complementary Medicine*, vol. 9, no. 1, pp. 38–44, 2019.

[42] F. Sauter, U. Jordis, J. Frolich, K. Gewald, F. Grohmann, and E. K. Ahmed, "Synthesis of fully aromatic pyrido4', 3': 4, 5thieno2, 3-dpyrimidine derivatives," *Models in Chemistry*, vol. 131, pp. 489–498, 1994.

[43] M. A. Ameen, S. Karsten, and J. Liebscher, "A convenient method for constructing novel tetrahydropyrido[4′,3′:4,5]thieno[2,3-*d*]-pyrimidinones-carbohydrate and amino acid conjugates via copper(I)-catalyzed alkyne-azide 'Click Chemistry'," *Tetrahedron*, vol. 66, no. 12, pp. 2141–2147, 2010.

[44] A. W. Roberts and D. C. S. Huang, "Targeting BCL2 with BH3 mimetics: basic science and clinical application of venetoclax in chronic lymphocytic leukemia and related B cell malignancies," *Clinical Pharmacology and Therapeutics*, vol. 101, no. 1, pp. 89–98, 2017.

[45] C. A. Lipinski, F. Lombardo, B. W. Dominy, and P. J. Feeney, "Experimental and computational approaches to estimate solubility and permeability in drug discovery and development settings," *Advanced Drug Delivery Reviews*, vol. 23, no. 1-3, pp. 3–25, 1997.

[46] M. Anuar, N. Najmi, N. S. N. Hisam, S. L. Liew, and A. Ugusman, "Clinical review: navitoclax as a pro-apoptotic and anti-fibrotic agent," *Frontiers in Pharmacology*, vol. 11, p. 1817, 2020.

[47] Y. H. Zhao, M. H. Abraham, J. Le et al., "Rate-limited steps of human oral absorption and QSAR studies," *Pharmaceutical Research*, vol. 19, pp. 1446–1457, 2002.

[48] M. Wan, L. Xu, L. Hua et al., "Synthesis and evaluation of novel isoxazolyl chalcones as potential anticancer agents," *Bioorganic Chemistry*, vol. 54, pp. 38–43, 2014.

[49] M. A. Khedr, K. M. Abu-Zied, W. A. Zaghary, A. S. Aly, D. N. Shouman, and H. Haffez, "Novel thienopyrimidine analogues as potential metabotropic glutamate receptors inhibitors and anticancer activity: Synthesis, *In-vitro*, *In-silico*, and SAR approaches," *Bioorganic Chemistry*, vol. 109, 2021.

[50] A. Ayati, S. Moghimi, M. Toolabi, and A. Foroumadi, "Pyrimidine-based EGFR TK inhibitors in targeted cancer therapy," *European Journal of Medicinal Chemistry*, vol. 221, 2021.

[51] S. Blondy, V. David, M. Verdier, M. Mathonnet, A. Perraud, and N. Christou, "5-Fluorouracil resistance mechanisms in colorectal cancer: from classical pathways to promising processes," *Cancer Science*, vol. 111, no. 9, pp. 3142–3154, 2020.

[52] R. S. Hotchkiss, A. Strasser, J. E. McDunn, and P. E. Swanson, "Cell death," *The New England Journal of Medicine*, vol. 361, no. 16, pp. 1570–1583, 2009.

[53] F. Peng, C.-W. Meng, Q.-M. Zhou, J.-P. Chen, and L. Xiong, "Cytotoxic evaluation against breast cancer cells of isoliquiritigenin analogues fromSpatholobus suberectusand their synthetic derivatives," *Journal of Natural Products*, vol. 79, no. 1, pp. 248–251, 2016.

[54] C. Bagul, G. K. Rao, V. K. K. Makani, J. R. Tamboli, M. Pal-Bhadra, and A. Kamal, "Synthesis and biological evaluation of chalcone-linked pyrazolo [1, 5-a] pyrimidines as potential

anticancer agents," *MedChemComm*, vol. 8, no. 9, pp. 1810–1816, 2017.

[55] S. M. Awad, O. A. Fathalla, J. Wietrzyk, M. Milczarek, A. M. Soliman, and M. S. Mohamed, "Synthesis of new pyrimidine derivatives and their antiproliferative activity against selected human cancer cell lines," *Research on Chemical Intermediates*, vol. 41, no. 3, pp. 1789–1801, 2015.

[56] Z. A. Muhammad, M. M. Edrees, R. A. M. Faty, S. M. Gomha, S. S. Alterary, and Y. N. Mabkhot, "Synthesis, antitumor evaluation and molecular docking of new morpholine based heterocycles," *Molecules*, vol. 22, no. 7, p. 1211, 2017.

[57] C.-Y. Hsieh, P.-W. Ko, Y.-J. Chang et al., "Design and synthesis of benzimidazole-chalcone derivatives as potential anticancer agents," *Molecules*, vol. 24, no. 18, p. 3259, 2019.

[58] S. Schwertheim, F. Wein, K. Lennartz, K. Worm, K. W. Schmid, and S.-Y. Sheu-Grabellus, "Curcumin induces G2/M arrest, apoptosis, NF-κB inhibition, and expression of differentiation genes in thyroid carcinoma cells," *Journal of Cancer Research and Clinical Oncology*, vol. 143, no. 7, pp. 1143–1154, 2017.

[59] V. Peyrot, D. Leynadier, M. Sarrazin et al., "Interaction of tubulin and cellular microtubules with the new antitumor drug MDL 27048:," *The Journal of Biological Chemistry*, vol. 264, no. 35, pp. 21296–21301, 1989.

[60] C.-S. Park, Y. Ahn, D. Lee et al., "Synthesis of apoptotic chalcone analogues in HepG2 human hepatocellular carcinoma cells," *Bioorganic & Medicinal Chemistry Letters*, vol. 25, no. 24, pp. 5705–5707, 2015.

[61] A. Kamal, J. S. Reddy, M. J. Ramaiah et al., "Design, synthesis and biological evaluation of imidazopyridine/pyrimidine-chalcone derivatives as potential anticancer agents," *MedChemComm*, vol. 1, no. 5, pp. 355–360, 2010.

[62] P. Takac, M. Kello, M. Vilkova et al., "Antiproliferative effect of acridine chalcone is mediated by induction of oxidative stress," *Biomolecules*, vol. 10, no. 2, p. 345, 2020.

[63] D. B. Longley, D. P. Harkin, and P. G. Johnston, "5-Fluorouracil: mechanisms of action and clinical strategies," *Nature Reviews. Cancer*, vol. 3, no. 5, pp. 330–338, 2003.

[64] M. Redza-Dutordoir and D. A. Averill-Bates, "Activation of apoptosis signalling pathways by reactive oxygen species," *Biochimica et Biophysica Acta (BBA) - Molecular Cell Research*, vol. 1863, no. 12, pp. 2977–2992, 2016.

[65] P. E. Czabotar, G. Lessene, A. Strasser, and J. M. Adams, "Control of apoptosis by the BCL-2 protein family: implications for physiology and therapy," *Nature Reviews. Molecular Cell Biology*, vol. 15, no. 1, pp. 49–63, 2014.

[66] R. M. Kluck, E. Bossy-Wetzel, D. R. Green, and D. D. Newmeyer, "The release of cytochrome c from mitochondria: a primary site for Bcl-2 regulation of apoptosis," *Science*, vol. 275, no. 5303, pp. 1132–1136, 1997.

[67] B. Z. Carter, M. Gronda, Z. Wang et al., "Small-molecule XIAP inhibitors derepress downstream effector caspases and induce apoptosis of acute myeloid leukemia cells," *Blood*, vol. 105, no. 10, pp. 4043–4050, 2005.

[68] T.-J. Fan, L.-H. Han, R.-S. Cong, and J. Liang, "Caspase family proteases and apoptosis," *Acta Biochimica et Biophysica Sinica*, vol. 37, no. 11, pp. 719–727, 2005.

[69] P. Takac, M. Kello, M. B. Pilatova et al., "New chalcone derivative exhibits antiproliferative potential by inducing G2/M cell cycle arrest, mitochondrial-mediated apoptosis and modulation of MAPK signalling pathway," *Chemico-Biological Interactions*, vol. 292, pp. 37–49, 2018.

[70] Y. Hsu, C. Chia, P. Chen, S. Huang, S. Huang, and P. Kuo, "Shallot and licorice constituent isoliquiritigenin arrests cell cycle progression and induces apoptosis through the induction of ATM/p53 and initiation of the mitochondrial system in human cervical carcinoma HeLa cells," *Molecular Nutrition & Food Research*, vol. 53, no. 7, pp. 826–835, 2009.

[71] D. Deeb, X. Gao, H. Jiang, A. S. Arbab, S. A. Dulchavsky, and S. C. Gautam, "Growth inhibitory and apoptosis-inducing effects of xanthohumol, a prenylated chalone present in hops, in human prostate cancer cells," *Anticancer Research*, vol. 30, pp. 3333–3339, 2010.

[72] S. Syam, S. I. Abdelwahab, M. A. Al-Mamary, and S. Mohan, "Synthesis of chalcones with anticancer activities," *Molecules*, vol. 17, no. 6, pp. 6179–6195, 2012.

[73] N. Dong, X. Liu, T. Zhao et al., "Apoptosis-inducing effects and growth inhibitory of a novel chalcone, in human hepatic cancer cells and lung cancer cells," *Biomedicine & Pharmacotherapy*, vol. 105, pp. 195–203, 2018.

[74] S. Gupta, P. Maurya, A. Upadhyay et al., "Synthesis and bioevaluation of indole-chalcone based benzopyrans as promising antiligase and antiproliferative agents," *European Journal of Medicinal Chemistry*, vol. 143, pp. 1981–1996, 2018.

[75] H.-M. Wang, L. Zhang, J. Liu et al., "Synthesis and anti-cancer activity evaluation of novel prenylated and geranylated chalcone natural products and their analogs," *European Journal of Medicinal Chemistry*, vol. 92, pp. 439–448, 2015.

[76] S. Albrecht, A. Elpelt, C. Kasim et al., "Quantification and characterization of radical production in human, animal and 3D skin models during sun irradiation measured by EPR spectroscopy," *Free Radical Biology & Medicine*, vol. 131, pp. 299–308, 2019.

[77] E. V. Shakhristova, E. A. Stepovaya, N. V. Ryazantseva et al., "Role of glutathione system redox potential in apoptosis dysregulation in mcf-7 breast adenocarcinoma," *Bulletin of Experimental Biology and Medicine*, vol. 160, no. 3, pp. 364–367, 2016.

[78] C. H. Lau, X. J. Jiang, D. K. P. Ng, and P. C. Lo, "A disulfide-linked conjugate of $_{\text{ferrocenyl}}$ chalcone and silicon(iv) phthalocyanine as an activatable photosensitiser," *Chemical Communications*, vol. 49, no. 39, pp. 4274–4276, 2013.

[79] Y. Hseu, Y. Huang, V. Thiyagarajan et al., "Anticancer activities of chalcone flavokawain B fromAlpinia priceiHayata in human lung adenocarcinoma (A549) cells via induction of reactive oxygen species-mediated apoptotic and autophagic cell death," *Journal of Cellular Physiology*, vol. 234, no. 10, pp. 17514–17526, 2019.

[80] J. H. Weisburg, D. B. Weissman, T. Sedaghat, and H. Babich, "In vitro cytotoxicity of epigallocatechin gallate and tea extracts to cancerous and normal cells from the human oral cavity," *Basic & Clinical Pharmacology & Toxicology*, vol. 95, no. 4, pp. 191–200, 2004.

[81] R. J. DeBerardinis and N. S. Chandel, "Fundamentals of cancer metabolism," *Science Advances*, vol. 2, no. 5, 2016.

[82] J. Guzy, J. Vašková-Kubálková, Z. Rozmer et al., "Activation of oxidative stress response by hydroxyl substituted chalcones and cyclic chalcone analogues in mitochondria," *FEBS Letters*, vol. 584, no. 3, pp. 567–570, 2010.

[83] D.-J. Fu, J.-H. Li, J.-J. Yang et al., "Discovery of novel chalcone-dithiocarbamates as ROS-mediated apoptosis inducers by inhibiting catalase," *Bioorganic Chemistry*, vol. 86, pp. 375–385, 2019.

[84] T.-H. Kim, W. D. Seo, H. W. Ryu et al., "Anti-tumor effects by a synthetic chalcone compound is mediated by c-Myc- mediated reactive oxygen species production," *Chemico-Biological Interactions*, vol. 188, no. 1, pp. 111–118, 2010.

[85] Y.-C. Hseu, M.-S. Lee, C.-R. Wu et al., "The chalcone flavokawain B induces G2/M cell-cycle arrest and apoptosis in human oral carcinoma HSC-3 cells through the intracellular ROS generation and downregulation of the Akt/p38 MAPK signaling pathway," *Journal of Agricultural and Food Chemistry*, vol. 60, no. 9, pp. 2385–2397, 2012.

[86] I. Moriguchi, S. Hirono, Q. LIU, I. Nakagome, and Y. Matsushita, "Simple method of calculating octanol/water partition coefficient," *Chemical & Pharmaceutical Bulletin*, vol. 40, no. 1, pp. 127–130, 1992.

Hindawi
Oxidative Medicine and Cellular Longevity
Volume 2021, Article ID 8207283, 16 pages
https://doi.org/10.1155/2021/8207283

Research Article

The Antioxidant Supplementation with *Filipendula ulmaria* Extract Attenuates the Systemic Adverse Effects of Nanosized Calcium Phosphates in Rats

Radomir Scepanovic,[1,2] Dragica Selakovic,[2] Jelena S. Katanic Stankovic,[3] Natalija Arsenijevic,[4] Marija Andjelkovic,[5] Jovana Milenkovic,[4] Pavle Milanovic,[4] Miroslav Vasovic,[4] Nemanja Jovicic,[6] and Gvozden Rosic[2]

[1]*Military Medical Academy, University of Defense, Belgrade, Serbia*
[2]*Department of Physiology, Faculty of Medical Sciences, University of Kragujevac, 34000 Kragujevac, Serbia*
[3]*Department of Science, Institute for Information Technologies Kragujevac, University of Kragujevac, 34000 Kragujevac, Serbia*
[4]*Department of Dentistry, Faculty of Medical Sciences, University of Kragujevac, 34000 Kragujevac, Serbia*
[5]*Department of Biochemistry, Faculty of Medical Sciences, University of Kragujevac, Kragujevac, Serbia*
[6]*Department of Histology and Embryology, Faculty of Medical Sciences, University of Kragujevac, 34000 Kragujevac, Serbia*

Correspondence should be addressed to Nemanja Jovicic; nemanjajovicic.kg@gmail.com
and Gvozden Rosic; grosic@medf.kg.ac.rs

Radomir Scepanovic and Dragica Selakovic contributed equally to this work.

Received 9 July 2021; Accepted 10 August 2021; Published 17 August 2021

Academic Editor: Daoud Ali

The aim of this study was to investigate and compare the systemic toxicity of three nanosized calcium phosphates (CaPs): hydroxyapatite (HA), tricalcium phosphate (TCP), and amorphous calcium phosphate (ACP) in rats. Since those metallic compounds are widely used as bone replacement materials, including their use in oral surgery, CaPs were applied (*per os*) equimollary (17.8 mg/kg, 11 mg/kg, and 9.65 mg/kg b.w., respectively) for 30 days in order to mimic the previously described release rate from dental composites. Also, we employed antioxidant supplementation with *Filipendula ulmaria* (FU) extract. All the applied CaPs significantly increased serum calcium, triglycerides, LDL, and LDH, while serum levels of testosterone and LH declined, with no alterations in the liver enzymes. The evaluation of oxidative stress markers (in the liver, kidney, and testicle) showed an increase in TBARS values, while SOD and CAT activities and GSH levels were significantly reduced. The relative gene expression of Bax and Bcl-2 was shifted to proapoptotic action, accompanied by intense characteristic histological changes in architecture in all investigated organs. The toxic effects were most prominent in groups treated by ACP. FU administration attenuated the majority of nanosized CaP-induced adverse effects, thus recommending this therapeutic approach to minimize nano-CaP systemic toxicities.

1. Introduction

Calcium phosphates (CaPs) represent compounds of special interest in many scientific fields, with the evidently growing need for their use in medicine. In contrast to the synthetic polymers used in biomedical applications, those metal compounds are naturally present in the human body [1]. Due to the fact that CaPs express the highest levels of biocompatibility, it is not surprising that they are well accepted by the body and that they are optimally integrated into a human body [2]. They are widely accepted as materials of choice for hard tissue regeneration [3], artificial bone substitution [4], and treatment of bone defects [5]. However, the most frequent application of CaPs usually takes place in various interventions in dentistry,

such as numerous endodontic treatments [6], coating in dental implants [7], failing subperiosteal metal implants [8], periodontal defects [9], and restoration of edentulous atrophic ridges [10]. From the clinical point of view, numerous investigations have been conducted with different CaP polymers, including hydroxyapatite (HA), monocalcium phosphate, dicalcium phosphate, tricalcium phosphate (TCP), tetracalcium phosphate, and amorphous calcium phosphate (ACP), as bioactive components of composites [11]. However, recent advances in biomaterials direct clinical indications for CaP application to nanoparticles in order to increase their remineralization potential [12].

Nevertheless, despite a number of studies that lead to a conclusion for the absolute safety of those composites, it has been reported that the medical administration of CaPs is accompanied by growing concerns based on their adverse effects. Even though there are only a few published reports evaluating nano-CaP toxicities, it is possible to notice that the finding is evidently in accordance with their results. Namely, it has been confirmed that nano-CaP (HA, TCP, and ACP) administration is accompanied by various systemic morphofunctional abnormalities. In both the *in vitro* and *in vivo* investigations, nano-CaP application resulted in increased oxidative stress [13], apoptosis [14], and DNA damage [15], which were accompanied by various structural alterations. Moreover, numerous tissues and organs were affected by nano-CaPs. Depending on the investigated organ system, there are confirmations for neurotoxicity [11], nephrotoxicity [16], hepatotoxicity [17], and gonadotoxicity [18]. Since the common pathophysiological mechanisms of nano-CaP toxicities involve oxidative damage, with consequent apoptotic turnover, it is not surprising that cosupplement application of antioxidants has become a routine procedure in the treatment of nano-CaP-induced toxicities. At the same time, the use of natural products, as compounds abundant in the antioxidant defense potential, is currently a topic of actual interest for medical applications. Therefore, based on the results of several reports, it seems that toxicities induced by different CaPs could be attenuated by a variety of antioxidant-rich products.

Filipendula ulmaria (L.) Maxim. (Rosaceae) (FU) is a medicinal plant widely investigated for its confirmed antioxidant, antimicrobial, anti-inflammatory, and antiproliferative properties [19–23]. In the aerial part of the plant, there is considerable content of phenolic compounds, especially total phenolic acids and flavonoids [21]. It has been described that FU extract exerted high antioxidant activities [24]. In addition, our recent investigation confirmed a beneficial response to FU in the prevention of behavioral manifestations in nano-CaP-induced neurotoxicity [11].

Due to the evident lack of comparative information on the toxicity of those nanoparticles, the aim of this study was to evaluate the potential systemic effects of different CaPs applied in the form of nanoparticles, by means of the morphofunctional status of the kidney, liver, and testis. Furthermore, following the possible involvement of oxidative stress in the mediation of nano-CaP systemic actions, we included the simultaneous administration of antioxidant-rich *Filipendula ulmaria* extract, as a potential therapeutic approach that could minimize the role of oxidative stress in the pathogenesis of nano-CaP systemic toxicities.

2. Materials and Methods

2.1. Animals and Treatment. A total of 42 male Wistar albino rats (2 months old, 250–300 g) that were used in the study were purchased from the Military Medical Academy (Serbia) and housed in groups of three per transparent polyethylene cage under standard environmental conditions (temperature: 23 ± 1°C; light: 12/12 h light/dark cycle). The rats had access to food and water *ad libitum*. The animals were randomly divided into seven equal groups as follows: control group; three groups that orally (dissolved in tap water) received individual nanosized calcium phosphates: hydroxyapatite (17.8 mg/kg b.w.) (HA) group, tricalcium phosphate hydrate (11 mg/kg b.w.) (TCP) group, and amorphous calcium phosphate (9.65 mg/kg b.w.) (ACP) group; and three groups that along with calcium phosphates simultaneously orally received *Filipendula ulmaria* extract (100 mg/kg b.w.): HA+FU, TCP+FU, and ACP+FU groups (Figure 1).

The mineral components of dental composites in nanoparticles were purchased from Sigma-Aldrich, Germany: hydroxyapatite nanopowder: <200 nm particle size (BET), ≥97%, and synthetic; tricalcium phosphate hydrate nanopowder: <200 nm particle size (BET); and calcium phosphate: amorphous nanopowder and <150 nm particle size (BET). The doses for nanosized calcium phosphates were determined to meet the following criteria, as previously described by Arsenijevic and coworkers [11]: to achieve the equimolarity, to level the lowest dose of calcium phosphates (HA) that showed toxic effects according to literature data [25] for experiments performed *in vivo* with nanosized particles, and to achieve the doses of calcium phosphates daily released from dental composites *in vitro* [26]. The route of administration (*per os*) was chosen to mimic the authentic way of application in humans. From the plant material (aerial part of FU), the preparation of the extract, as well as the content identification, was performed by using the previously described procedure [24]. The daily dose of FU extract was selected according to the results of our previous study with confirmed biological effectiveness of this extract [24]. The final concentrations of all substances applied in this study were determined according to the average water intake measured in the past 24 hours. All applied protocols lasted for 30 days, with continuous monitoring by a veterinarian on a daily basis. The day before sacrifice, food intake was totally restricted to all animals at 8 pm.

2.2. Sample Preparation. Twenty-four hours after completing the experimental protocols, the animals were anesthetized by short-term narcosis, induced by intraperitoneal application of ketamine (10 mg/kg) and xylazine (5 mg/kg), and then sacrificed by decapitation. Trunk blood samples were collected for the determination of serum biochemical parameters and sex hormone levels, while (simultaneously)

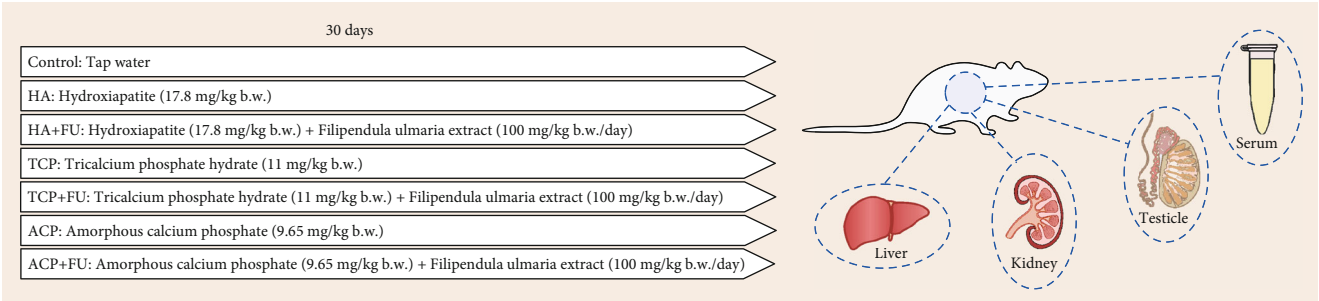

Figure 1: Experimental design.

organs (kidney, liver, and testis) were rapidly removed for tissue sample analysis. The collected blood samples were allowed to clot at room temperature for 2 h in anticoagulant-free tubes and then centrifuged at 3500 g for 15 min at 4°C. The clear supernatant was kept at −80°C until analysis. The tissue supernatants were obtained from the fresh liver, kidney, and testis tissues using phosphate-buffered saline (PBS; 0.01 M, pH 7.4). Briefly, fresh tissue was homogenized with PBS in a 1 : 5 ratio using a manual tissue homogenizer and centrifuged at 4000 rpm for 15 min at 4°C. Obtained supernatants were carefully separated and stored in the freezer until further use.

2.3. Biochemical Parameter Determination. The biochemical parameters—creatinine, urea, calcium, triglycerides, total cholesterol, HDL (high-density lipoprotein) cholesterol, LDL (low-density lipoprotein) cholesterol, lactate dehydrogenase (LDH), alkaline phosphatase (ALP), alanine aminotransferase (ALT), and aspartate aminotransferase (AST)—were estimated by using standard kits in an automatic clinical chemistry analyzer (Abbott Alinity c analytical system, Abbott Core Laboratory, Abbott Diagnostics).

2.4. Serum Hormone Assays. The testosterone and LH (luteinizing hormone) levels were measured by the enzyme-linked immunosorbent assay kits, according to the manufacturer's instructions (Abcam, Cambridge, MA, USA). The limits of detection were 6 pg/mL and 0.01 ng/mL, respectively. The intra- and interassay coefficients of variation were 4.5% for testosterone and 3.9% for LH.

2.5. The Determination of Oxidative Stress Markers. The activity of enzymes included in the protection of the organism against induced oxidative stress, catalase (CAT) and superoxide dismutase (SOD), was estimated using spectrophotometric methods reported by Beers and Sizer [27] and Misra and Fridovich [28], respectively. The level of enzymatic activity was expressed as units per milligram of proteins (U/mg) in the sample. Ellman's spectrophotometric assay [29], employing 5,5-dithio-bis-(2-nitrobenzoic acid), was used for the evaluation of the content of reduced glutathione (GSH), a significant endogenous antioxidant. The GSH content was expressed as mg GSH/g proteins. The production of thiobarbituric acid reactive substances (TBARS) during oxidative stress-induced lipid oxidation in tissues was monitored according to the method of Ohkawa and coworkers [30]. The TBARS levels were estimated as nmol of malondialdehyde (MDA)/mg proteins. The concentration of proteins in each tissue homogenate sample was evaluated by Lowry et al.'s assay [31] using bovine serum albumin as a standard. The instrument used for all measurements was a UV-Vis double-beam spectrophotometer (model Halo DB-20S, with a temperature controller, Dynamica GmbH, Dietikon, Switzerland). The preparation of tissue homogenates was done following the procedure from Kumburovic and colleagues [32].

2.6. Chemicals for the Oxidative Stress Determination. 2-Thiobarbituric acid (TBA) was obtained from abcr GmbH (Karlsruhe, Germany). 1,1,3,3-Tetraethoxypropane (malonaldehyde bis(diethyl acetal), MDA) was purchased from Acros Organics (Geel, Belgium). Bovine serum albumin was obtained from HUMAN GmbH (Wiesbaden, Germany). All other reagents for the determination of oxidative stress parameters in tissue homogenates were purchased from Sigma-Aldrich Chemie GmbH (Darmstadt, Germany).

2.7. RNA Isolation and Real-Time PCR Analysis. Total RNA was extracted from the liver, renal, and testicular tissues using a PureZOL reagent (Bio-Rad, USA) according to the manufacturer's instructions. Reverse transcription was done using iScript Reverse Transcription Mastermix (Bio-Rad, USA). Quantitative RT-PCR was performed using SsoAdvanced Universal SYBR Green Supermix (Bio-Rad, USA). mRNA-specific primers for Bax, Bcl-2, and β-actin as a housekeeping gene were used. Quantitative RT-PCR reactions were done in the Applied Biosystems 7500 (Applied Biosystems, USA), and after data analysis, relative gene expression was calculated according to Livak and Schmittgen [33].

2.8. Histological Analysis. Livers, kidneys, and testes were excised, fixed in 10% buffered formalin, and embedded in paraffin. Tissue sections (5 μm) were stained with H&E. Oil Red O staining was performed on liver tissue cryosections (5 μm). Tissue sections were fixed in paraformaldehyde (10%), rinsed with 60% isopropanol, and stained with freshly prepared Oil Red O working solution for 10 minutes. After rinsing with 60% isopropanol, the sections were counterstained with Mayer's hematoxylin and mounted with glycerin jelly.

All research procedures were carried out in accordance with the European Directive for the welfare of laboratory animals No 86/609/EEC and the principles of Good Laboratory Practice and according to ARRIVE guidelines. All experiments were approved by the Ethical Committee of the Faculty of Medical Sciences, University of Kragujevac, Serbia.

2.9. Statistical Analysis. Statistical analysis was performed with the SPSS version 20.0 statistical package (IBM SPSS Statistics 20). The results are expressed as the mean ± standard error of the mean (SEM). The parameters were initially submitted to the Levene test for homogeneity of variance and to the Shapiro-Wilk test for normality. One-way ANOVA, followed by the Bonferroni post hoc test, was used for comparisons between the groups. The significance was determined at $p < 0.05$ for all tests.

3. Results

As shown in Figure 2(a), prolonged intake of nanosized CaPs significantly altered serum calcium levels ($F = 3.517$, df = 6). The highest calcemia was observed in the ACP group, where the increase was significant when compared to the control ($p < 0.05$) and TCP groups ($p < 0.01$). However, simultaneous antioxidant supplementation with FU extract reversed ACP-induced hypercalcemia ($p < 0.05$) to the control values. In contrast, none of the applied protocols significantly influenced serum levels of creatinine (Figure 2(b), $F = 2.002$) and urea (Figure 2(c), $F = 0.810$).

Serum markers of lipid status were significantly affected by prolonged oral administration of nanosized calcium phosphates (Figure 3). As presented in Figures 3(a) and 3(b), serum triglycerides and LDL cholesterol levels were significantly above the control values ($p < 0.05$, $F = 3.192$ and 3.086) in rats solely treated with ACP but lowered after FU extract administration ($p < 0.05$) and leveled to the control values. At the same time, serum HDL levels were not significantly affected by any of the applied nanosized CaPs (Figure 3(c), $F = 1.139$). More significant impact following the 30-day protocol with nanosized CaPs was achieved on total cholesterol levels (Figure 3(d), $F = 3.693$), where the treatment with ACP resulted in a significant increase when compared to the control ($p < 0.05$), and attenuated by FU extract administration that significantly reduced serum total cholesterol levels ($p < 0.01$) when compared with the group where only ACP was administered. The most prominent alterations of lipid status induced by ACP intake were confirmed by the cholesterol ratio (Figure 3(e), $F = 3.386$) that was also significantly increased following the treatment with nanosized ACP particles ($p < 0.01$) and declined after simultaneous FU extract administration ($p < 0.05$).

Serum LDH levels (Figure 4(a)) were seriously affected by the applied protocols ($F = 3.457$), which was manifested in the ACP group by LDH elevation when compared to both the control and TCP groups ($p < 0.05$), and reversed to the control values after FU extract application. Unlike LDH, neither of the evaluated liver enzymes, ALP, ALT, and AST (Figures 4(b)–4(d)), was significantly altered following any of the applied protocols ($F = 0.059$, 0.443, and 0.159, respectively).

As shown in Figure 5(a), serum testosterone levels were significantly influenced by the protocols with nanosized CaPs ($F = 3.579$). Although all applied CaPs declined testosterone levels (significant for HA and ACP, $p < 0.05$), when applied along with CaP nanoparticles, FU extract prevented the lowering of the levels of testosterone. Even more significant hormonal disturbance following prolonged nanosized CaP intake was observed by means of serum LH levels (Figure 5(b), $F = 7.130$). All three applied forms of nano-CaPs induced a significant reduction in serum LH ($p < 0.01$). The deterioration of LH levels was persistent even following antioxidant supplementation with FU extract, with values significantly below the control ($p < 0.01$).

Lipid peroxidation in kidney tissue, expressed as TBARS (Figure 6(a)), was significantly altered following the applied protocols ($F = 12.801$). TBARS values were significantly above the control values ($p < 0.01$) in all three groups solely treated with CaPs. However, the significant reduction of the lipid peroxidation was observed after simultaneous administration of FU extract in groups treated with HA and TCP, while antioxidant supplementation failed to prevent the increase in TBARS values with ACP, since the values remained significantly above the control ($p < 0.01$). The enzymatic antioxidant defense (Figures 6(b) and 6(c)) was significantly affected by the applied protocols ($F = 7.687$ and 39.195, respectively). The activity of SOD was significantly reduced by all three nano-CaPs individually ($p < 0.05$ for HA and TCP, and $p < 0.01$ for ACP) and reestablished by simultaneous antioxidant supplementation. The significant reduction of CAT activity, also achieved with all three nano-CaPs ($p < 0.01$), although significantly enhanced by FU extract ($p < 0.01$), still remained significantly below the control values ($p < 0.01$) in all three combined groups. Nonenzymatic antioxidant capacity (Figure 6(d)), like the enzymatic mechanism, was also significantly influenced by the applied treatments ($F = 5.248$). The significant reduction of GSH levels was observed following HA administration ($p < 0.01$) but was successfully compensated by FU extract that resulted in a significant increase of kidney tissue GSH concentration ($p < 0.05$). The impact of nanosized CaPs on the relative expression of apoptosis-related genes was estimated by the determination of the Bax, Bcl-2, and Bax/Bcl-2 ratio (Figures 6(e)–6(g), $F = 3.081$, 2.919, and 12.099, respectively). While the relative mRNA expression of Bax was significantly enhanced only in the ACP group ($p < 0.05$) and successfully attenuated by FU extract administration, no significant impact of the applied protocols was observed in antiapoptotic Bcl-2. However, when expressed as a pro/antiapoptotic gene expression ratio, the nanosized CaPs significantly shifted the ratio to proapoptotic. Although this ratio was observed with all three nano-CaPs, the significant augmentation was achieved only with ACP. ACP administration resulted in the Bax/Bcl-2 ratio enhancement even when compared to the other two CaPs used in this study ($p < 0.05$), and it was persistently low following antioxidant supplementation with FU extract. Observed results were in line with pathohistological findings of

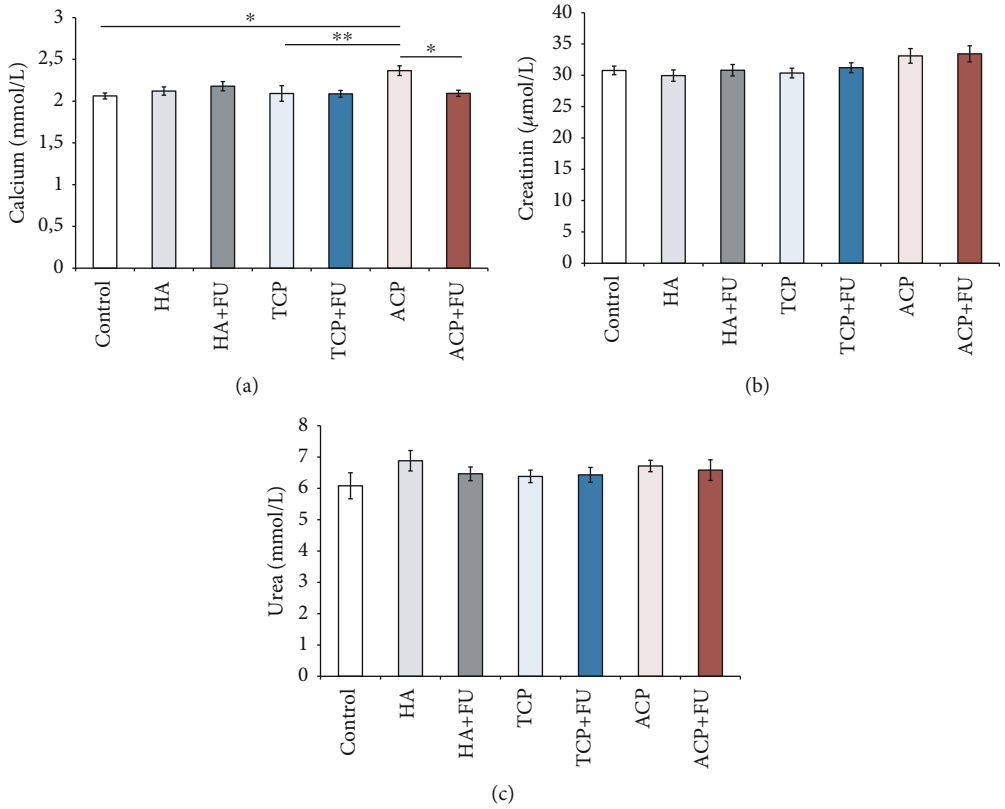

Figure 2: Serum levels of calcium, creatinine, and urea (a–c). The values are mean ± SEM; ∗ denotes a significant difference, $p < 0.05$; ∗∗ denotes a significant difference, $p < 0.01$.

vacuolation of the proximal convoluted tubule epithelium and glomerular cells that were most prominent in the ACP group (Figures 6(h) and 6(i)).

As presented in Figure 7(a), the applied protocols with nanosized CaPs showed a significant impact on lipid peroxidation, expressed as TBARS ($F = 40.750$), in the liver. While TCP administration did not produce a significant alteration of TBARS, oral intake of HA induced a significant increase when compared to the control values ($p < 0.05$). However, the most prominent enhancement of lipid peroxidation was observed following ACP application. The TBARS values in animals solely treated with ACP were significantly above the control values ($p < 0.01$), even when compared to the HA and TCP groups ($p < 0.01$). Although supplementation with FU extract significantly decreased lipid peroxidation induced by ACP ($p < 0.01$), the values remained significantly above the control ($p < 0.01$). The activity of antioxidant enzymes (Figures 7(b) and 7(c)) was also significantly altered by the applied protocols ($F = 29.663$ and 51.663, respectively). All three applied nanosized CaPs significantly reduced the activity of both SOD and CAT when compared to the control values ($p < 0.01$). Interestingly, the decline in SOD and CAT activities observed in the HA and ACP groups was even more pronounced when compared to that in the TCP group ($p < 0.01$). Although antioxidant supplementation resulted in augmentation of enzymatic activity (significant for SOD in the HA+FU group, $p < 0.05$), the values in all combined groups remained significantly below the control ($p < 0.01$). The nonenzymatic antioxidant capacity in the liver (Figure 7(d)) was less affected than the enzymatic one ($F = 2.889$), since only individual administration of ACP resulted in a significant decline ($p < 0.05$), which was also reversed by supplementation with FU extract. The analysis of the relative gene expression of apoptotic markers revealed a very strong influence of nanosized CaP administration on both the proapoptotic (Figure 7(e), $F = 34.431$) and antiapoptotic (Figure 7(f), $F = 29.141$) markers, as well as on their ratio (Figure 7(g), $F = 62.482$). When individually applied, all three CaPs employed in this study significantly enhanced the relative expression of Bax ($p < 0.01$), with the most prominent proapoptotic action observed in the ACP group, where the values were also significantly above the HA and TCP groups ($p < 0.01$). The antioxidant supplementation with FU extract, which significantly lowered Bax relative expression in the ACP combined group ($p < 0.01$), was insufficient to prevent the nano-CaP-induced increase of Bax, except in the TCP+FU group. In the same manner, the trials with individually applied nanosized CaPs significantly declined Bcl-2 relative gene expression when compared to the control ($p < 0.01$). Again, the most prominent alteration was observed in the ACP group, where the deterioration of Bcl-2 expression was significant even when compared to the TCP group ($p < 0.01$). Like Bax, the antioxidant supplementation successfully prevented the decline of this antiapoptotic marker only in the TCP+FU group. Finally, the Bax/Bcl-2 ratio confirmed the

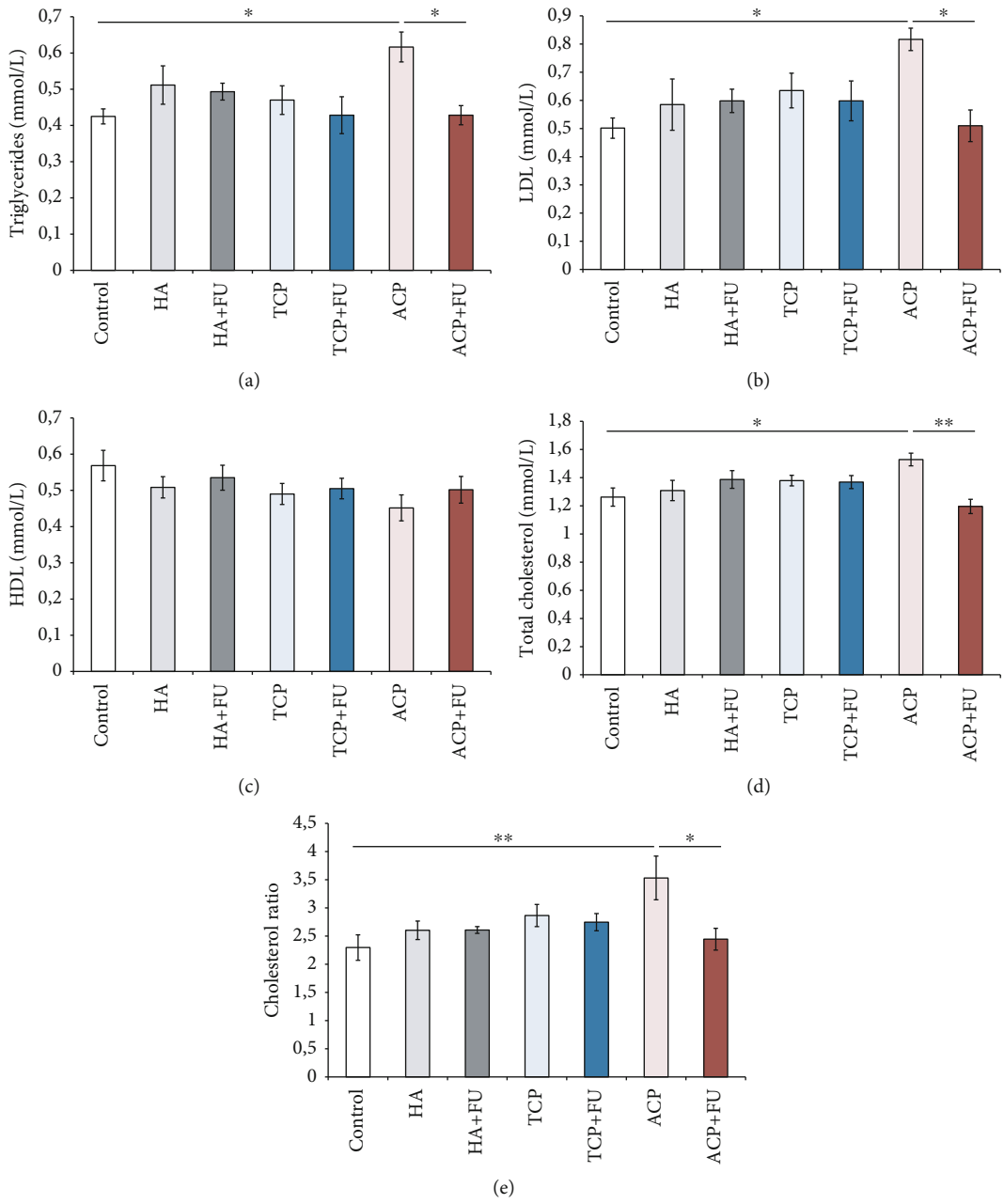

FIGURE 3: Serum levels of triglycerides, LDL, HDL, and total cholesterol and the cholesterol ratio (a–e). The values are mean ± SEM; ∗ denotes a significant difference, $p < 0.05$; ∗∗ denotes a significant difference, $p < 0.01$.

proapoptotic effect of the protocols with the individual nanosized CaPs when compared to the control ($p < 0.05$ for HA, and $p < 0.01$ for ACP), except in the TCP group. The proapoptotic action was the most prominent in the ACP group again, with the values of the Bax/Bcl-2 ratio significantly above the other two CaPs ($p < 0.01$). Unlike HA and TCP, simultaneous administration of FU extract in the applied dose, although it significantly reduced the ratio ($p < 0.01$), failed to prevent ACP-induced proapoptotic action ($p < 0.01$). Pathohistological analysis of accumulated lipids in liver tissue sections demonstrated intralobular microvesicular steatosis, which was the most prominent in the ACP group (Figures 7(h) and 7(i)).

As shown in Figure 8, all applied protocols in this study significantly affected oxidative status in rats' testicular tissue by means of lipid peroxidation (TBARS, Figure 8(a), $F = 10.130$), as well as both the enzymatic (SOD and CAT, Figures 8(b) and 8(c), $F = 12.157$ and 8.045, respectively) and nonenzymatic antioxidant mechanisms (GSH, Figure 8(d), $F = 7.512$). HA and ACP administration increased TBARS values when compared to the control ($p < 0.01$) and even when compared to the TCP group ($p < 0.01$) for ACP-treated animals. While antioxidant supplementation, when applied simultaneously with HA, resulted in a significant decline of lipid peroxidation compared to the HA group ($p < 0.01$) and reversed TBARS

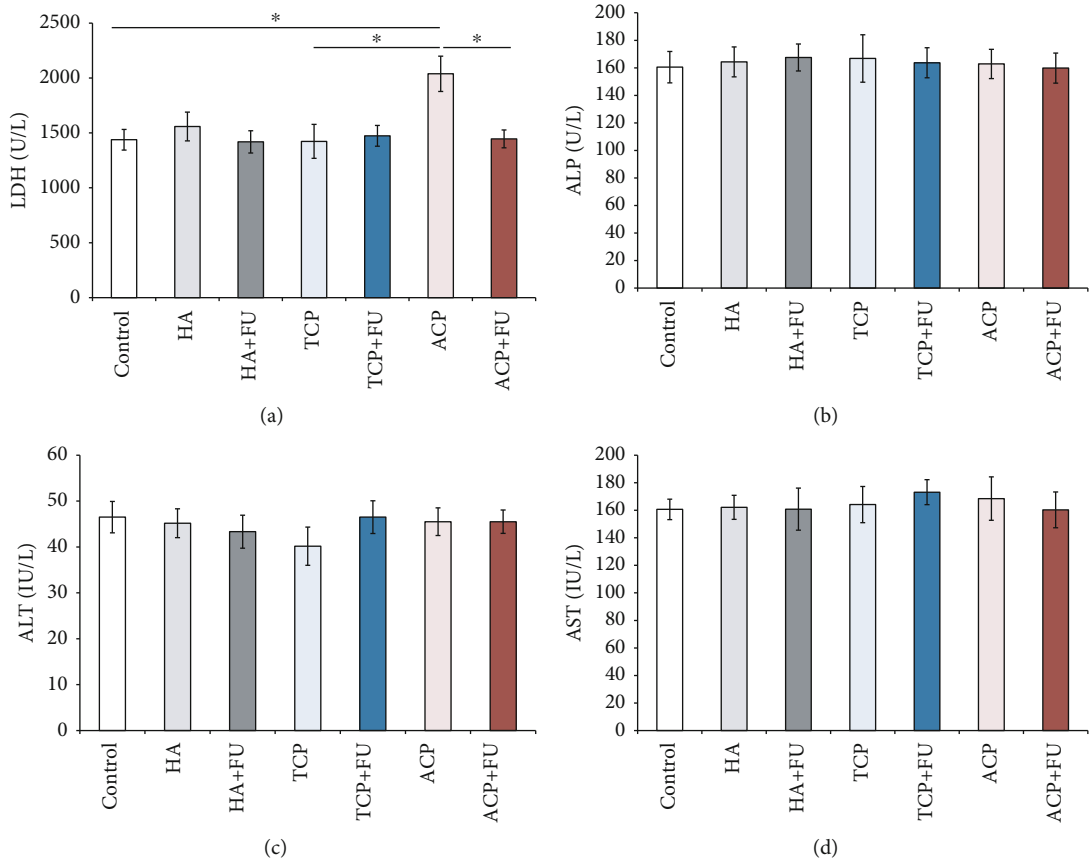

Figure 4: Serum levels of LDH, ALP, ALT, and AST (a–d). The values are mean ± SEM; ∗ denotes a significant difference, $p < 0.05$; ∗∗ denotes a significant difference, $p < 0.01$.

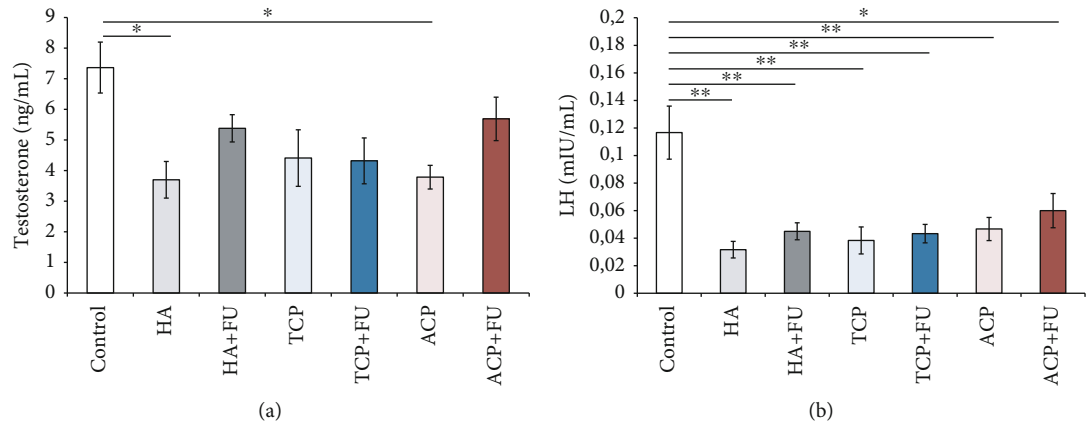

Figure 5: Serum levels of testosterone and LH (a, b). The values are mean ± SEM; ∗ denotes a significant difference, $p < 0.05$; ∗∗ denotes a significant difference, $p < 0.01$.

values to the control levels, FU extract did not significantly affect the ACP-induced increase in TBARS, and the values remained significantly above the control ($p < 0.01$). Interestingly, CAT activity in the testis was significantly reduced only in the ACP group when compared to the control group ($p < 0.01$), while the much more profound decline in SOD activity was observed in both the HA and ACP groups ($p < 0.01$). The prooxidant effect of ACP was even significant when compared to that of the TCP group ($p < 0.01$) and remained below the control values after simultaneous FU extract administration ($p < 0.01$). The ACP prooxidative action was also observed by means of GSH concentration in testicular tissue. Prolonged intake of ACP significantly declined GSH when compared to the control and TCP groups ($p < 0.01$). When FU extract was administered along with ACP, GSH levels remained below the control values

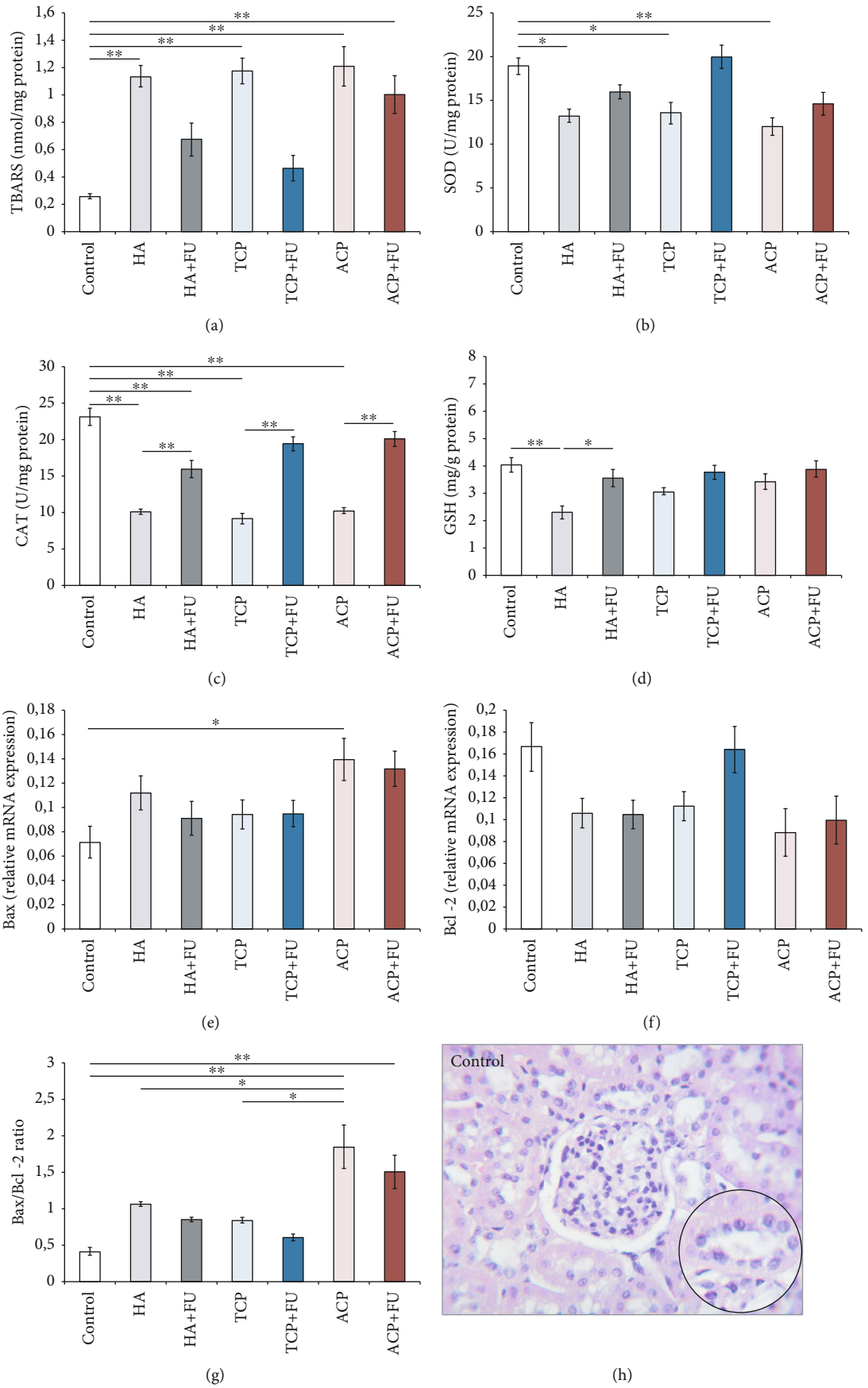

Figure 6: Continued.

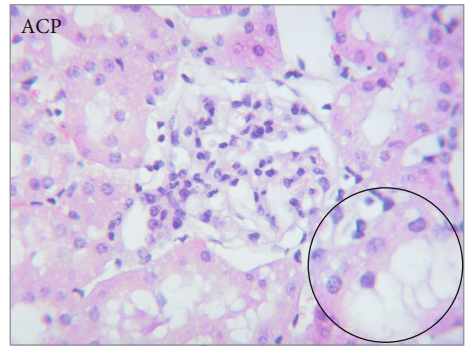

(i)

Figure 6: Oxidative stress (a–d) and apoptotic (e–g) markers with representative H&E staining in the kidney (h, i). The values are mean ± SEM; ∗ denotes a significant difference, $p < 0.05$; ∗∗ denotes a significant difference, $p < 0.01$.

($p < 0.05$). The equilibrium in the relative gene expression of pro- and antiapoptotic factors was also significantly shifted toward the apoptosis by means of the relative Bax (Figure 8(e), $F = 31.611$) and Bcl-2 expression (Figure 8(f), $F = 17.877$). Bax relative gene expression in testicular tissue was significantly enhanced by HA and ACP administration when compared to the control ($p < 0.01$), as well as to the TCP group ($p < 0.05$ for HA, and $p < 0.01$ for ACP). Also, Bax observed in the ACP group was significantly above the values in the HA group ($p < 0.05$). Although the antioxidant supplementation significantly reduced Bax relative gene expression when compared to the group where CaPs were applied solely ($p < 0.05$ for HA, and $p < 0.01$ for ACP), Bax was significantly above the control values in the ACP+FU group ($p < 0.01$). At the same time, Bcl-2 expression in testicular tissue was significantly declined by all three applied nanosized CaPs when compared to the control ($p < 0.01$), with the most prominent response to ACP ($p < 0.01$ when compared to TCP). The antioxidant supplementation with FU extract failed to significantly improve the antiapoptotic capacity since the values were kept persistently below the control values ($p < 0.05$ for HA, and $p < 0.01$ for TCP and ACP). The proapoptotic action of nanosized CaPs in the male rat testis was confirmed by significant alterations in the Bax/Bcl-2 ratio (Figure 8(g), $F = 62.745$). However, the most significant changes were observed in the ACP group where the Bax/Bcl-2 ratio was significantly above the control, as well as the HA and TCP groups ($p < 0.01$). Although FU extract, when applied along with ACP, induced a significant decline in the Bax/Bcl-2 ratio ($p < 0.01$), the values remained above the control ($p < 0.01$). Pathohistological analysis of testicular tissue demonstrated notable changes in tissue architecture in ACP-treated rats. A remarkably lower number of testicular interstitial cells were present. Also, in interstitial spaces of ACP-treated rats, cells with condensed chromatin with pyknotic nuclei were present. In this experimental group, the seminiferous tubule structure was also notably altered with a diminished number of cells in the germinal epithelium (Figures 8(h) and 8(i)).

Summarizing the results obtained in individual organs, we presented (Table 1) the comparison of the observed effects for each experimental protocol.

4. Discussion

Although calcium phosphates may be considered materials for the future in various biomedical applications, potential health risks related to their usage are often underestimated, especially since the exposure to nanoparticles is continual and usually occurs without explicit consent. Even more, there is an evident imbalance in public views between the promotion of the benefits for new nanomaterials, including nano-CaPs, and the caution considering their side effects (Table 1). Therefore, it seems necessary to alert the public about the potential risk factors associated with their medical applications. In that sense, in order to allow a better insight into the nanoparticles' side effects, the knowledge in this field should be presented more systematically. First of all, investigations in this medical problem should be standardized by means of the particle size and shape, surface composition, and release of biologically active species [34]. Finally, the administration route should be considered one of the most important aspects of experimental design.

Although chronic nano-CaP administration resulted in negligible alterations in renal function indicators in peripheral blood, the analysis of oxidative stress indicators in renal tissue revealed that nano-CaP protocols produced significant worsening in oxidative stress markers. Prooxidative action of all three applied nano-CaPs was manifested by both increased ROS production (augmentation of the index of lipid peroxidation, Figure 6(a)) and diminished antioxidant capacity. Interestingly, both the enzymatic (SOD and CAT activities, Figures 6(b) and 6(c), respectively) and nonenzymatic (GSH, Figure 6(d)) antioxidant mechanisms were impaired, but it should be noticed that GSH levels were minimized only following prolonged HA administration. Furthermore, it seems obvious that simultaneous antioxidant supplementation with FU extract prevented the prooxidative action of the applied nano-CaPs within all estimated oxidative stress indicators in renal tissue. Thus, FU extract not only successfully diminished nano-CaP-induced ROS overproduction (except in the ACP group) but also restored the antioxidant capacity by means of increased enzymatic antioxidant activity, as well as by reversing GSH levels to the control values. Due to the lack of data for the action of other

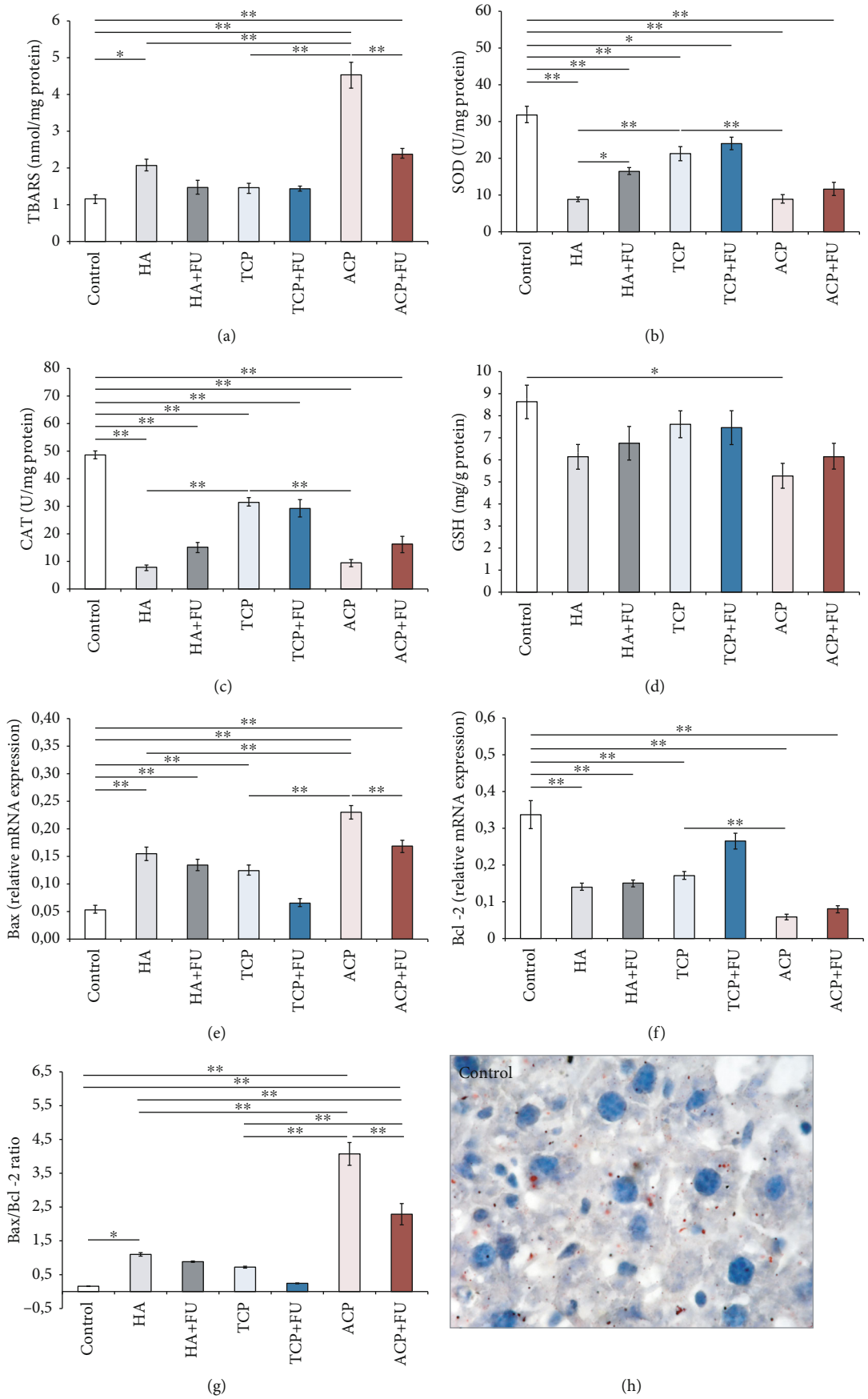

Figure 7: Continued.

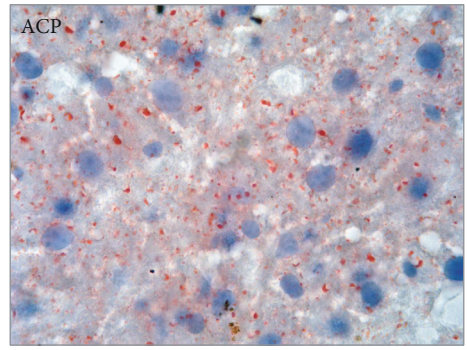

(i)

Figure 7: Oxidative stress (a–d) and apoptotic (e–g) markers with representative photomicrographs of Oil Red O staining in the liver (h, i). The values are mean ± SEM; ∗ denotes a significant difference, $p < 0.05$; ∗∗ denotes a significant difference, $p < 0.01$.

nano-CaPs on renal function *in vivo*, we can only compare our results with the most comprehensively evaluated nephrotoxic effects of HA. Indeed, our results are in accordance with the results for HA-induced nephrotoxicity obtained under various experimental conditions. Mosa and coworkers also reported prooxidative action of HA in renal tissue following chronic administration in male rats [16], which was manifested by the increased ROS production and marked decline in all antioxidant defense mechanisms, including total antioxidant capacity. The proposed mechanism of HA prooxidative action was based on previous findings that nanoparticles inside the cell promote imbalance between oxidants and antioxidants with consequent intracellular oxidative stress [35]. The intracellular prooxidative action of nanoparticles may be manifested by the affection in various intracellular structures based on the modification of lipids, proteins, and nucleic acids [36]. Although with no specific data for renal tissue, the observed proapoptotic action of nano-CaPs following the protocols applied in this study can be only compared to the previously reported general prooxidant pathways described for nano-HA *in vitro*. Xu and collaborators observed the dose-dependent prooxidative action in C6 cells as an acute response to nano-HA particles [36]. A similar prooxidant effect of nano-HA was confirmed on osteoblastic MC3T3-E1 cells, particularly affecting mitochondrial pathways [13]. These investigators, although with different doses and time exposure, reported both increased ROS production and diminished antioxidant capacity following HA administration.

The impact of the applied nano-CaPs on apoptotic markers was significant only in the ACP group (Figures 6(e)–6(g)). Interestingly, the proapoptotic action of ACP was confirmed not only when compared to the control group but also in comparison to the other two applied nano-CaPs and persisted even after antioxidant supplementation with FU extract. Again, with no specific data for the impact of nano-CaPs on apoptotic indicators in renal tissue, we can only state that our results are in line with previous reports for proapoptotic action of nano-CaPs obtained in *in vitro* studies. HA nanoparticle administration resulted in potentiating apoptosis in osteoblasts and macrophages via the augmentation of p53 expression and caspase family activity and the simultaneous downregulation of Bcl-2 [37, 38]. At the same time, it has been reported that ACP nanoparticles induced apoptosis of leukemia cells by the selective effect in the G1 phase [39].

The most prominent prooxidative and apoptotic actions, as observed in the ACP group, were accompanied by the morphological alterations in renal tissue, predominantly manifested by vacuolation of the proximal convoluted tubule epithelium and glomerular cells (Figures 6(h) and 6(i)). It is not surprising that kidney tissue undergoes significant alterations following potentially toxic substances due to the high flow rate of blood, which in turn delivers elevated concentrations of nano-CaPs to the kidney. Moreover, the proximal tubule epithelium is more vulnerable to nephrotoxicity, as confirmed in this study. This specific local affection can be attributed to the fact that these cells express various transporters, which enable active intake and intracellular accumulation of toxic compounds [40].

Under the standardized conditions that allow the comparison of individual nano-CaP effects on renal function, as performed in this study, it seems that the nephrotoxicity by means of all estimated levels was the most prominent in the ACP-treated group, with the less harmful effect observed in the HA group, and especially in TCP-treated rats. However, it should also be taken into account that the increased phosphate load itself may significantly affect kidney morphology and function [41]. Therefore, it is not surprising that hypercalcemia was confirmed only following the treatment with ACP. The observed serum calcium level elevation achieved with prolonged ACP oral intake was significant not only when compared to the control but also when compared to the TCP group. However, simultaneous administration of FU extract was sufficient to attenuate the ACP-induced calcemia rise.

As expected, we are not able to compare our results for the impact of antioxidant supplementation with FU extract to other reports that used the same antioxidant-rich natural compound. Therefore, we can confirm that the protective role of antioxidants, as observed in this study, is in accordance with the previously reported beneficial effect of curcumin and chitosan on HA-induced nephrotoxicity mechanisms by means of their antioxidative and

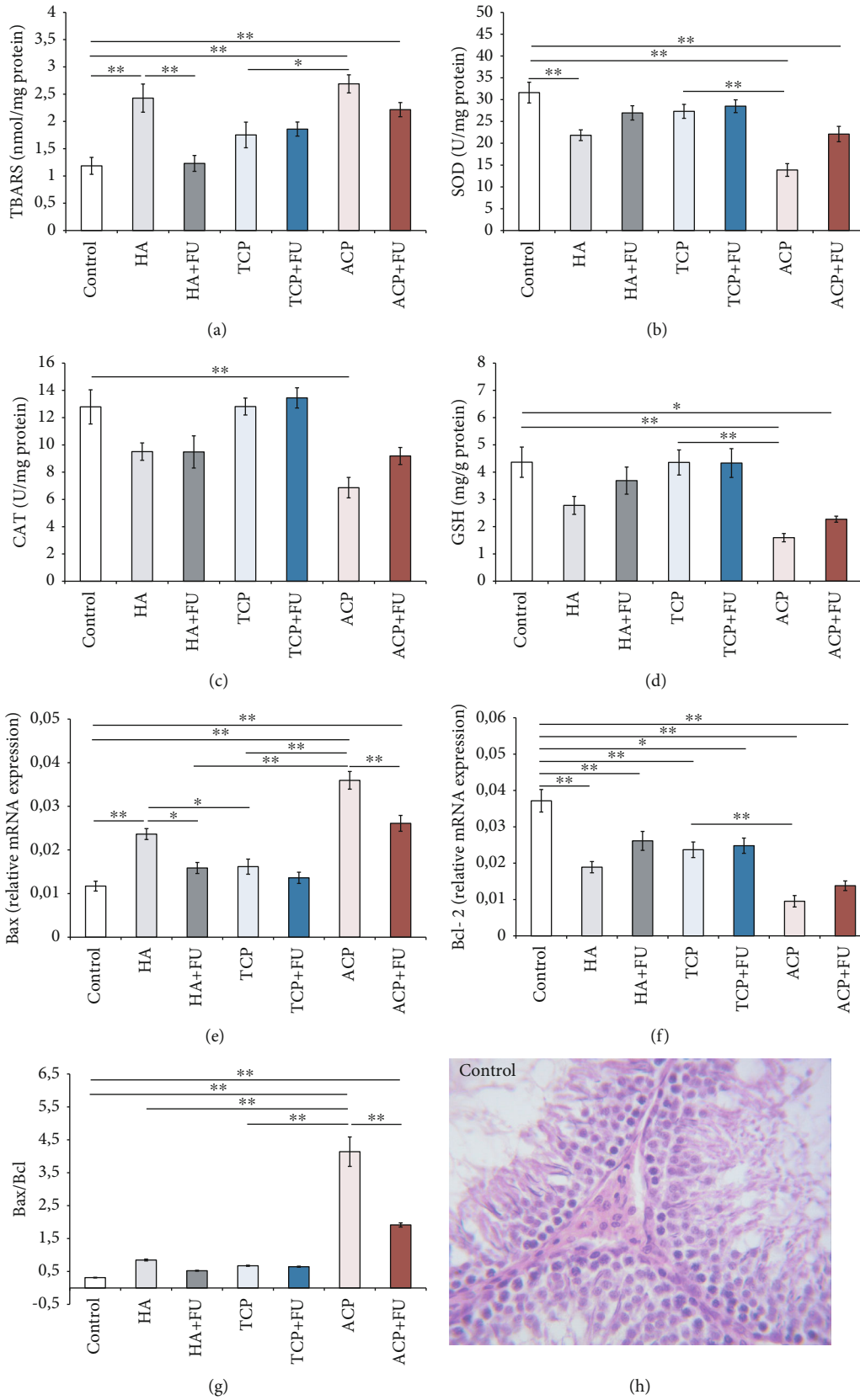

Figure 8: Continued.

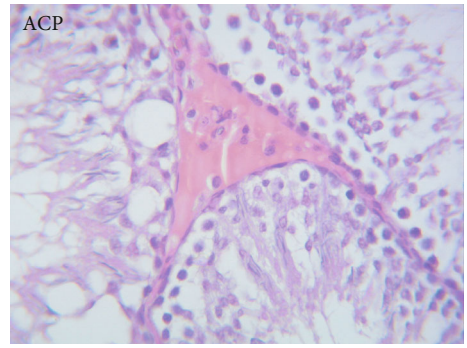

(i)

Figure 8: Oxidative stress (a–d) and apoptotic (e–g) markers with representative H&E staining in the testis (h, i). The values are mean ± SEM; ∗ denotes a significant difference, $p < 0.05$; ∗∗ denotes a significant difference, $p < 0.01$.

Table 1: Summary of the organ-specific results.

Treatment		Effect (organ)					
		Oxidative damage		Apoptosis		Structural alterations	
				Kidney			
HA	HA+FU	↑↑↑	↓↓	n.c.	n.c.	n.c.	n.c.
TCP	TCP+FU	↑↑↑	↓↓	n.c.	n.c.	n.c.	n.c.
ACP	ACP+FU	↑↑↑	↓↓	↑↑	↓↓	↑	↓
				Liver			
HA	HA+FU	↑↑	↓↓	↑↑	↓	n.c.	n.c.
TCP	TCP+FU	↑	↓	↑	↓	n.c.	n.c.
ACP	ACP+FU	↑↑↑	↓	↑↑↑	↓↓	↑	↓
				Testis			
HA	HA+FU	↑↑	↓↓↓	↑↑	n.c.	n.c.	n.c.
TCP	TCP+FU	n.c.	n.c.	↑	n.c.	n.c.	n.c.
ACP	ACP+FU	↑↑↑	↓	↑↑↑	↓↓	↑↑	↓

The arrows represent the description of alterations in the evaluated parameters. n.c. = no change.

antiapoptotic actions, accompanied by the restoration of tissue architecture [16].

None of the evaluated liver enzymes was affected by the prolonged oral intake of nano-CaPs in doses applied in this study (Figures 4(b)–4(d), respectively), but LDH levels were significantly above the control values following prolonged ACP administration. The serum LDH observed in the ACP group was also significantly higher when compared to that in TCP-treated animals. However, this effect of ACP was prevented by simultaneous administration of FU extract (Figure 4(a)). On the other hand, the indicators of liver metabolic functions were significantly influenced by the applied protocols. Interestingly, while neither HA nor TCP altered serum levels, ACP administration increased serum levels of triglycerides, LDL, and total cholesterol, as well as the cholesterol ratio (Figures 3(a)–3(e)). Those manifestations of dyslipidemia were abolished by antioxidant supplementation with FU extract. The results obtained in this study are in accordance with previous findings of Chen and colleagues [42], in terms of increased LDH and unaltered ALP levels following nano-HA administration. A similar increase in serum LDH levels following HA nanoparticle application was also achieved in a dose-dependent manner in an *in vitro* experimental model [17]. In contrast to the previously mentioned investigation, treatments with nano-CaPs applied in this study did not increase serum ALT and AST levels. Those discrepancies could be attributed to differences in experimental design, including the applied dose (three times above ours), the exposure duration, and the route of administration. This can also be considered an indirect confirmation that liver injury following nano-CaP administration in this study was not as severe as in the investigation conducted by Chen et al. Indeed, a recent study by Paraš and coworkers [43] also showed no significant alterations in AST and ALT levels following chronic administration of nano-HA (120 days). The lipid profile alterations observed in our study are also in accordance with the reported increase in serum total cholesterol and LDL levels following nano-HA administration [42].

The evaluation of oxidative stress markers in hepatic tissue revealed a significant impact of the applied protocols. ROS production was significantly enhanced by HA and ACP, with no significant effect of TCP (Figure 7(a)). This manifestation of prooxidative action was successfully abolished by FU extract in the HA group but remained above the control values in ACP-treated animals. At the same time, the enzymatic antioxidant defense was markedly reduced by HA and ACP, again with no significant impact of TCP (Figures 7(b) and 7(c), respectively). Interestingly, the decline in enzymatic antioxidant activity in the HA and ACP groups was significantly augmented even when compared to that in the TCP group and remained lower after simultaneous antioxidant supplementation. Furthermore, GSH levels in hepatic tissue samples were reduced only in ACP-treated rats, but this was prevented by FU extract. Our results correspond to the data obtained in the rat liver cell model [17], where HA nanoparticles induced the dose-dependent augmentation of total oxidative stress and the simultaneous decline in total antioxidant capacity. Also, a single dose of 50 mg/kg nano-HA resulted in prooxidative action in rat liver samples [42]. Like in our study, even an acute response to HA nanoparticles was manifested by

increased lipid peroxidation, decreased SOD activity, and diminished GSH content. Due to the lack of literature data for other nano-CaPs, we can only compare our results with other nanometallic compounds and assume that the prooxidative action, as observed in this study, might be mediated via the JNK/p53 and NF-κB pathways [44].

The proapoptotic effect of the applied nano-CaPs was expressed by means of both the increase of the relative proapoptotic gene expression (Figure 7(e)) and the decline in the relative antiapoptotic gene expression (Figure 7(f)) and confirmed by their ratio (Figure 7(g)). Unlike the oxidative stress, apoptotic markers were significantly affected by all three applied nano-CaPs, but this effect was prevented by simultaneous FU extract administration except in ACP-treated rats. Structural alterations accompanied by prooxidative and apoptotic actions of nano-CaPs in liver tissue samples were manifested predominantly through lipid accumulation in the form of intralobular microvesicular steatosis. Not surprisingly, the morphological changes were the most prominent in the ACP group (Figures 7(h) and 7(i)). Again, although with a different experimental design, it is obvious that our results are in line with the previously reported proapoptotic action of nano-HA [42]. However, structural changes described in that investigation do not correspond to ours. Namely, in contrast to Chen et al.'s report that potentiates inflammatory response in the liver following HA administration, our experimental protocols resulted in microvesicular steatosis. The observed differences could be explained by the fact that the acute response to the high dose of nano-HA could trigger an immediate hepatotoxic effect manifested by inflammatory cell infiltration, while chronic treatment with the lower dose of nano-HA predominantly caused the steatotic effect.

The obvious beneficial role of antioxidant supplementation with FU extract on nano-CaP-induced hepatotoxicity cannot be compared to similar reports. However, although already known for its protective role by means of antioxidant and anti-inflammatory effects [24], the confirmation of benefits of using FU extract following nano-CaP administration could be found only in certain brain regions [11].

A significant decline in serum testosterone levels (for approximately 50%) was observed in the HA and ACP groups, with no significant impact of TCP (Figure 5(a)). Serum testosterone levels decrease induced by nano-HA, and ACP was successfully attenuated by FU extract administration. All applied nano-CaPs diminished LH levels in sera, but unlike testosterone, the decline in serum LH persisted in all experimental groups even with simultaneous antioxidant supplementation (Figure 5(b)). The decline of testosterone, as observed in this study, following nano-CaPs is in accordance with the recently reported effect of chronic nano-HA on serum testosterone levels, while the lowering of LH is not in line with the results of a similar investigation [18]. Therefore, we must notice that there was a significant difference in experimental design in the mentioned study in which the pretreatment was 50% longer, and the daily dose was more than 15-fold higher. However, the principal mechanism of sex hormone level alterations may be found in the significant reduction of interstitial cells in testes that are the main source of testosterone. Furthermore, this mechanism is probably responsible for the observed changes in the germinal epithelium.

The prooxidative action of nano-CaPs in testicular tissue was confirmed by various aspects. The increased ROS production and decline in SOD activity were observed in HA- and ACP-treated animals (Figures 8(a) and 8(c)), while only nano-ACP administration reduced CAT activity and GSH levels (Figures 8(b) and 8(d)). The most pronounced prooxidative action of ACP remained persistent after simultaneous administration of FU extract. It is worth noticing that TCP administration induced no significant prooxidative response. The same response to nano-HA was observed in the study that evaluated the reproductive toxicity [18]. Due to the lack of other literature sources for nano-CaPs, we can only compare our results with previously reported oxidative damage in other species induced by different metallic nanoparticles [45].

While all three administered nano-CaPs induced a decline in Bcl-2 relative gene expression (Figure 8(f)), only nano-HA and ACP increased Bax relative gene expression in testicular tissue. On the other hand, FU extract application significantly lowered Bax but did not affect Bcl-2 alterations induced by nano-CaPs. Again, the proapoptotic potential, expressed as the Bax/Bcl-2 ratio, reached the highest levels in ACP-treated animals. The results obtained in this study for the proapoptotic action may be supported by the previously reported effect of nano-HA that involves the increase in p53 and TNF-α [18].

In testicular tissue, we observed significant alterations in tissue architecture following ACP treatment. The most prominent difference, when compared to the control group, was a reduction in the number of testicular interstitial cells. This was accompanied by the diminished number and altered structure of the germinal epithelial cells (Figures 8(h) and 8(i)). Our results are in line with the reduction of Leydig cells as the consequence of nano-HA treatment [18], as well as with the report that nano-Ag particles reduced the number of germline stem cells in testes [45].

The beneficial response to simultaneous administration of FU extract manifested by counteracting nano-CaP-induced gonadal dysfunction was confirmed at different estimated levels: sex hormone serum levels, oxidative and proapoptotic indicators, and structural changes in testicles. However, there is no literature data for this specific action of FU, so we can only comment that our results are in accordance with the previously reported protective role of other antioxidants (such as curcumin and chitosan) on nano-CaP-induced gonadotoxicity [18].

5. Conclusions

The results of our study clearly demonstrate that chronic intake of nano-CaPs may be accompanied by serious systemic and organ-specific adverse effects. Therefore, we suggest that further investigations for potential medical application of novel materials for tissue engineering should

include at least a basic systematic estimation of side effects, in order to achieve the biosafety of new therapeutic compounds. Yet, at least some aspects of observed toxicities may be prevented by safe and reliable supplementation with antioxidants.

Data Availability

All data is available upon request.

Ethical Approval

The study was approved by an institutional review board of the Faculty of Medical Sciences, University of Kragujevac (approval ID 01-304/3).

Conflicts of Interest

The authors declare no conflict of interest.

Authors' Contributions

The contributions of the authors involved in this study are as follows: conceptualization: R.S., D.S., N.J., and G.R.; methodology: R.S., D.S., J.S.K.S., N.A., M.A., J.M., P.M., M.V., N.J., and G.R.; validation: R.S., D.S., N.J., and G.R.; formal analysis: R.S., D.S., J.S.K.S., N.A., M.A., J.M., P.M., M.V., N.J., and G.R.; investigation: R.S., D.S., J.S.K.S., N.A., M.A., J.M., P.M., M.V., N.J., and G.R.; resources: D.S., N.J., and G.R.; data curation: R.S., D.S., J.S.K.S., N.A., M.A., J.M., P.M., M.V., N.J., and G.R.; writing—original draft preparation: R.S., D.S., J.S.K.S., N.A., M.A., J.M., P.M., M.V., N.J., and G.R.; writing—review and editing: R.S., D.S., N.J., and G.R.; visualization: R.S., D.S., N.J., and G.R.; and funding acquisition: D.S., N.J., and G.R. All authors have read and agreed to the published version of the manuscript. Radomir Scepanovic and Dragica Selakovic contributed equally to this work.

Acknowledgments

This work was supported by the Faculty of Medical Sciences, University of Kragujevac, Serbia (JP 01/19).

References

[1] W. Habraken, P. Habibovic, M. Epple, and M. Bohner, "Calcium phosphates in biomedical applications: materials for the future?," *Materials Today*, vol. 19, no. 2, pp. 69–87, 2016.

[2] S. V. Dorozhkin and M. Epple, "Biological and medical significance of calcium phosphates," *Angewandte Chemie (International Ed. in English)*, vol. 41, no. 17, pp. 3130–3146, 2002.

[3] M. Epple and A. Kovtun, "Functionalized calcium phosphate nanoparticles for biomedical application," *Key Engineering Materials*, vol. 441, pp. 299–305, 2010.

[4] R. Z. LeGeros, "Calcium phosphates in oral biology and medicine," *Monographs in Oral Science*, vol. 15, pp. 1–3, 1991.

[5] P. W. Brown and B. Constantz, *Hydroxyapatite and Related Materials*, CRC Press, Boca Raton, Florida, United States, 1st edition, 1994.

[6] C. Liu, W. Wang, W. Shen, T. Chen, L. Hu, and Z. Chen, "Evaluation of the biocompatibility of a nonceramic hydroxyapatite," *Journal of Endodontia*, vol. 23, no. 8, pp. 490–493, 1997.

[7] E. Munting, M. Verhelpen, F. Li, and A. Vincent, "Contribution of hydroxyapatite coatings to implant fixation," in *Handbook of Bioactive Ceramics*, T. Yamamuro, L. Hench, and J. Wilson, Eds., vol. 2pp. 143–148, CRC press, Boca Raton, Florida, United States, 1st edition, 1990.

[8] T. S. Golec, "The use of hydroxylapatite to coat subperiosteal implants," *The Journal of Oral Implantology*, vol. 12, no. 1, pp. 21–39, 1985.

[9] M. L. Rabalais Jr., R. A. Yukna, and E. T. Mayer, "Evaluation of durapatite ceramic as an alloplastic implant in periodontal osseous defects. I. Initial six-month results," *Journal of Periodontology*, vol. 52, no. 11, pp. 680–689, 1981.

[10] J. F. Piecuch, "Augmentation of the atrophic edentulous ridge with porous replamineform hydroxyapatite (Interpore-200)," *Dental Clinics of North America*, vol. 30, no. 2, pp. 291–305, 1986.

[11] N. Arsenijevic, D. Selakovic, J. S. Katanic Stankovic et al., "The beneficial role of *Filipendula ulmaria* extract in prevention of prodepressant effect and cognitive impairment induced by nanoparticles of calcium phosphates in rats," *Oxidative Medicine and Cellular Longevity*, vol. 2021, Article ID 6670135, 12 pages, 2021.

[12] R. N. Jardim, A. A. Rocha, A. M. Rossi et al., "Fabrication and characterization of remineralizing dental composites containing hydroxyapatite nanoparticles," *Journal of the Mechanical Behavior of Biomedical Materials*, vol. 109, p. 103817, 2020.

[13] Y. Jin, X. Liu, H. Liu et al., "Oxidative stress-induced apoptosis of osteoblastic MC3T3-E1 cells by hydroxyapatite nanoparticles through lysosomal and mitochondrial pathways," *RSC Advances*, vol. 7, no. 21, pp. 13010–13018, 2017.

[14] Z. Liu, Y. Xiao, W. Chen et al., "Calcium phosphate nanoparticles primarily induce cell necrosis through lysosomal rupture: the origination of material cytotoxicity," *Journal of Materials Chemistry B*, vol. 2, no. 22, pp. 3480–3489, 2014.

[15] H. Turkez, M. I. Yousef, E. Sönmez et al., "Evaluation of cytotoxic, oxidative stress and genotoxic responses of hydroxyapatite nanoparticles on human blood cells," *Journal of Applied Toxicology*, vol. 34, no. 4, pp. 373–379, 2014.

[16] I. F. Mosa, M. I. Yousef, M. Kamel, O. F. Mosa, and Y. Helmy, "The protective role of CsNPs and CurNPs against DNA damage, oxidative stress, and histopathological and immunohistochemical alterations induced by hydroxyapatite nanoparticles in male rat kidney," *Toxicology Research*, vol. 8, no. 5, pp. 741–753, 2019.

[17] E. Sonmez, I. Cacciatore, F. Bakan et al., "Toxicity assessment of hydroxyapatite nanoparticles in rat liver cell model in vitro," *Human & Experimental Toxicology*, vol. 35, no. 10, pp. 1073–1083, 2016.

[18] M. I. Yousef, H. H. Abd, Y. M. Helmy, and M. A. N. Kamel, "Synergistic effect of curcumin and chitosan nanoparticles on nano-hydroxyapatite-induced reproductive toxicity in rats," *Environmental Science and Pollution Research International*, vol. 28, no. 8, pp. 9362–9376, 2021.

[19] L. Barros, L. Cabrita, M. V. Boas, A. M. Carvalho, and I. C. F. R. Ferreira, "Chemical, biochemical and electrochemical assays to evaluate phytochemicals and antioxidant activity of wild plants," *Food Chemistry*, vol. 127, no. 4, pp. 1600–1608, 2011.

[20] N. Harbourne, E. Marete, J. C. Jacquier, and D. O'Riordan, "Stability of phytochemicals as sources of anti-inflammatory nutraceuticals in beverages – A review," *Food Research International*, vol. 50, no. 2, pp. 480–486, 2013.

[21] J. Katanić, T. Boroja, N. Stanković et al., "Bioactivity, stability and phenolic characterization of Filipendula ulmaria (L.) Maxim," *Food & Function*, vol. 6, no. 4, pp. 1164–1175, 2015.

[22] P. Trouillas, C. A. Calliste, D. P. Allais et al., "Antioxidant, anti-inflammatory and antiproliferative properties of sixteen water plant extracts used in the Limousin countryside as herbal teas," *Food Chemistry*, vol. 80, no. 3, pp. 399–407, 2003.

[23] S. Vogl, P. Picker, J. Mihaly-Bison et al., "Ethnopharmacological *in vitro* studies on Austria's folk medicine –An unexplored lore *in vitro* anti-inflammatory activities of 71 Austrian traditional herbal drugs," *Journal of Ethnopharmacology*, vol. 149, no. 3, pp. 750–771, 2013.

[24] J. Katanić, S. Matić, E. M. Pferschy-Wenzig et al., "*Filipendula ulmaria* extracts attenuate cisplatin-induced liver and kidney oxidative stress in rats: *In vivo* investigation and LC-MS analysis," *Food and Chemical Toxicology*, vol. 99, pp. 86–102, 2017.

[25] O. A. Abbas, I. G. Ibrahim, and A. E. Ismail, "Therapeutic effects of nano-HAp in a rat model of $AlCl_3$ induced neurotoxicity," *Iranian Journal of Pharmaceutical Research*, vol. 18, no. 3, pp. 1309–1322, 2019.

[26] K. Zhang, L. Cheng, M. D. Weir, Y. X. Bai, and H. H. K. Xu, "Effects of quaternary ammonium chain length on the antibacterial and remineralizing effects of a calcium phosphate nanocomposite," *International Journal of Oral Science*, vol. 8, no. 1, pp. 45–53, 2016.

[27] R. F. Beers Jr. and I. W. Sizer, "A spectrophotometric method for measuring the breakdown of hydrogen peroxide by catalase," *The Journal of Biological Chemistry*, vol. 195, no. 1, pp. 133–140, 1952.

[28] H. P. Misra and I. Fridovich, "The role of superoxide anion in the autoxidation of epinephrine and a simple assay for superoxide dismutase," *The Journal of Biological Chemistry*, vol. 247, no. 10, pp. 3170–3175, 1972.

[29] G. L. Ellman, "Tissue sulfhydryl groups," *Archives of Biochemistry and Biophysics*, vol. 82, no. 1, pp. 70–77, 1959.

[30] H. Ohkawa, N. Ohishi, and K. Yagi, "Assay for lipid peroxides in animal tissues by thiobarbituric acid reaction," *Analytical Biochemistry*, vol. 95, no. 2, pp. 351–358, 1979.

[31] O. H. Lowry, N. J. Rosebrough, A. L. Farr, and R. J. Randall, "Protein measurement with the Folin phenol reagent," *The Journal of Biological Chemistry*, vol. 193, no. 1, pp. 265–275, 1951.

[32] I. Kumburovic, D. Selakovic, T. Juric et al., "Antioxidant effects of *Satureja hortensis* L. attenuate the anxiogenic effect of cisplatin in rats," *Oxidative Medicine and Cellular Longevity*, vol. 2019, Article ID 8307196, 15 pages, 2019.

[33] K. J. Livak and T. D. Schmittgen, "Analysis of Relative Gene Expression Data Using Real-Time Quantitative PCR and the $2^{-\Delta\Delta C_T}$ Method," *Methods*, vol. 25, no. 4, pp. 402–408, 2001.

[34] M. Epple, "Review of potential health risks associated with nanoscopic calcium phosphate," *Acta Biomaterialia*, vol. 77, pp. 1–14, 2018.

[35] D. Nemenqani, O. El-Gharib, A. M. Ahmed, and A. R. Baiuomy, "The protective effects of antioxidant (vitamin C) against hepatic oxidative damage induced by zinc oxide nanoparticals," *International Research Journal of Applied and Basic Sciences*, vol. 9, pp. 502–509, 2015.

[36] J. Xu, P. Xu, Z. Li, J. Huang, and Z. Yang, "Oxidative stress and apoptosis induced by hydroxyapatite nanoparticles in C6 cells," *Journal of Biomedical Materials Research. Part A*, vol. 100A, no. 3, pp. 738–745, 2012.

[37] Z. Xu, C. Liu, J. Wei, and J. Sun, "Effects of four types of hydroxyapatite nanoparticles with different nanocrystal morphologies and sizes on apoptosis in rat osteoblasts," *Journal of Applied Toxicology*, vol. 32, no. 6, pp. 429–435, 2012.

[38] J. Sun and T. Ding, "p53 reaction to apoptosis induced by hydroxyapatite nanoparticles in rat macrophages," *Journal of Biomedical Materials Research. Part A*, vol. 88, no. 3, pp. 673–679, 2009.

[39] G. Li, J. Huang, Y. Li et al., "In vitro study on influence of a discrete nano-hydroxyapatite on leukemia P388 cell behavior," *Biomedical Materials and Engineering*, vol. 17, no. 5, pp. 321–327, 2007.

[40] S. E. Hart, "Assessment of renal function," in *Drug Discovery and Evaluation: Pharmacological Assays*, F. Hock, Ed., pp. 1–44, Heidelberg, Springer, Berlin, 2015.

[41] L. L. Haut, A. C. Alfrey, S. Guggenheim, B. Buddington, and N. Schrier, "Renal toxicity of phosphate in rats," *Kidney International*, vol. 17, no. 6, pp. 722–731, 1980.

[42] Q. Chen, Y. Xue, and J. Sun, "Hepatotoxicity and liver injury induced by hydroxyapatite nanoparticles," *Journal of Applied Toxicology*, vol. 34, no. 11, pp. 1256–1264, 2014.

[43] S. Paraš, D. Trišić, O. Mitrović Ajtić et al., "Toxicological profile of nanostructured bone substitute based on hydroxyapatite and poly(lactide-co-glycolide) after subchronic oral exposure of rats," *Nanomaterials*, vol. 10, no. 5, p. 918, 2020.

[44] X. Liu and J. Sun, "Endothelial cells dysfunction induced by silica nanoparticles through oxidative stress via JNK/p53 and NF-κB pathways," *Biomaterials*, vol. 31, no. 32, pp. 8198–8209, 2010.

[45] C. Ong, Q. Y. Lee, Y. Cai et al., "Silver nanoparticles disrupt germline stem cell maintenance in the *Drosophila* testis," *Scientific Reports*, vol. 6, no. 1, p. 20632, 2016.